FLEXIBLE ELECTROLYTE GATED ORGANIC FIELD EFFECT TRANSISTORS FOR SENSING

FRANZ XAVER WERKMEISTER

München 2016

Flexible Electrolyte Gated Organic Field Effect Transistors for Sensing

Franz Xaver Werkmeister

Dissertation
durchgeführt an der Fakultät für Physik
der Ludwig–Maximilians–Universität
München

vorgelegt von
Franz Xaver Werkmeister
aus Kitzingen

München, den 26.09.2016

ZUSAMMENFASSUNG

Biosensoren sind ein aktives Forschungsfeld der Organischen Elektronik. Das hohe Potential rührt von der Biokompatibilität und der guten elektronischen Kopplung zwischen Gewebe und Organischen Bauteilen her. Dies hat zum Feld der organischen Bioelektronik geführt. Zusätzlich sind durch günstige Massenproduktion mit geringem Energieverbrauch und biologische Abbaubarkeit nachhaltige Einweg-Instrumente möglich.

In dieser Arbeit wird die Fertigung von mechanisch flexiblen Organischen Feldeffekttransistoren (OFETs) demonstriert, welche als Double Gate Transistoren unter wässriger Lösung betrieben wurden. Ein Polymer der Poly-Para-Xylylen Polymergruppe wurde als Gate-Isolator und Substrat verwendet, um die mechanische Flexibilität zu erreichen. Diese Polymerfilme weisen typischerweise eine quadratisch gemittelte Oberflächenrauigkeit von mehreren Nanometern (nm) auf. In diesem Zusammenhang haben wir *In-Situ* Wachstumsexperiemente durchgeführt, um die Bildung des Transistorkanals auf rauen parylene-C Isolatoren zu untersuchen. Durch eine während der Deposition des organischen Halbleiters durchgeführte elektrische Charakterisierung konnten wir hier den Beginn des Transistorbetriebs bei einer Beschichtung von weniger als einer Molekularlage von Pentacen beobachten. Die weitere Entwicklung der OFET Eigenschaften mit der Filmdicke unterschied sich nicht von der auf glatten Isolatoren. Dementsprechend ist unsere Interpretation, dass der Transistorkanal sich ungestört durch die Oberfächenrauigkeit des Isolators bildet, falls die vertikalen Höhenunterschiede für benachbarte Moleküle klein genug sind.

Der gleiche Isolator wurde weiterhin verwandt, um OFETs für die Detektion von Harnstoff zu fertigen. In diesem Fall wurde das Enzym Urease kovalent an die OFET Oberfläche angebunden, um die Hydrolyse von Harnstoff zu ermöglichen. Die Hydrolyse von Harnstoff resultierte in Ammoniak, der in den Transistor diffundierte und den Ladungstransport durch die Immobilisierung von mobilen Ladungsträgern verringerte. Mit dem daraus folgenden Stromabfall konnten Harnstoffkonzentrationen im Bereich von 0,75 - 7,5 mM in gepufferter Lösung detektiert werden. Dies entspricht physiologischen Konzentrationen an Harnstoff in Blut.

Die Reaktion von OFETs auf Ammoniak wurde weiter untersucht. Hierfür wurden OFETs über den Elektrolyt geschaltet und die elektrochemischen Eigenschaften der verwendeten Dünnfilme des organischen Halbleiters DNTT gemessen. DNTT wies hinreichende Stabilität sowie geringe Dotierung durch elektrochemische Prozesse auf; Das Energieniveau für Lochleitung wurde zu -5.16 ± 0.05 eV bestimmt. Die Antwortzeit auf Ammoniak konnte auf 1-2 s reduziert werden, wobei die Antwort(zeit) von der Fertigung und der daraus resultierenden DNTT Filmmorphologie abhängt. Die Verkapselungsschicht bestimmt hier die Diffusionsstrecke, die die Ammoniakmoleküle passieren müssen. In der Folge wird die Antwortzeit von dieser Schichtdicke dominiert. Dies impliziert, dass für eine optimale Antwort sowohl die Morphologie des organischen Halbleiterfilms optimiert werden muss, als auch die Dicke der Verkapselungsschicht minimiert werden muss. In der Zukunft könnten solche optimierten OFETs für die Beobachtung von Zellsignalen verwendet werden.

Summary

Biosensors are a focus of organic electronics. The high potential stems from the biocompatibility and the good electronic coupling between tissue and organic electronic devices, which has lead to the field of organic bioelectronics. Additionally, cheap mass production with little energy consumption and biodegradability render disposable devices possible.

In this thesis the fabrication of mechanical flexible Organic Field Effect Transistors (OFETs) is demonstrated, which were operated as double gate transistors in aqueous solution. A polymer of the poly-para-xylylene family was used as gate dielectric and substrate to achieve the mechanical flexibility. These polymer films typically possess a surface roughness of several nanometer (nm) root mean squared. Related to this, we performed *In-Situ* growth experiments to study the transistor channel formation on rough parylene-C dielectrics. Here, by electrical characterization during deposition of the organic semiconductor pentacene, we could observe onset of transistor operation for less than one monolayer pentacene coverage. Further evolution of the OFET characteristics with film thickness was the same as in the case for smooth dielectrics. Consequently, our interpretation is that the transistor channel forms unperturbed from the dielectric surface roughness, if the vertical height changes are small for close-by molecules.

The same dielectric was further employed to fabricate OFETs for the detection of urea in solution. Here, the enzyme urease was covalently attached to the OFET surface to facilitate the hydrolysis of urea. The hydrolysis of urea gave rise to ammonia, which diffused into the transistor and decreased charge transport via trapping of mobile charge carriers. With the consequential decrease of current, urea concentrations in the range of 0.75 - 7.5 mM in buffered solutions were detected. This fits to physiological concentrations of urea in blood.

OFET response to ammonia was further investigated. To this end OFETs were solution gated and electrochemical properties of the used organic semiconductor DNTT thin films were measured. DNTT was found to display sufficient stability and low electrochemical doping, and a energy frontier level of -5.16 ± 0.05 eV for hole transport. The response time towards ammonia could be decreased to 1-2 s, where the response (time) depends on the fabrication and the resulting DNTT film morphology. Here, the encapsulation layer sets the diffusion distance for the ammonia molecules to pass. Consequently, the response time gets dominated by this layer thickness. This implies that for optimized response the organic semiconductor film morphology has to be optimized as well as the encapsulation layer thickness minimized. In future, such optimized OFETs could be applied to monitor signaling of living cells.

CONTENTS

INTRODUCTION

Electronics are ubiquitous in everyday life, such as in the control of public transport and operation/control of individual vehicles, or smartphones, and home entertainment. These devices are typically based on inorganic semiconductor technology, most notably silicon based integrated circuits. More recently, research introduced new materials, as metal-oxide nanoparticles, 2D materials like graphene and organic semiconductors to supplement silicon based technology. Here, these new materials can unlock device structures, such as mechanical flexible electronics. These are not feasible with the established technology due to mass production cost or incompatible physical properties.

A current example is display technology: for displays, Organic Light Emitting Diodes (OLEDs) have entered mass production, since they offer higher contrast and lower power consumption compared to LCD displays. Interestingly, the driving transistors in the active matrix displays are still fabricated from silicon, however, replacement of this material by printable metal-oxides and organic semiconductors is under investigation.[5] An additional benefit of these new materials is the possibility of fabrication of mechanical flexible displays on foils or even paper.[6]

Another thrust of organic electronics in particular is biosensing.[7] For example Organic Electrochemical Transistors (OECTs) are a promising candidate for printable sensors for metabolites.[8, 9]

1.1 BIOSENSING

A bio-receptor coupled to a transducer in an integrated device is a biosensor.[10] The term biosensor is by definition only applicable, if the bio-receptor is of biological origin. The bio-receptor is an element of biological origin, which provides recognition of the chemical or molecular substance to be analyzed, the analyte. The output (signal) from the bio-receptor is then transferred into the detection signal, e.g. a current or voltage, by the transducer.

Several approaches can be taken to achieve a biosensor or more general a sensor. One part is the readout mechanisms, which can be implemented by diverse principles: optical readout via changes in e.g. reflectance or fluorescence. This is especially interesting, if coupled with abundant tools for readout, such as a blue ray disk reader.[11] Further, mechanical readout can be used, such as changes in stiffness or resonance frequency of cantilevers, Quartz Crystal Microbalances (QCMs) or similar mechanical systems.[12] Another possibility is readout via electrical signals, such as change in resistance[13] or via Field Effect devices.[14]

Readout via electronic properties is advantageous, since it can be easily interfaced with or built from readily available electronic elements and devices. Further, detection can be done label-free. Label-free detection has the advantage to dispense the need for multi-step attachment of e.g. fluorescent labels.[15] This greatly reduces complexity of measuring substances of interest, which is important for the intended application as mass-produced transducer/sensor systems, e.g. in point of care applications.[7, 16] Here, the interest is not to replace the analytical methods in laboratories, but to provide easy-to-use and cheap sensor systems to monitor medically relevant parameters with portable systems, as for blood sugar measurements.

Of the different electrical readout mechanisms, nearly all can be and are implemented utilizing the different established and new materials, such as Si-technology and GaAs, in contrast to graphene, Carbon nanotubes and organic semiconductors. One case is a chemresistor, i.e. a semiconductor two-terminal device, whose resistance changes upon interaction with the analyte are evaluated.[13] Another possibility is the interaction via a Field-Effect to change the charge carrier concentration and corresponding measurements for the readout.[14] Examples are impedance sensors[17] as well as Ion Sensitive Field Effect Transistors (ISFETs).[18, 19] ISFETs can be extended via enzymes and proteins for further analytes.[10] Compared to electrochemical and optical sensing techniques,[16] transistors offer the advantage of signal amplification.[14, 20, 21] ISFETs have been commercially implemented for DNA sequencing. [22] However, some approaches for implementation have failed due to biocompatibility.[18] Also calibration before use and stability is often an issue,[18] which can be avoided with differential measurements.[23] In differential measurements, two, a functionalized and an unfunctionalized sensors are employed, and the signal taken as the response of the biosensor versus the reference. This approach can solve operation issues, such as drift.

A relatively new material class for application in transistors intended for biosensing are organic semiconductors. Several device architectures and sensing principles have been proposed and demonstrated, which include highly specific and sensitive detection schemes.[7, 24] Compared to inorganic semiconductors and inorganic nanoparticles based transistors,[25] organic semiconductor based transistors can be fabricated on low cost substrates at low processing temperatures. Further, the possibility to directly graft the detection elements to organic semiconductors is an exciting route to fabricate transistors for biosensing.[26] Furthermore, organic molecules can be chosen biocompatible or even biodegradable,[27] which is important for medical sensors and implants. Another advantage is that organic transistors are comparably mechanical flexible, such that they can conform to tissue,[28] which decreases irritation and decreases immune response. Especially, the properties of organic electronics make them

promising candidates for neuronal interfaces.[21, 29, 30]

1.2 SMALL MOLECULE ORGANIC SEMICONDUCTORS

Organic electronics encompasses application of products of organic chemistry as electronic active materials to realize electronic circuitry elements. Sometimes also pure carbon substances such as graphene and fullerenes are included in the field. In any case, fullerenes are typically considered part of organic electronics. In this work, organic semiconductors are considered to be only materials from organic chemistry. These are polymers and small molecules, individual as well as in solid state, which can be conductors and semiconductors.[31]

Conducting and semiconducting polymers[32] have the advantage of deposition by solution processes. However, they are often effectively doped by traces of the synthesis chemicals and metal catalysts, which are in fact impurities.[32] Small molecules can be solution processable depending on the molecule and are otherwise deposited by physical vapor deposition (PVD), with the advantage that PVD is a very clean and well controlled process.

Limited to small molecule organic semiconductors, the common characteristic is the presence of aromatic π-electron systems, i.e. the π electrons are delocalized over a molecular orbital. In molecules, the covalent bonds give rise to molecular orbitals, which get occupied up to the Highest Occupied Molecular Orbital (HOMO). The next higher, unoccupied energy level after the HOMO is the Lowest Unoccupied Molecular Orbital (LUMO), which is separated from the HOMO by an energy gap. In difference to the atoms building inorganic semiconductors,[33] these individual molecules are already semiconducting.[31, 34]

This type of small molecule organic semiconductors is also semiconducting in the van-der Waals bonded solid state, especially as polycrystalline thin film layers or crystals,[31] with their thin film transport levels originating from the individual molecules' HOMO and LUMO
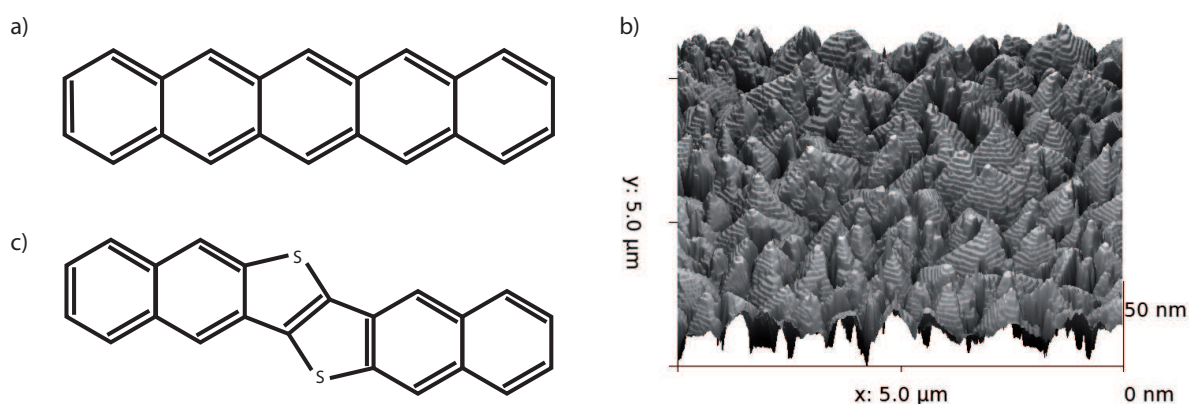

Figure 1.1: *a) Chemical structure of pentacene. b) A 3D representation of an Atomic Force Microscope (AFM) micrograph of pentacene thin film exhibiting Stranski-Krastanov growth. c) Chemical structure of a) Dinaphtho[2,3-b:2',3'-f]thieno[3,2-b]thiophene (DNTT).*

levels. The conduction states in these materials are also commonly referred to as HOMO and LUMO, even if these state involve single particle states of electrons and holes on ionized molecules.[35] The charge transport mechanism of such materials is still under debate. To date it is established that the two limiting cases of band-like transport and hopping transport through localized states, i.e. single molecules, exist both. This depends on the molecules and their solid state structure. Band-like transport is reported for single crystal samples, hopping transport is reported in rather disordered thin films.[36] Recent models point to the fact that the relatively large thermal motion in the van-der Waals bonded crystals is leading to localization, which is currently limiting the charge transport.[36, 37] Such thermal motions have been measured lately and correlated with transport properties.[38]

In the following, some important aspects of the two organic semiconductors utilized in this work will be discussed shortly.

1.2.1   PENTACENE

Pentacene (see Fig. 1.1 a)) is often applied as a model system, since it is one of the most studied small molecule organic semiconductor. High performance has been reported for Organic Field Effect Transistors (OFETs) based on pentacene polycrystalline thin films.[39, 40] Among other aspects of interest, its growth on dielectric[41] and metallic surfaces and the resulting electronic properties[42] have been rather well studied. Interestingly, polycrystalline thin films of pentacene can consist of different crystalline phases, namely the thin film phase and the bulk phase.[43, 44] While the bulk phase is the thermodynamically stable phase, the thin film phase is induced by the substrate during growth.[43] While pentacene enjoys wide use as a model system, it suffers from limited environmental stability, and consequently, new organic semiconductors have been investigated for practical applications.[45–47]

1.2.2   DINAPHTHO[2,3-B:2',3'-F]THIENO[3,2-B]THIOPHENE (DNTT)

One of these new organic semiconductors is Dinaphtho[2,3-b:2',3'-f]thieno[3,2-b]thiophene (see Fig. 1.1 c)).[46] In difference to pentacene, it has high stability versus oxidation from oxygen,[46] yet displays similar performance as pentacene.[48] This was already used to fabricate OFETs, which were resistant to conditions encountered upon sterilization procedures, which was not possible with pentacene.[49] However, compared to pentacene, the properties of DNTT, such as thin film growth, are not as deeply studied yet.[50, 51] Consequently, pentacene still fulfills the role as a model system with readily available literature data for comparison.
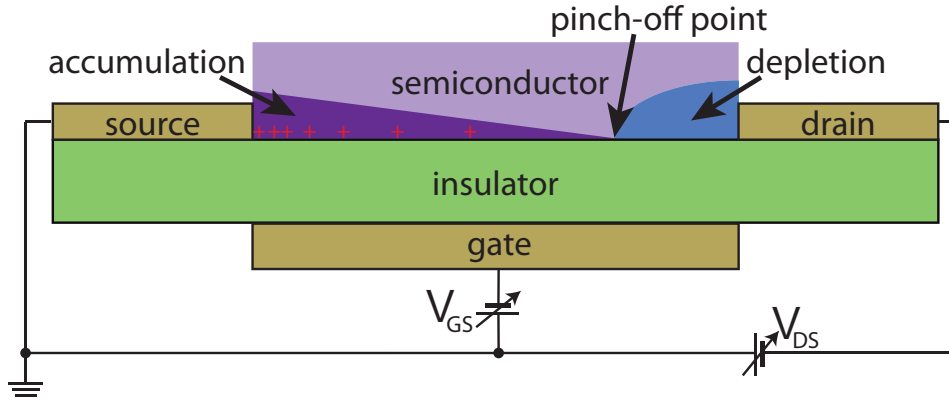
1.3 FIELD EFFECT TRANSISTORS (FETS)

Figure 1.2: *FET scheme. Scheme of a FET in saturation mode for p-type charge carriers. The accumulation layer in the channel is pinched-off and charge carriers between the pinch-off point and the drain are transported through a space-charge region for $V_{DS} < V_{GS} - V_{Th}$.*

Field Effect Transistors are basic electronic devices constructed from semiconductors.[33] In FETs the semiconducting channel between two electrical contacts, the source and the drain, is separated from the gate by a thin insulating layer (Fig. 1.2). The charge carrier density in the channel is controlled via an electrical field imposed by the gate voltage. Upon application of a voltage between source and drain, current is transported, if charges are accumulated by the gate. The transistor is in its on state. If the channel is depleted from charge carriers by the gate, the transistor is in the off state.

If charge transport takes place in the channel, one differentiates between the subthreshold, the saturation and the linear regime. In the subthreshold regime the charge sheet is not yet completely accumulated and the current rises exponentially with gate potential. In the saturation regime, the charge sheet would be in principle complete. However, all charge carriers near the drain, in the so called pinch-off region, are collected by the drain. This leads to a space charge transport region near the drain, where no charge carriers are accumulated between the pinch-off point and the drain. Finally, for higher gate potentials charges are accumulated through the whole channel and the transistor is in the linear regime.

A special case of FETs are Thin Film Transistors (TFTs). In TFTs the semiconductor is formed as a thin layer. In FETs in general the transistor can be formed at the top of the bulk material, e.g. MOSFETs on silicon wafers, which gives rise to influences from currents through the bulk material.

The TFT current in the linear regime is given by:[33]

$$I_{SD} = \frac{W}{L} \cdot \mu \cdot C_i \cdot (V_{GS} - V_{Th} - \frac{V_{DS}}{2}) \cdot V_{DS} \tag{1.1}$$

Here, W is the width and L the length of the transistor channel, μ the mobility of the semiconductor, C_i the areal capacitance of the gate dielectric, and V_{Th} the threshold voltage of the transistor. V_{DS} is the drain voltage and V_{GS} the gate voltage, which are both applied versus the
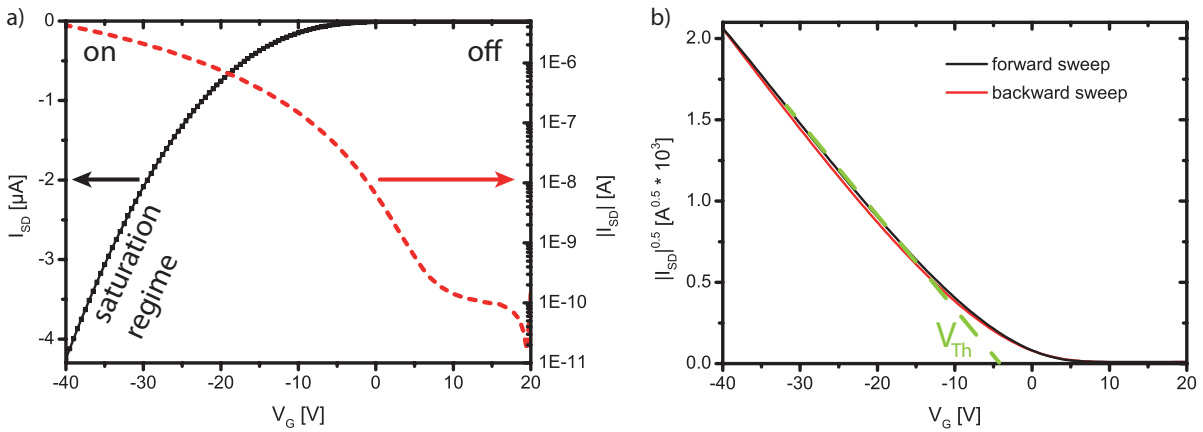
Figure 1.3: *(O)FET characteristics. a) Transconductance curve of a OFET plotted in linear as well as logarithmic representation. b) Plot of the transconductance with the squareroot of the source-drain current. From the linear slope extracted from this plot the threshold voltage as well as the mobility of a FET in the saturation regime can be extracted with equation 1.2. Also displayed is the effect of hysteresis: The forward and backward sweeps of the transistor do not necessarily overlap due to the presence of traps.[52, 53]*

source.

In the saturation regime the TFT current is given by:[33]

$$I_{SD} = \frac{W}{2L} \cdot \mu \cdot C_i \cdot (V_{GS} - V_{Th})^2 \qquad (1.2)$$

Here, the notation is the same as for the linear current. Note that in practice the saturation mobility μ_{sat} and the linear mobility μ_{lin} as well as the respective threshold voltages differ between the saturation and the linear regime. A transconductance (gate) sweep of a TFT from off state into saturation is displayed in Fig. 1.3.

In Organic Field Effect Transistors (OFETs) the inorganic semiconductor is replaced by an organic semiconductor (see 1.2). Moreover, dielectrics and electrodes can also be replaced with organic alternatives.[27, 54] In distinction from the prevalent Si MOSFETs, which operate in inversion and are fabricated on a bulk crystal, OFETs work in accumulation and the organic semiconducting film is usually formed as a thin film. The theory from classical TFTs is readily adopted to OFETs.[55] For OFETs gate-voltage dependence of the mobility, which can be also seen as charge density dependence of the mobility, as well as contact resistance modify the behaviour in real OFETs, and introduce additional dependencies, such as gate voltage dependent charge injection/extraction.[56]

1.4 BIOSENSING WITH ORGANIC TRANSISTORS

There are two distinct architectures for organic transistors used in biosensing, one is the organic field effect transistor (OFET) and the other one the organic electrochemical transistor

(OECT).[57] OFETs and OECTs differ by their operation principle. In OFETs mobile charge carriers are accumulated at the dielectric-semiconductor interface, while in OECTs the doping level is controlled. In the following, the basic properties are shortly discussed.

1.4.1 OECTs

OECTs are based on the doping and de-doping of the organic semiconducting layer. This is driven via the electrochemical potential in the electrolyte, which is in direct contact with the transistor channel (Fig. 1.4 d). With this approach, high transconductance has been reached, since the complete film height is contributing to the current change, outperforming most other architectures and materials.[58] On the other hand, this limits the obtainable switching frequency. Chemical reactions resulting in electrochemical potential shifts, e.g via pH value shifts, can be conveniently monitored, since this shifts the effective gate potential.[8] OECTs for biosensing are compatible with high throughput printing techniques,[9] and fabrication
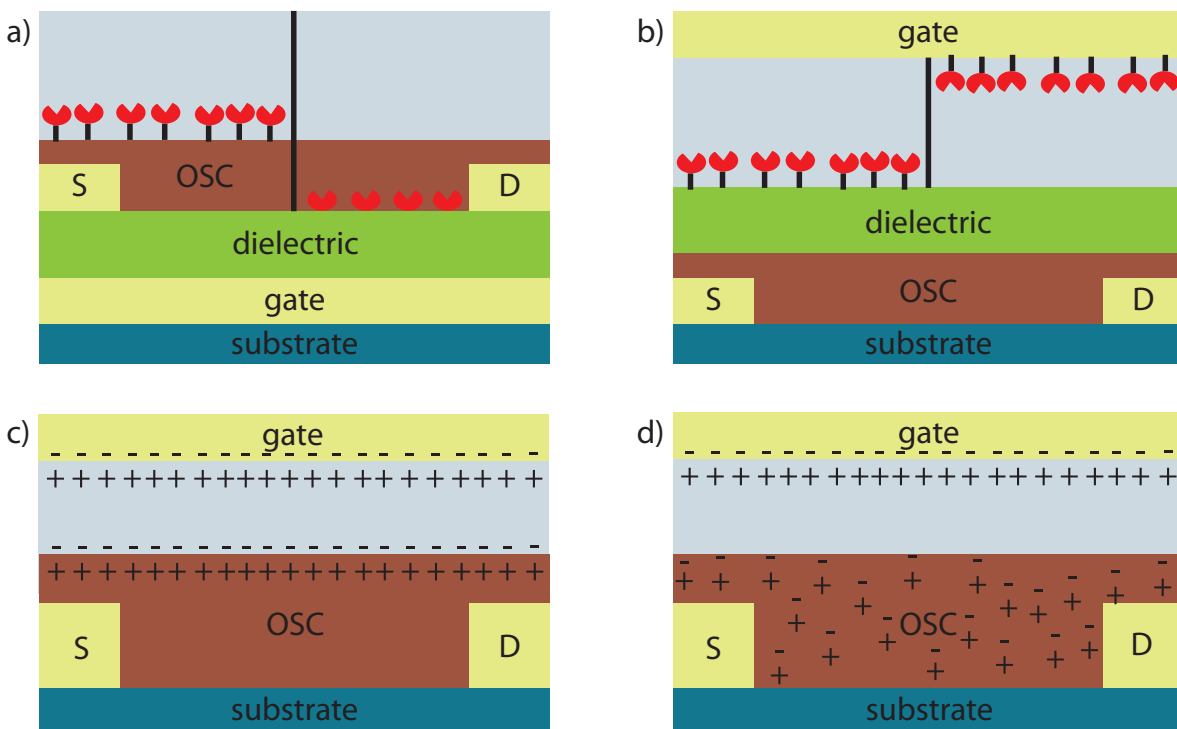
Figure 1.4: *Schematics of the different (bio)sensor architecture principles of organic transistors. a) Bottom gate OFET with the solution not in contact with the gate potential. Indicated are the possible positions of bio-recognition elements on the organic semiconductor (OSC) or between the OSC and the dielectric. b) The electrochemical potential in solution is set by the gate. The solution is in contact with the dielectric or c,d) directly with the OSC. Bio-recognition elements can be attached to either the gate, the dielectric or the OSC surface. In c) and d) the difference between OFETs and OECTs is indicated: In OFETs a charge carrier sheet is accumulated at the OSC-solution/dielectric interface, while in OECTs the complete film is doped and de-doped.*

pathways to include chemical attachment sites for subsequent immobilization of functional elements.[59] Utilizing OECTs detection of neurotransmitters,[60] uric acid,[61] cholesterol, [61] and glucose,[8, 9, 61] amongst others, have been reported.

1.4.2   OFETs

OFETs are operated via charge modulation through the field effect. In distinction from OECTs, the doping level of OFETs does not change, only the charge carrier densities are changed via the applied electrical fields.

There are three basic gating principles available:

First, the gate potential can be applied via a gate separated from the organic semiconductor by the gate dielectric. The solution to be tested is brought into contact with the semiconducting channel without connection to the gate potential (Fig. 1.4 a).

Second, the gate potential can be applied via the solution to test, which is in direct contact with the semiconducting channel or a dielectric on top of the organic semiconductor (Fig. 1.4 b and c). At the solution-solid interface, the potential drops at the electrochemical double layer (EDL).[62] Charge transfer is only present with electrochemical reactions, otherwise the potential gives rise to a concentration gradient of ions at the interface, the diffuse double layer. Since EDLs are very thin, they have a high capacitance of ca. $10 \frac{\mu F}{cm^2}$, giving rise to low operating voltages.

Third, the OFET can be separated from the solution. The solution sets the potential of a floating gate or the gate potential is controlled via the solution in an extended gate.

In extension, a bottom gate as well as a gate in the solution can be applied, which leads to Double-Gate-OFETs.[63, 64] With this geometry, the threshold voltage of the bottom (top) channel can be adjusted by the electric potential of the top (bottom) gate, provided the semiconducting layer is thin enough. If the semiconducting layer is thin enough, the depletion layer induced by the top gate can extend to the bottom, and effectively increase the threshold voltage of the bottom channel, and vice versa.[65] The individual gate potentials couple to the channel(s) governed by their capacitance. Thus the threshold shift V_{th}, which will result from a potential shift in the other gate δV_{other}, will be given by ratio of the capacitance of the individual gates:[63]

$$\delta V_{th} = -\frac{C_{other}}{C} \cdot \delta V_{other}$$
(1.3)

With this, a potential shift at one gate can be amplified in the threshold voltage shift of the other gate.

1.5 OFET PARAMETERS FOR BIOSENSING

The detection of a substance of interest is based on its interaction with the OFET and its impact on the electrical characteristics. Mostly, OFETs are operated in saturation in biosensing. As it can be seen from equation 1.2, there are three basic parameters which can change or can be influenced: the mobility μ, the threshold voltage V_{Th} and the areal capacitance C_i of the gate. Further, the On-Off ratio, i.e. the ratio between the On current and the Off current of the OFET, can decrease or increase upon interaction with a substance. One of these parameters, or a combination of several, must change in order to enable detection of a substance.[7]
Changes of On/Off ratio and the Off current were mostly described for OFETs operated as gas sensors[66], and can also be expected for biosensors operated in solution.[7] While changes in the On current can be related to shifts in the other parameters, the Off current might yield an interesting parameter for evaluation in some cases.
Out of the parameters in equation 1.2, a shift in the threshold voltage V_{Th} is a classical measurement parameter. Any change in charge δQ at the dielectric interface will give rise to a corresponding electrical field. This field couples via the capacitance to the transistor channel and generates an effective offset $\delta V_{Th} = -\delta Q/C$ to the threshold voltage V_{Th}.[19] This is used in the principle of ISFETs;[18, 19] any change in charge at the dielectric interface can be detected in the transconductance curve or, more simple, the source-drain current. E.g. adsorption of charged particles gives rise to a change in a transistor's threshold voltage.[64] This also yields to sensitivity to pH value changes. Upon pH-value change, the corresponding change of chemical potential can lead to a change in charge of chemical surface groups, such as hydroxyl-groups $|-OH$:[19]

$$|-OH_2^+ + OH^- \rightleftharpoons |-OH + H_2O \rightleftharpoons |-O^- + H_3O^+ \tag{1.4}$$
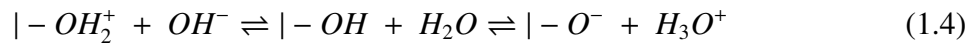
A surface potential shift of $\alpha \cdot (-59.2 mV/pH)$ at 298 K results, with a sensitivity parameter α between 0 and 1 depending on the solid-electrolyte interface.[18] The same mechanism at metal-electrolyte interfaces is used for solid state pH sensitive electrodes.[67] Also other changes in chemical potentials can be transduced via a shift of the threshold voltage, such as ion concentrations, and OFETs can be made to be selective by application of ion-selective membranes.[68, 69]
A critical issue for consideration of threshold voltage shifts is that electrical fields in solution decay exponentially.[70] Here, the lengthscale for field decay is the Debye's screening length λ_D. The Debye length is dependent on the ionic concentration in the solution. With a Deybe length $\lambda_D \approx 1nm$ it was found that detection of proteins via electrostatic fields in solutions of physiological strength is impossible.[70]
But on the other hand, in solutions of physiological strength, interactions of e.g. proteins with OFETs are detectable via monitoring the changes in capacitance C_i.[71] With this approach binding of odorant molecules was demonstrated with distinction between chiral enantiomers. [72]

Last, interaction of molecules in the solution with the organic semiconductor can change charge carrier mobility. This can be directly monitored via the OFET current.[3]

There are several device architectures, which are recent additions to organic electronics.

- In extended gate OFETs for sensing, the gate is separated from the actual OFET and the site of detection.[73] Thus, this setup separates the detection site in electrolyte from the transistor, such that each individually can be optimized. Such setups have also been realized with commercial silicon electronics for sensors.[74]

- In Charge-Modulated OFETs, the gate is directly implemented on the same substrate, but the gate is exposed to solution separately. No potential is set in or via the solution, which makes Charge-Modulated OFETs an interesting approach, since they do not need an electrode in the electrolyte.[75, 76]

- Another type has a functional interlayer between the organic semiconductor and the gate dielectric, such that any changes or interaction in this interlayer couple directly to the transistor channel.[77] This design may be exclusive to organic electronics, since the analyte must diffuse through the semiconductor layer[78] and the semiconductor must be deposited in a way not to damage the functional interlayer.

1.6 THIS WORK

This work focuses on the application of OFETs for biosensing. In previous work in our group, stable operation of OFETs in aqueous solutions and detection of adsorption of fatty acids via electrostatic interactions was demonstrated.[64, 79] However, these OFETs were still based on Si-chips as gates and the silicon dioxide as gate dielectrics.

The first aim of my work was to implement mechanically flexible OFETs, which could be operated in contact with aqueous solution. To improve the signal, i.e. the electrical current, and approach biological length scales of cellular assemblies, these OFETs had to be micropatterned. This was realized by utilizing photolithography. The OFETs were fabricated with thin layers of parylene as gate dielectric and substrate. These layers can also be released from the substrate, which results in mechanical flexible OFETs. Finally, operation in contact with solution was demonstrated.[2]

While parylene is an established dielectric for OFETs,[80] and pentacene film growth on parylene has attracted some attention,[81, 82] information on the channel formation, i.e. the growth of the first few monolayers of the organic semiconductor, was still missing. Here, we performed In-Situ electrical characterization during pentacene deposition to investigate OFET formation on the relatively rough parylene-C dielectrics.[2] The OFETs showed transistor performance even before the first pentacene monolayer was concluded. Indeed, evolution of the OFET characteristics were the same as for smooth dielectrics.

The architecture established with parylene dielectrics was then applied for an urea biosensor.[3]

Urea is a medical indicator[83, 84] and heavily used as fertilizer in agriculture.[85] Urea is selectively hydrolyzed by the enzyme urease.[83] Here, urease was covalently attached to the OFET interface to the electrolyte. For the covalent attachment procedure, DNTT, a more stable organic semiconductor than pentacene, was chosen. For these measurements an assembly of the OFET with a commercial available flowchamber was developed. The response of the OFET to pH-value changes in solution as well as to ammonia concentrations was tested. The ammonia response was found to dominate. It was rationalized by the diffusion of uncharged ammonia through the hydrophobic encapsulation layer and direct interaction of ammonia with the inorganic semiconductor as in gas sensors. Finally, detection of urea in buffer solutions via the ammonia produced by the hydrolysis of urea was demonstrated.

A major feature of the demonstrated OFETs for urea detection was their long response time for ammonia. For ammonia gas sensors, strategies have been demonstrated in the literature, on how to improve response time; Namely, thin films with high surface to volume ratio have been demonstrated to improve response.[86] In my study, DNTT morphology was found to be set by a 3D growth mode on a different gate dielectric, SU-8. With this morphology, the film was composed of many lowly connected islands, if the deposition process was stopped at the correct time. As it can be expected from the results on gas sensors, this gave a short response time also in solution.

FLEXIBLE ORGANIC THIN FILM TRANSISTORS (OTFTs) FOR OPERATION IN SOLUTION

Part of findings in this discussion have been published in Werkmeister et al. [1]. The publication is attached as full text in Appendix A.

To take full advantage of organic electronics it is crucial to fabricate flexible OFETs. Further, for (bio)sensing purposes, the single OFETs' components should be patterned on the microscale. And, of course, the OFETs should display stable operation in solution. To address the patterning of single layers in the device stack, photolithography has been chosen.

2.1 PHOTOLITHOGRAPHY

Photolithography is an efficient, highly parallel method to produce patterns on substrates. First, the pattern is produced in the illuminating light field by appropriate masking and mirror techniques. This patterned illumination then is transfered into structures on the substrate by photo-excitation of a functional photosensitive layer.
In the special case of this work, the photosensitive layer is always a commercial photoresist. It is patterned in a process flow, where the pattern is defined by the photo-illumination pattern (Fig. 2.1 a). This pattern then can be transferred to other functional layers, e.g. by subsequent material deposition or etching. During the so called Lift-Off process, the materials are deposited onto the patterned photoresist. When the photoresist gets dissolved later, all material not deposited directly onto the substrate will get lifted off and only the material directly on the substrate will remain (Fig. 2.1 b). Lift-Off is an additive process. In contrast, if the substrate with a patterned photoresist on top is etched, only the uncovered areas will get etched (Fig.
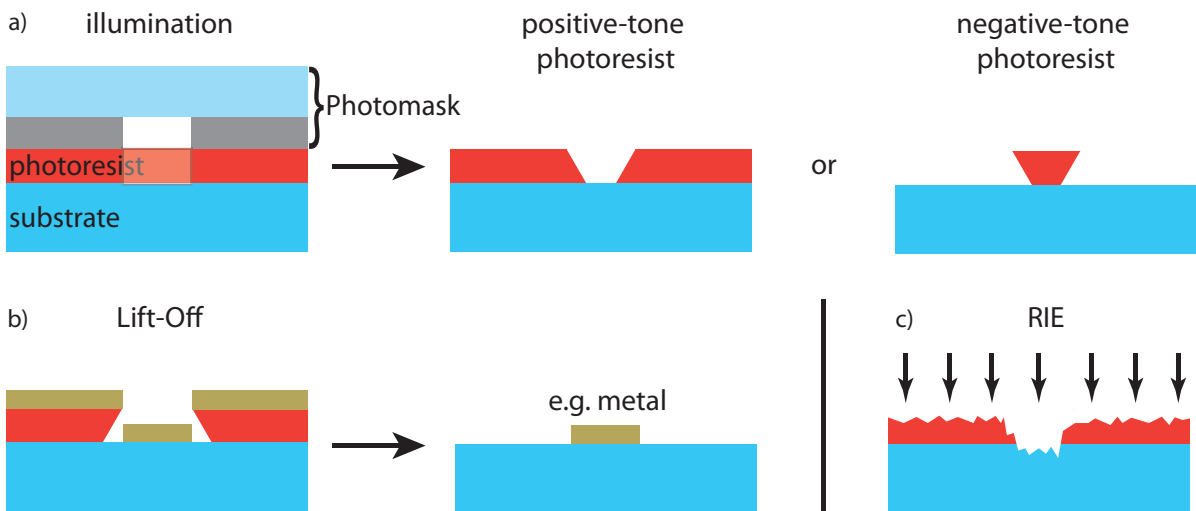
Figure 2.1: *a) Schematic of photopattern generation for positive-, as well as negative-tone photoresists. b) Schematic of a Lift-Off process. c) Schematic of a reactive ion etching (RIE) process with a photoresist as etchmask.*

2.1 c), which is a subtractive process. Related to such different aims, there exists a wealth of different photoresists, which are each optimized for a number of purposes.

The typical process flow to arrive at a photoresist pattern consists multiple steps: coating, softbake, illumination, post exposure bake, and development. During coating, a homogenous layer of photoresist is deposited onto the substrate, e.g. by spincoating. Next, the substrate is baked to remove residual solvent, which also makes the film more dense and mechanically stable. This is the so called softbake. After the softbake, the sample is aligned with the later photo-pattern, e.g. by alignment of the sample to the structures on a mask, and then illuminated with a chosen illumination dose. Depending on the photoresist used, a post exposure bake is necessary, in which by heating photo-activated chemical reactions occur. For example, a crosslinking agent gets generated by illumination and the crosslinking reaction is then driven by supplement of thermal energy. Last, the pattern is generated by the development step. Here, the system is subjected to the developer, a solution which will selectively dissolve or etch either the illuminated or the not illuminated areas of the photoresist layer. If the illuminated areas get dissolved, the photoresist is denoted as positive-tone, and in the other case as negative-tone.

Consequently, to reach the needed patterns in photoresists, many steps of the process flow have to be optimized. These are namely, amongst others; the photoresist deposition parameters, the soft- and postbake temperature(s) and time(s), the illumination dose and the development time.

For the work presented in this chapter, a Lift-Off process for patterning the electrodes was used, the parameters are given in Appendix C. A bi-layer of Lift-Off resist combined with a positive photoresist was chosen for the Lift-Off process,[87] since a single positive photoresist layer for Lift-Off usually is accompanied by fencing. In Fencing, the electrodes are not well defined, but have a fence at the edge from material deposited onto the photoresist sidewalls.

This may disrupt the organic semiconductor layer in the channel and lead to electrical contact between the electrodes and solution. Another way to avoid fencing is to use (single layer) negative-tone photoresists designed for Lift-Off. However it can be difficult to dissolve this layer completely afterward, otherwise unwanted resist residuals remain on the surface.[88]

2.2 CHOICE OF DIELECTRIC

The choice of photolithography as processing technique limits the suitable substrates and especially dielectrics. All these layers have to be compatible with the employed photoresists, process temperatures and process chemicals. Also, they should stand UV irradiation from photolithography. Furthermore, the dielectrics should be optically transparent and mechanical flexible, corresponding to the application in biosensors and should enable OFET operation in solution. The surface properties of the dielectric are of great importance for the resultant performance of the fabricated OFETs. Reactive and charged surface groups have been found to limit charge transport to the extend that electron transport is completely suppressed depending on the choice of dielectric.[89] Further, different surface energies give rise to different growth (modes) of the organic semiconductor, which also determines the transistor properties.[90]
With this prerequisites in mind, one can exclude all dielectric layers, which are soluble in either water or solvents. Further, they should withstand temperatures of > 100°C, which are typically encountered in photolithography processes. Combined with the desired optical transparency and mechanical flexibility, this leaves some polymer foils/layers as suitable dielectrics and substrates. Two of the best candidates are parylenes and polyimides. Polyimides, however, pose limitations on the choice of substrate, since the polymerization process necessitates process temperatures of typically 180°C or higher,[39, 91] which limits the possible substrates. Further, polyimides are sensitive to basic solution, e.g. most developers, which makes photolithography more complicated.[92] Consequently, parylenes were chosen as gate dielectrics, especially because they were already reported to facilitate operation in solution.[28]

2.3 PARYLENE

Parylenes, i.e. Poly(para-xylylene) (parylene-N) and its derivatives, form a family of polymers. Strictly speaking, parylene can also be just the designation of parylene-N and not the complete polymer family. These polymers are used in a range of fields, e.g. as protection coatings and electrical insulating layer.[93] It has widespread industrial application[93, 94] and is FDA approved.[28] Consequently, there is a wealth of studies available on its properties.[93–99] It is deposited via the Gorham route in rough vacuum in a Chemical Vapor Deposition (CVD) process; In the Gorham route a precursor (a dimer) is first sublimated, then cracked by pyrolysis and finally polymerizes on the substrates placed in the coating chamber (see Fig.
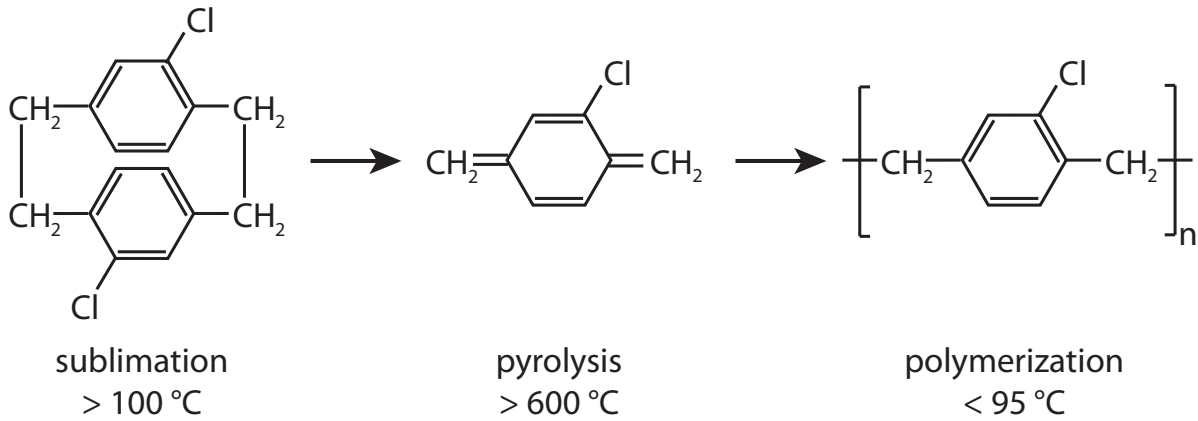
Figure 2.2: *Gorham route for the CVD process of parylene-C: The precursor, the dimer, is sublimated and pyrolytically split at high temperatures. The monomers will deposit and polymerize on all surfaces at room temperature. The process is run in vacuum and the vacuum pump is protected by a cold trap.*

2.2).[93] In this CVD process all surfaces are coated conformal and, depending on the derivative, deposition is performed at room temperature (RT). Further, the surface is clean after deposition without the need for additional cleaning procedures.

Parylene-C is most used, since it is compatible with standard parylene-CVD equipment and has a higher deposition rate than parylene-N and thus enables a better throughput. The deposition of both, parylene-N and parylene-C, on the sample can be modeled via adsorption of the monomers, which consequential either desorb or polymerize with a suitable polymer chain end.[93] A characterization of the dielectric properties of parylene-N and -C layers, as well as of OFETs fabricated on these dielectrics can be found in my master's thesis.[100]

Interestingly, this growth is influenced by the chemical composition of the substrate.[101] On transition metals, polymerization of parylenes can be inhibited until a passivisation layer is formed on the metals. This leads to a greatly selective growth, which has been used to obtain patterned CVD of a reactive parylene-derivative.[102] In particular for the application as gate dielectrics in OFETs, this property is undesired, since the gate electrodes are usually fabricated from metals. Consequentially, if parylene growth is inhibited or disturbed on the electrode, the parylene layer will be absent precisely at the position where it is desired. This problem can be solved by a thin (6 nm) aluminum layer on top of the Au electrode.[1] The Al can be deposited and patterned in the same process as the Au electrode. Most likely, the formation of a thin aluminum-oxide layer passivises the electrode surface for uninhibited parylene deposition. Note that this is only true for electrodes patterned via photolithography. For electrodes deposited through shadow masks, there usually is still an area of disturbed parylene growth at the rim of the electrodes. At this rim of the electrodes, the half shadow could give rise to a material gradient, which could lead to uncovered Au surfaces.

Parylenes are widely applied as gate dielectrics in OFETs, in particular poly(chloro-para-xylylene) (parylene-C). It is compatible with photolithography[1, 28, 100] and forms optical transparent foils, which can serve as flexible substrates for organic transistors (see Fig. 2.3 b)).[1, 28, 100, 103] The substrates or even finished devices can simply be peeled of their

solid support, which is a convenient pathway to arrive at mechanical flexible OFETs.

2.4   MECHANICAL FLEXIBILITY

One of the great advantages of organic semiconductors is the ability to fabricate mechanical flexible electronic circuits. Organic semiconductors form their polycrystalline structures from relatively weak van-der-Waals bonds, which can accommodate more mechanical strain than covalent bonds.[6] This makes them suitable to build flexible electronics. Additionally the relatively low processing temperatures, room temperature or less, enable to use cheap plastic foils[104] as well as paper as substrates.[105, 106]. For electronics integrated onto such mechanical flexible substrates of thickness h, the bending radius R of the curvature induced by the bend, relates to the mechanical strain ϵ on the surface of the substrate via[103] (see Fig. 2.3 a)):

$$\epsilon = \frac{h}{2R} \qquad (2.1)$$

In such bent substrates, there exists an neutral strain position, which is in first approximation in the middle of the height of the samples. The precise position of the neutral strain layer depends on the precise material stack in general, and this in turn modifies the strain onto the electronic layer depending on the material stack.[6] Here, the layers above and below will get compressed or stretched upon bending, i.e. the layer in neutral strain position suffer no strain. In theory this neutral strain layer is infinitesimal thin. In practice, layers close to the neutral strain layer remain operational under otherwise unfeasible bending radii, such that the strain must be greatly reduced.[107] Bending radii down to 200 μm were achieved for simple OFETs[103] with thin substrates and bending radii down to 5 μm were achieved for embedding the OFET structure in the neutral strain position.[104]

 There are several factors governing behavior of small molecule based OFETs under mechanical deformation: The intrinsic strain response of the organic semiconductor crystal itself, the behaviour of the polycrystalline organic thin film, but also the robustness of the dielectric and the electrical leads. The first intrinsic component was investigated by the group of Daniel Frisbie on rubrene single crystals recently.[108] The work function of the crystal surfaces was found to increase under tensile strain and decrease under compressive strain. This is expected to influence charge transport in organic semiconductor crystals,[108] since charge transport of organic crystals is dependent on energetic disorder.[37]

Moving from the intrinsic crystal behavior to the behavior of a polycrystalline thin film, several aspects are important. A phase transition in pentacene due to mechanical bending has been reported.[109] The change in lattice constant takes bending energy and reduces the stress. In contrast, such behavior has not been observed in another study.[110] One difference between the studies is that for films, which have displayed phase transitions, a phase coexistence had been observed initially.[109] For the phase pure films, no phase transition or change in pentacene crystal lattice spacing was observed. Instead, the morphological distance increased
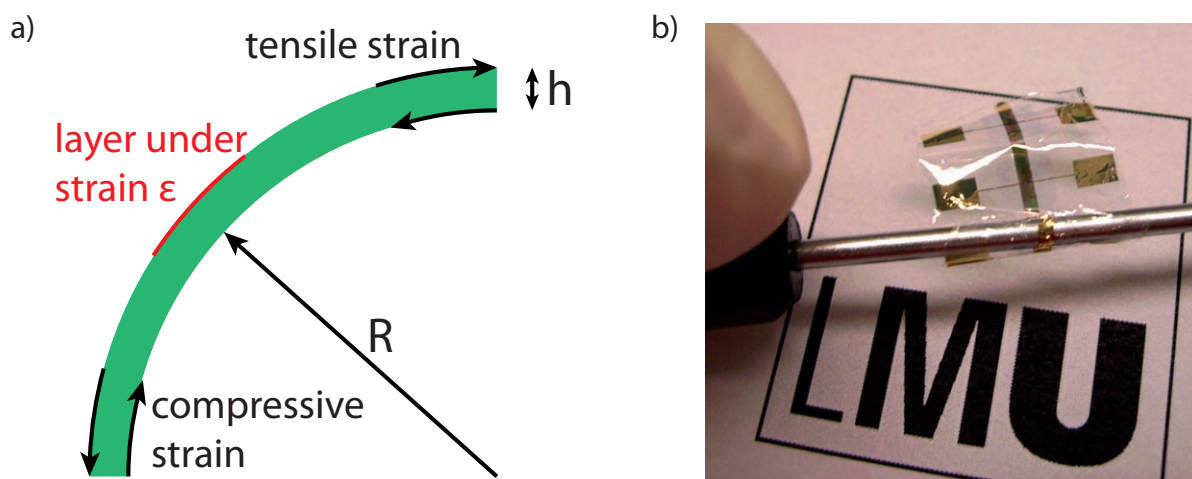
Figure 2.3: *a) Schematic of the situation of a bend substrate of thickness h with the bending radius R. b) Photograph of a flexible OFET fabricated on a parylene-C foil.*

between individual grains in the polycrystalline pentacene films.[110] In agreement with these results, smaller grain size in OFETs lead to less dependence on mechanical strain.[111]
Apart from the organic semiconductor, it was further found that rupture of the gold electrodes lead to OFET breakdown rather than degradation of the organic semiconductor thin film.[91, 110] Further, OFET breakdown can occur via gate dielectric breakdown.[107]
There exist several strategies for reducing the strain of the active FET, which have been used for organic as well as inorganic electronics: First, one can produce very thin FETs, in the best case dispensing the substrate.[103] Our approach to bendable OFETs falls into this category, with the total thickness of the OFET in the range 3-4 μm and sufficient transistor performance down to a bending radius of 800 μm (see Fig. 2.3 b)).[1, 100] Especially for stretchable circuits, another viable architecture is to place the active electrical elements onto stiffer regions within a more stretchable matrix.[112] With this strategy, it is also possible to integrate commercial (not-stretchable) microelectronics into stretchable architectures.[113] Yet another approach is to embed the active components in the neutral strain position, which enables highly bendable integrated circuits.[106, 107] This strategy is however not easily applicable to biosensors, since the FET must be coupled to the bio-recognition element, which should be close to the solution at test.

2.5　OPERATION IN SOLUTION

After demonstration of the mechanical flexibility of the OFET design, next, the operation in solution was tested. For this purpose, the transistor channel was encapsulated with 50 nm thick layer of tetratetracontane (TTC), which has been shown to be suitable for encapsulation in previous works.[64, 79] To protect the electrical leads, these were coated with a layer of S1812 G2, a positive-tone photoresist, which was suitable patterned, before deposition of

TTC. As a model solution, 10 mM Phosphate Buffered Saline (DPBS) buffer solution was chosen, since it is an isotonic solution, which is often applied in biological model systems. The PBS was used at 10 mM buffer strength prepared from premixed powder. This gave a total ionic strength of > 130 mM. Often (buffer) solutions are used diluted compared to isotonic ionic strength to improve operational stability or detection. However, this is in contrast to the idea of a biosensor and may not be possible in a point-of-care setting.

The OFETs were operated in a Double Gate mode: The bottom gate with parylene-C as gate dielectric was the conventional gate, as used in the previous characterizations and to check transistor performance during fabrication. On top of the TTC encapsulated OFET channel a droplet of DPBS was put, which was electrically connected via an immersed Pt/Ir wire (80% Pt, 20% Ir). It was not possible to use parylene-N as gate dielectric, since it showed good dielectric properties only for limited times. These limited operation times were unsuitable for measurements, i.e. the samples suffered dielectric breakdown, before a complete set of characterizations could be recorded.

With parylene-C as bottom gate dielectric, the OFETs could be operated as Double-Gate-OFETs.[1] Related to the threshold voltage ratio in equation 1.3, the transconductance $g_{individual}$

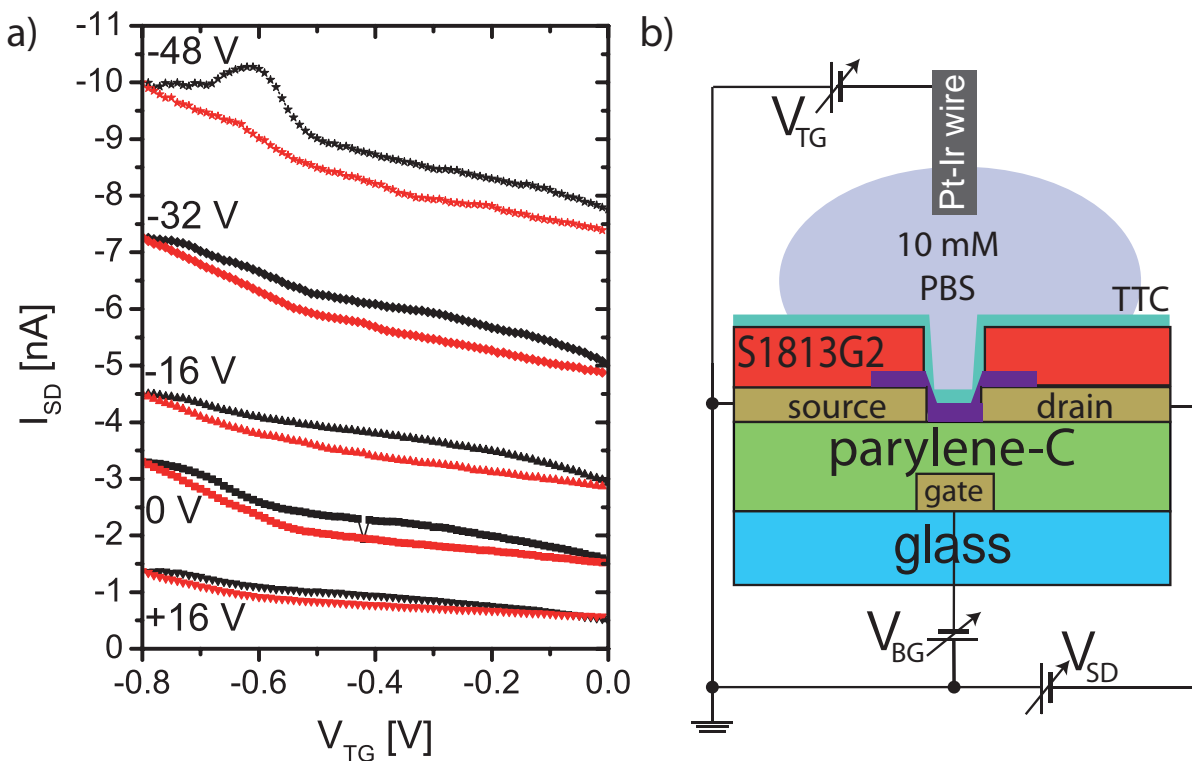**Figure 2.4:** *a) Schematic of the OFET and the measurement situation. b) Top gate transconductance curves at different applied bottom gate voltages. The forward sweep is drawn in black, the backwards sweep in red. The bottom gate voltages are given next to each transconductance curve. A peak is visible in the $V_{BG} = +48V$ curve, which is potentially an electrochemical reaction of pentacene shortly before dielectric breakdown.*

of the individual channels is directly proportional to the corresponding capacitance;

$$g_{top} = \frac{C_{top}}{C_{bottom}} \cdot g_{bottom} \tag{2.2}$$

(simplified for the case that C_{top} and C_{bottom} are much smaller than the intrinsic capacitance of the semiconductor layer). Consequently, the ratio of the transconductance of the bottom gate vs. the top gate is given by the ratio of the corresponding capacitances.[1] This results in higher transconductance for the channel with the higher capacitance, which is typically the solution-side gate.

The operation time of these OFETs in solution was limited by breakdown of the top gate dielectric, i.e. the TTC encapsulation layer, to at best several hours. A typical OFET behaviour before breakdown is shown in Fig. 2.4. Before breakdown, a peak in the transistor current at $V_{TG} = -0.6\ V$ for $V_{BG} = -48\ V$ is visible. This peak corresponds quite well to the potential, which must be applied to a platinum electrode to drive oxidation of pentacene molecules (for more information on electrochemical reactions see section 3.2.3). Thus, one can rationalize the breakdown as either by electrolyte passing through the encapsulation layer, or by thinning, e.g. by dissolution or ablation, of the encapsulation layer. A possible pathway to improve the encapsulation layer is to change to a crosslinked system to improve layer integrity.

An important point is the relatively low operation voltage of solution gates. Here, one has the advantage of low voltage operation, which is necessary for medical applications. Even not considering this, low operation voltages are more realistic with respect to practical application, e.g. easily attainable with batteries. Consequently, I chose gating via the solution gate as the main operation mode for further sensing experiments.

2.6   INFLUENCE OF DIELECTRIC'S SURFACE ROUGHNESS

Part of findings in this discussion have been published in Werkmeister et al. [2]. The publication is attached as full text in Appendix A.

Parylene films display a high surface roughness, when the film has sufficient thickness to serve as a dielectric.[1, 2] Among the physical properties of dielectrics, the surface roughness is a particularly interesting one. On a rough surface adhesion promoting layers can be dispensed, which greatly simplifies device architecture and production.[104, 114] Early studies implied a decrease in device performance due to a roughened surface.[115] The roughness of the dielectric's surface is typically described by the rms roughness extracted via AFM. The rms roughness is defined for N points with individual height deviations r_i from the mean:

$$R_{rms} = \sqrt{\frac{1}{N} \sum_{i=1}^{N} r_i^2} \tag{2.3}$$

In further studies, a limiting rms. roughness of 0.9 nm was found, for higher rms. roughness the OFET performance degraded.[116] Typical rms roughness for parylene films are several nm rms.[1, 2]

In contrast, OFET performance was found to be independent from roughness in other cases. [117] This was rationalized as a consequence of the lateral length scale of the roughness.[118] If the height variations on a small length-scale, i.e. the unit cell of individual semiconducting molecules, are negligible, crystal growth can be unaffected and surface scattering small. Only recently, systematic studies of the height correlation length versus OFET performance have been conducted,[119] which support these findings and interpretations.

In this line, we performed an In-Situ growth experiment:[2] The OFET operation onset and evolution during deposition of the organic semiconductor pentacene on rough parylene-C dielectrics were recorded and evaluated. The OFET current was found to set on below one monolayer of pentacene and further evolution of the OFET characteristics showed no influence of the surface roughness. We demonstrated that the pentacene polycrystalline film grew unaffected by the parylene-C surface roughness, which was found to display a lateral correlation length of ca. 100 nm by AFM analysis.

Due to early studies on artificially roughened surfaces, it was found necessary to apply planarization layers, i.e. a additional material layer which gives a reduced surface roughness compared to the original surface it is applied to.[120] However, planarization layers were also applied in systems,[107] where recent results imply that it is unnecessary and surface roughness actually has the advantage of making adhesion promoters unnecessary.[104] Thus, the findings on the influence are important for potential industrial implementation of OFETs.

AMMONIA READOUT IN SOLUTION APPLIED TO ENZYMATIC UREA DETECTION AND SEMICONDUCTOR MORPHOLOGY BASED OPTIMIZATION OF RESPONSE TIME

Part of findings in this discussion have been published in Werkmeister et al. [3]. The publication is attached as full text in Appendix A.

In the previous chapter OFET operation in solution was demonstrated. This OFET architecture was designed such that mechanical flexible device structures were possible. Next, this architecture was further developed to an selective biosensor: the enzyme urease was covalently bound to the surface of the OFET and urea detected via measurement of the ammonia, which resulted from the hydrolysis of urea.

3.1 UREA BIOSENSORS

The urea cycle is the strategy of higher animals, e.g. humans, to bind nitrogen waste. Nitrogen waste results for example from enzymatic conversion of glutamine to glutamate[60] and more in general, is an endpoint of amino acid metabolism. The nitrogen waste is present as ammonia, which would be toxic in high concentrations, thus it is converted into urea. Therefore, it is a medical indicator,[121, 122] which has stimulated research in urea (bio)sensors.[83, 84] Progress of dialysis can be monitored with urea sensors to adjust the treatment time to the needs of individual patients.[123] Urea is also used as fertilizer,[85] and consequently, mea-

surement of urea concentrations in water supplies is of high interest.[83, 84] As fertilizer, urea is the source of nitrogen for plant growth. Here, urea is enzymatically hydrolyzed into carbon dioxide and ammonia, where evaporation of the later is a major nitrogen loss mechanism.[85] The enzyme facilitating the hydrolysis of urea is urease, which is also applied in urea biosensors.[83, 84, 124]

Urea (bio)sensors based on various readout mechanism have been demonstrated. As such conductivity,[124] pH-shifts at pH-sensitive membranes[74] and with ISFETs,[125] and recording of electron transfer of electrochemical reactions,[126] have been used to detect urea and measure its concentrations. Interestingly, also inhibition of urease by several substances can be used to determine concentrations of these substances, e.g. arginine.[127]

Urease catalyzes the hydrolysis of urea $CO(NH_2)_2$ to ammonium and carbon dioxide:

$$CO(NH_2)_2 + 3\,H_2O \rightarrow CO_2 + 2\,NH_4^+ + 2\,OH^- \tag{3.1}$$

Ammonium and ammonia coexist in solution coupled by an chemical equilibrium.[3, 128] Ammonia can diffuse through unpolar encapsulation layers. Then it can interact with the organic semiconductor and change the OFET performance, which is utilized in gas sensors.[86, 129–131] Thus, this mechanism can be used for the detection of urea with OFETs instead of the previously applied mechanisms, such as pH shifts. This detection scheme has been utilized for urea sensors with inorganic capacitive gas sensors.[132]

3.1.1 MEASUREMENT CHAMBER AND OFET DESIGN

The starting point for the design of the measurement chamber was a commercial flow chamber, the sticky-Slide VI $^{0.4}$ from ibidi GmbH (Germany). For this sticky-Slides, the bottom of the flowchamber is open and any planar sample or a foil can be glued to the sticky slide at the bottom of the flow-channel via double side adhesive tape. To facilitate electrical contacting of the OFETs glued to the flowchamber via spring contacts, holes were drilled into the
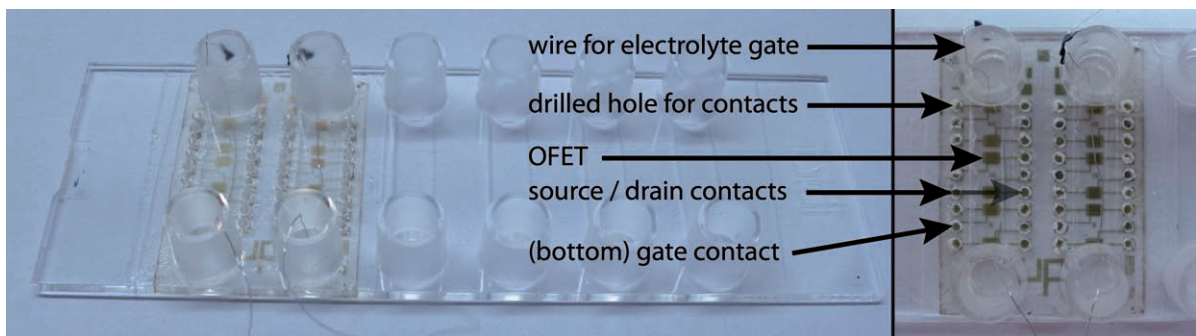

Figure 3.1: *Picture of an OFET glued to a modified flow-chamber. The Pt/Ir wires used as solution gates are visible in the individual channels. The right side displays a zoomed-in picture of the OFET sample.*

Slides at the later positions of the contact pads on the OFETs to facilitate electrical contact with a computer controlled milling machine. These holes, and the contacts, are isolated from the solution in the flow-channel by the adhesive tape. Since the factory applied adhesive tape gets ruptured during drilling, the original adhesive tape is first ripped off and after drilling a new tape is applied and patterned for use. The drilling and the glue limit the total number of applicable contacts on the OFET, since all these contacts must be placed in the areas outside of the flow-channel and the minimum distance is set by the minimum possible spacing of the spring-contacts and the contact pads as well as the distance necessary to obtain a seal by the glue. Here, 9 vias were drilled on each side of the flow-channel with a diameter of 0.8 mm each and a distance of 1.25 mm center to center and nominally 0.3 mm from the rim of the flow-channel to the rim of the via. Consequently, the design of the OFETs was done with respect to the Slides.

For the OFET design, photolithography was chosen for the patterning of electrodes and dielectrics, and microscopy cover slip slides were chosen as fabrication substrates. Their size of 18 mm times 24 mm was chosen because of two reasons. On the one hand, these slides covered the whole flow-channel in the sticky-Slide VI $^{0.4}$. On the other hand, they were compatible with the available processing equipment. Each OFET in the channel got its own gate electrode, so that the sample could still be used when one gate electrode displayed a short-circuit to the electrolyte. With this and the total 18 contact possibilities available per channel 6 OFETs per channel can be implemented. In each channel, 2 OFETs had a channel length L of 20 μm and channel width W of 24 mm, 2 a L of 10 μm and W of 49 mm, and 2 a L of μm and W of 99 mm. These different channel lengths make the design more general applicable for tests with respect to basic OFET properties, such as contact resistance[133]. Also, the contacts and contact resistance can be the actual detection mechanism, and this effect must be separated from the impact on the semiconducting channel,[134] which is possible with the designed architecture.

A fabricated OFET sample attached to a modified chamber is displayed in Fig. 3.1 and the preparation protocol for the flow-chambers as well as information on the measurement setup and protocols is given in Appendix D.

3.1.2 PARYLENE ENCAPSULATION LAYER

For the OFET architecture, parylene-C was chosen as a replacement for the previously applied TTC layer. As discussed in the previous chapter 2.5, the TTC encapsulation showed breakdown of the dielectric properties after several hours. One possible explanation is thinning of the encapsulation layer during the experiment. A crosslinked encapsulation layer would lessen or completely avoid this problem. Parylene-C showed good performance as bottom gate dielectric in solution (section 2.5), can be deposited as 100 nm thin films onto the OFET via CVD, and has a physically crosslinked structure. While, CVD of parylene-C does damage the organic semiconductor film to some extend, the OFETs retained good performance in the used
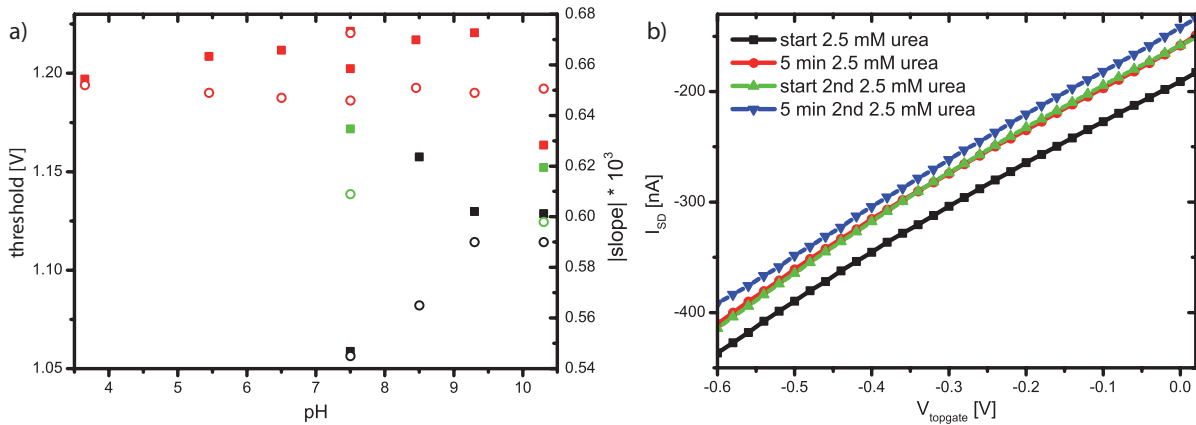
Figure 3.2: *a) Threshold voltage (squares) and slope/capacitance (circles) shifts with pH-value. Black symbols give the initial response with urease. Green symbols represent measurements after exposure to a pH-value of 10.3. Red symbols represent the behavior for and after exposure to pH of 3.65. b) Urea response for first exposure to 5 mM urea in DPBS and for a second exposure of the same concentration of urea. In the second exposure, nearly no further current drop takes place.*

sample architecture. The characterization of parylene-C coatings as an encapsulation layer for OFETs operated in solution was published as supporting information and can be found in the appendix B.

While chemically rather inert, the surface of parylene-C can be activated by oxygen plasma treatment for subsequent functionalization.[135] However, this treatment necessitates the use of an oxygen stable organic semiconductor, here DNTT, instead of pentacene, since pentacene displayed an insufficient stability versus the oxygen plasma treatment in the studied system.[3]

3.1.3 AMMONIA AND UREA DETECTION

Detection of urea is done via the hydrolysis of urea, and more specifically in the discussed case by the interaction of the OFET with the reaction products. The two noteable interaction mechanisms are the interactions with ammonia and the corresponding pH-value change of the solution. Consequently, it is imperative to investigate the pH-response of the proposed OFETs.

Note that pH-response of systems with additional layers changes. Such layers modify the capacitance, chemical concentrations, and chemical surface group composition at the OFET surface.[71] Most notably, these surface layers give rise to a Donnan's equilibrium, which can be modeled as an effective capacitance dependent on the ionic strength of the solution as well as the density of fixed charges in the surface layer.[71] The later will in turn depend on the (local) pH-value of the solution.

 As published,[3] the initial increases in current with pH-value are due to a threshold voltage shift and a change in capacitance (see Fig. 3.2 a). A change in the mobility can be excluded due to the hydrophobic parylene-C encapsulation. However, for pH-values, at which the ure-

ase would degrade, the pH response changes. For the alkaline regime after potential urease degradation, it was observed that the capacitance first stays constant and only the threshold voltage values change to different absolute values than before. The consequent test for acidic pH-values showed that the capacitance again jumps to a new value, which is constant within given accuracy during the rest of the experiments. For the threshold voltage shifts, a consistent step shift can again be observed for high pH-values, otherwise the threshold voltage shifts are negligible. The change of behavior with potential urease degradation can also be explained with breaking of the covalent surface anchoring or both effects occurring at different pH-values. Both processes would effectively change the surface composition and thus capacitance and surface charges. Here, it is noteworthy that the pH-dependence set by a pristine parylene-C encapsulation is given by the surface potential of the used Pt/Ir wire and no capacitance shifts occur.

In practice, the response is found to be ammonia dominated. The ammonia produced in the hydrolysis of urea causes a current decrease. Via this current decrease urea can be detected. This current decrease is the dominant signal, which is used for the urea detection.[3]

On the experimental timescale the current reduction remains constant. Further exposures to urea concentrations, which have been tested with the same concentration before, give rise to not significant response (see Fig. 3.2 b). The ammonia impact on individual OFET parameters is superimposed with the pH-response of the OFET. In total, ammonia effectively gives rise to a current decrease, which is the signal used for urea measurement. The current response is effected by the ammonia molecules, which diffuse to or into the organic semiconductor film. Thus, this process can be explained by 1D diffusion. The current response was modeled by a solution of Fick's second law of diffusion in 1D. A solution with the boundary conditions of $c(x = 0) = c_S$, a fixed surface concentration, and $c(x = \infty) = c_0$, a bulk concentration is, for the concentration $c(x, t)$ at time t and distance x from the reservoir is:

$$c(x, t) = c_S - (c_S - c_0) \cdot erf\left(\frac{x}{2\sqrt{D \cdot t}}\right) \tag{3.2}$$

D is the diffusion constant and $erf(x)$ the errorfunction. The transient current response of the OFETs upon ammonia introduction was fitted with the equation:

$$I(x, t) = I_0 - I \cdot erfc\left(\frac{x}{2\sqrt{D(t - t_0)}}\right) \tag{3.3}$$

Here, $I(x, t)$ is the OFET current at time t and distance x of the reservoir, with ammonia injection at time t_0. The function $erfc(x)$ is defined as $erfc(x) \equiv 1 - erf(x)$. This solution assumes a constant surface concentration at the reservoir interface and assumes a one-to-one correspondence of current decrease to ammonia concentration. Consequently, it is only applicable to short timescales, since this approximation is not valid any more at long timescales, when the film response begins to saturate. Equation 3.3 can be used to fit the transient current response and extract an effective diffusion constant.[3]

The physical interaction, which is the reason for the impact of ammonia on p-type organic

semiconductors is still under debate, however the two most likely candidates are base de-doping and dipolar disorder.[86] The current model typically applied is diffusion of ammonia into the organic semiconductor film.[86, 136] Another model is adsorption of the ammonia molecules onto the organic semiconductor film.[137] Here, adsorption in/at grain boundaries, which has been shown important for alcohol vapor detection,[138] could also give rise to the observed responses.

3.2 INVESTIGATION OF AMMONIA RESPONSE

Part of findings in this discussion have been published in Werkmeister et al. [4]. The publication is attached as full text in Appendix A.

While the OFETs based on parylene as substrates and dielectrics enable mechanical flexible device configurations, the use of the commercial flowchambers means that this property is not applicable. When the sample is glued to the bottom of the flowchamber, the mechanical properties of the flowchamber set the effective properties of the OFET to be flat and not mechanical flexible. While it is desirable to have mechanical flexibility in the biosensor in general, for the precise case of the flowchamber here, a rigid, planar structure is sufficient from a practical viewpoint. Therefore, the photoresist SU-8, which was already used for encapsulation of electrical leads, was investigated for its suitability to serve as dielectrics in OFETs.

3.2.1   SU-8

The commercial negative tone photoresist SU-8 from MicroChem has long been used to fabricate high resolution 3-D structures.[139] More recently, the dielectric properties were investigated[140] and the findings triggered use of SU-8 as a dielectric.[141] In particular, the possibility to apply photolithography for subsequent patterning of additional layers on top of SU-8 makes it an interesting candidate for OFET fabrication.[141]
For this study, SU-8 was utilized as an encapsulation for electrical leads, which would otherwise have been exposed to the electrolyte in biosensing experiments. Further, SU-8 2000.5 was used as a gate dielectric in OFETs. The detailed fabrication protocols developed for this purpose can be found in Appendix C. The advantage of SU-8 2000.5 compared to parylene-C is the fact that the fabrication of the layer as a permanent dielectric via photolithography includes the patterning of the layer in the very same step.
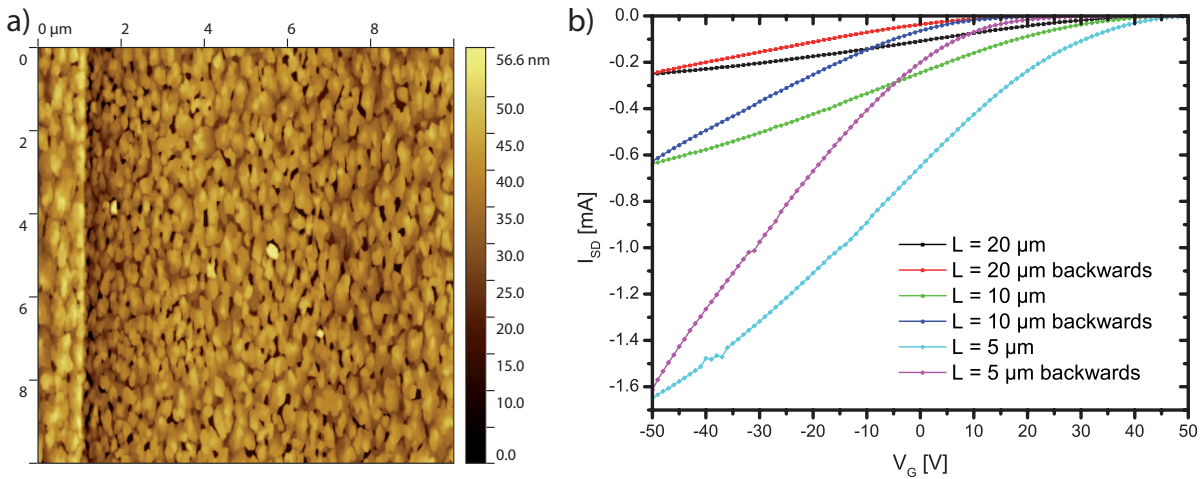
Figure 3.3: *a) AFM micrograph of a DNTT film in the channel and on the electrode for SU-8 dielectric based OFETs. b) Electrical characteristics for OFETs on SU-8 dielectrics with an SU-8 encapsulation applied to the electrical leads. Decreasing the channel length by a factor of 2 increases the channel width by a factor of 2 in the present design. Thus, the current should increase by a factor of 4 for a decrease of the channel length by a factor of 2. This increase by a a factor of 4 is not the case, which is an indication for contact resistance.*

3.2.2 DNTT-MORPHOLOGY ON SU-8 AND OFETS

It was found in this study that growth of PVD processed DNTT on SU-8 dielectrics depends on the prior processing of the dielectric. For as prepared SU-8 surfaces, DNTT films display a pyramidal surface morphology, as expected for the Stranski-Krastanov growth mode. For the Stranski-Krastanov growth mode, some layers grow layer by layer to later switch to the 3D growth, which gives rise to the pyramids. On SU-8 dielectrics, where the electrodes have been patterned by a Lift-Off process however, the DNTT films are composed of single islands, which percolate at later stages during growth (see Fig. 3.3 a). This growth mode is called Volmer-Weber. This is in line, with the reports in the literature that the growth of the organic semiconductor depends strongly on the dielectric's surface energy.[90]

Another feature visible in morphology studies is that DNTT grows in a similar structure on the Au electrodes as on the dielectrics (see Fig. 3.3 a). However, it should show disturbed growth on clean Au electrodes. This behavior can be reproduced, if a clean Au electrode is coated with SU-8, which is subsequently rinsed away. Consequently, SU-8 resist residuals are a likely candidate to induce this growth behavior on electrodes. Interestingly, for OFET samples without the last SU-8 encapsulation step, i.e. DNTT deposition after Lift-Off, the peculiar DNTT growth on the Au electrodes is recovered. This implies that the Lift-Off medium used, mr-Rem 400, does leave very little resist residuals on the Au electrodes.

Considering operation in solution, the well behaved growth of DNTT on the dirty Au electrodes has the advantage that it reduces exposure of Au to the electrolyte and thus blocks corresponding electrochemical reactions to some extend.

When evaluating the OFET parameters, the difference in DNTT morphology on the Au

electrodes is reflected in the threshold voltage. Typically, for OFETs without SU-8 encapsulation, the threshold is about +20 V, while for OFETs with SU-8 encapsulation the threshold is typically quite positive with about +50 V. Consequently, the encapsulation poses a tradeoff between highly positive threshold voltages of the bottom gate versus operation with a gate voltage applied via the solution. However, the preferred operation via the solution side gate was still feasible. The hysteresis is around 20 V, which is expected for an 3D growth semiconductor film morphology.[142] Saturation mobilities extracted from the OFET characteristics are $\approx 0.01 \frac{cm^2}{Vs}$. Figure 3.3 b) displays a transconductance curve set of OFETs on one sample.

3.2.3 ELECTROCHEMICAL CHARACTERIZATION OF DNTT

Before gating an OFET via a solution gate, it is instructive to perform electrochemical measurements. Such measurements can yield the possible potential window for operation as well as general behaviour under electrolytes, such as electrochemical doping.[143] The two typical measurements are cyclic voltammetry (CV) and Electrochemical Impedance Spectroscopy (EIS or also ECIS).[62] A detailed description and theory on CV and EIS can be found in the book of Bard and Faulkner.[62]

With CV, the electron transfer associated with reduction or oxidation reactions is measured. Here, the reaction is driven by an externally applied electrical potential. Consequentially, the potential, which governs the chemical equilibrium, is set by the combined chemical and electrical potential, the electrochemical potential. In CV, the electrical potential is cyclically swept, such that occurrence of oxidation and reduction, or the absence of the backreaction can be recorded via the charge transfer associated with the reaction. From the position of the peak-pairs of the reaction and corresponding backreaction, the potential of the energy level
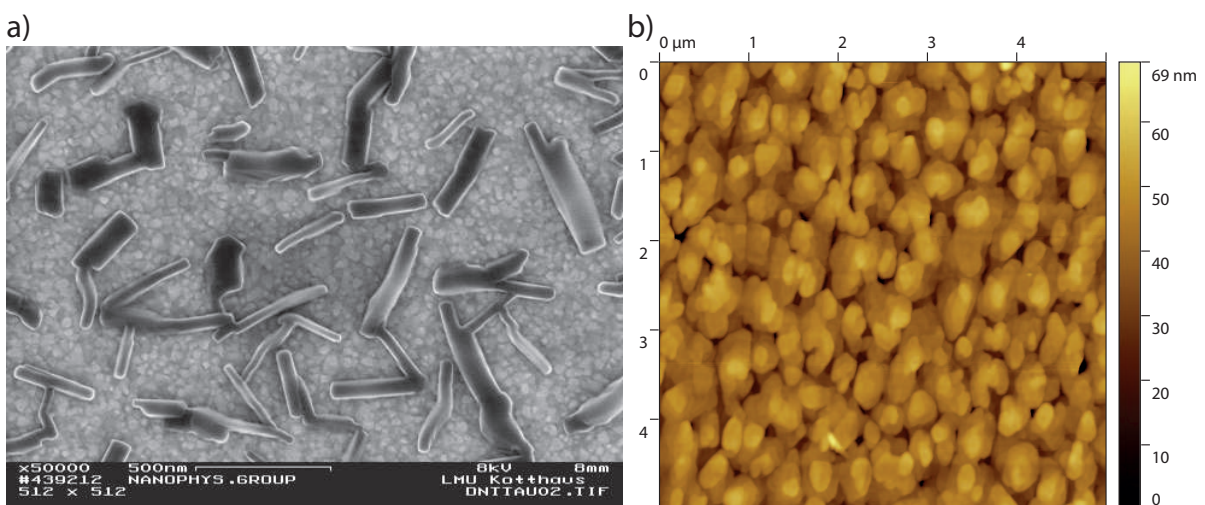

Figure 3.4: *a) SEM micrograph of a 46 nm DNTT layer deposited on bare Au. There are clearly visible big features. b) AFM micrograph of 50 nm DNTT on pretreated Au. The morphology is similar to the situation on SU-8 dielectrics.*

versus the potential reference, and thus versus the vacuum energy can be deduced. However, such measurements have systematic deviations, for example often organic semiconducting molecules in solution instead of in thin films are measured. This has to be considered if the absolute position of the molecular energy frontier levels shall be deduced.[35]

In this study, the organic semiconductor is deposited as a thin film on the electrode, which best resembles the situation in the OFETs. For PVD deposited small molecules organic semiconductors, growth on metal electrodes is often disturbed. Consequently, one has to take great care in measurements of DNTT thin films coated on electrodes, such as Au electrodes, since artifacts can arise from electrochemical reaction of the Au electrode with the electrolyte. On pristine Au electrodes, DNTT grows greatly disturbed with respect to OFET samples (see Fig. 3.4 a). In contrast, if the Au electrode is treated with an SU-8 encapsulation, which is rinsed away with the SU-8 developer, DNTT grew comparably to the situation on dielectrics (see Fig. 3.4 b). Indeed, only on treated Au electrodes one does not measure electrochemical reactions of the Au. The energy frontier level of DNTT was extracted on treated Au electrodes to -5.16 eV, with errors related to the potential extraction estimated to ±0.05 eV, owing to extraction of peak positions (see Fig. 3.5 a). However, the SU-8 residual layer on the Au as well as the different molecular orientation can reduce the charge transfer. This reduces signal level and makes the absolute measured current potentially to deviate from intrinsic properties. The energy frontier level measurement was only dependent on the potential to drive the reaction and its backreaction and is not sensitive to charge transfer limitations.

EIS is an investigation technique, which enables extraction of dielectric properties and properties of the interfaces of a sample structure.[143, 144] Because of chemical reactions, which can be driven by the electrical potential, the amplitude of the alternating voltage is typically chosen to be low. Here, it is 10 mV. Formation of an electrochemical double layer (EDL) and no electrochemical doping can be assumed, if the phase is close to -90 degree for low excitation frequencies (<100 Hz),[143] i.e. the measurement displays pure capacitive behavior. Indeed, for DNTT grown on treated Au electrodes, this is the case for no applied external potential.

The Escan is another investigation method for semiconductors.[143] It extends EIS measurements by conducting them with several potential offsets applied. This technique is related to the capacitance-voltage measurements in semiconductors.[33] The interesting feature of an Escan in the present sample geometry is that it can indicate whether or not electrochemical reactions/doping occur within the potential window of OFET operation. If the capacitance measured increases above the capacitance realistic for an EDL, obviously the relevant process cannot be charging of the EDL at the boundary. Indeed, changes in doping level can be responsible for higher apparent capacitance, a feature used in high performance OECTs.[58] Further, electrochemical reactions of the Au electrode can produce artifacts in the measurements, especially at low frequencies. Consequently, not only in CV measurements the growth of the organic semiconductor on the electrode has to be considered. With treated Au electrodes the capacitance tripled, as the potential is increased from 0.2 V to -0.4 V (see Fig. 3.5 b). This can be interpreted as the accumulation of charges at the semiconductor-electrolyte interface,
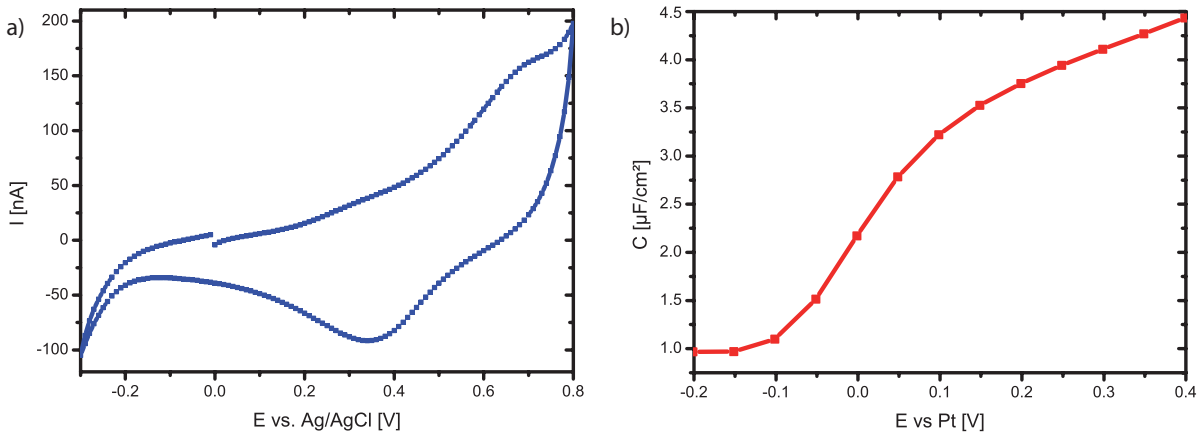
Figure 3.5: *a) Cyclic voltammetry of a 30 nm DNTT film on a pretreated Au-electrode. Potentials were applied versus a leakage-free Ag/AgCl reference electrode and the supporting electrolyte was 1 mM NaCl in water. b) Escan of the same sample as for a). The shift from depletion to accumulation is visible. For higher potentials the accumulation tends not to saturate, however, does not exceed typical EDL capacitance.*

so that the EDL at the interface gets the dominant contribution of the semiconductor layer. Before the semiconductor layer behaves rather as a dielectric layer. The capacitance increases further with potential, but stays at values acceptable for a EDL (ca. 10 μF/cm^2 [143]), which is an indication for the absence of electrochemical doping.

3.2.4   SOLUTION-GATED OFETS BASED ON DNTT

Given the results from the electrochemical characterization, it is reasonable to assume that DNTT based OFETs can be operated solution gated. Pentacene has a similar energy frontier level as DNTT and can be operated via a solution gate, if the operation voltages are limited to 0.4 V.[145] Indeed, DNTT OFETs can be operated via solution gate. Solution gate potential up to $V_{GS} = -0.5\ V$ can be applied. However, electrolyte current, i.e. current between the Pt wire and the source, increases with gate potential. This could be leakage current or Faradaic current associated with electrochemical reactions. Consequently, the applied gate potentials were limited to $V_{GS} \geq -0.4V$ in following experiments. With these samples operated as Double-Gate OFETs, one can extract the same information as in the previous chapter,[1] i.e. the ratio of the transconductances and extract the double layer capacitance. Here, the top-gate capacitance is a combination of the EDL at the electrolyte-semiconductor interface and the gate-electrolyte interface. Such behavior is important in some sensing approaches, where the change of gate capacitance is monitored.[72] The extracted value for the EDL capacitance is on the order $10^0 \frac{\mu F}{cm^2}$, in good agreement with values in the literature[145] and with the result from the previous Escan measurements (section 3.2.3).

 The shift of transistor characteristics with pH is different to the situation with urease attached, since there are no functionalization layers. Fig. 3.6 a) displays the shift of threshold values
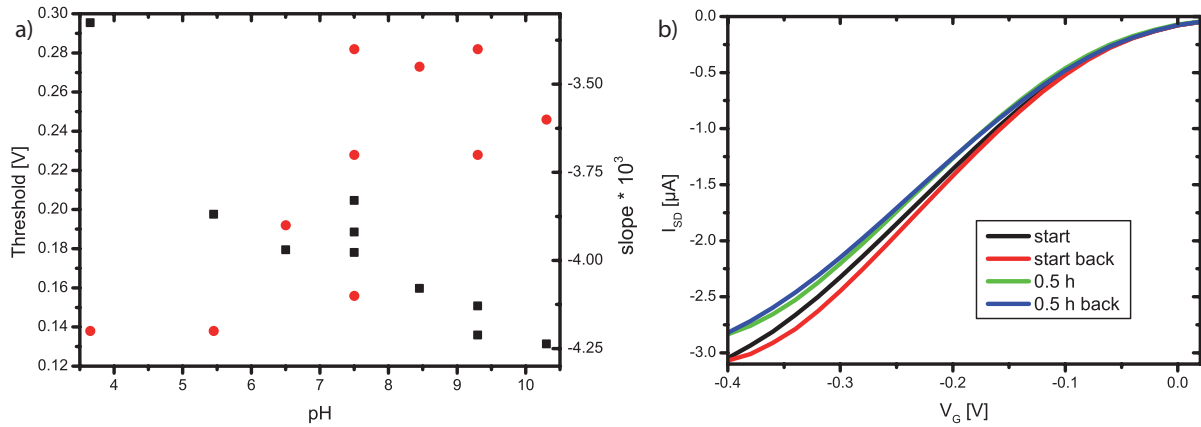
Figure 3.6: *a) pH dependence of the threshold voltage (black squares) and slope (red circles) on the pH value in solution. The slope change could be connected to the limited stability OFET characteristics instead of pH. b) Shift in OFET transconductance curves as measured after 0.5 h of operation.*

with pH of the buffer solution. The threshold shift is dominated by the potential dependence of the electrode; both, the semiconductor and the gate electrode interface can have chemical groups, which get recharged upon pH-change. DNTT is relatively stable and chemically inert, while Pt-interfaces are known to display potential shifts like the ones observed here.[67] In difference to the situation with urease attached, the slope of the OFET is nearly constant during the measurement. The slope change indicates only minor chemical doping or problems with parameters extraction.[4]

Some problems related to all measurements of directly solution gated OFETs in solutions of physiological strength is the stability of the OFET characteristics.[146] Also for the here reported OFETs such a drift is visible (see Fig. 3.6 b)). Here, the 3D morphology of the organic semiconductor film has negative impact,[142] since it increases the surface-to-volume ratio and has many grain boundaries. Regarding the stability, improvements are expected upon application of a encapsulation layer, such as the previously presented thin parylene-C layers[3] or lipid bilayer membranes.[146]

3.2.5   AMMONIA DETECTION

Ammonia detection was tested with the SU-8 dielectric OFETs.[4] Tests were performed with directly solution gated OFETs as well as parylene encapsulated ones. For the directly solution gated samples, the response time was ca. 2 s in the optimized case. Similar results were obtained with solution gated OFETs on parylene-substrates. A slower response with a higher residual current saturation was observed with different processing chemicals used.[4] For the encapsulated samples, the diffusion time had two different current response timescales. First, a fast component as in the solution gated case. Second, a slow response component was observed, which reproduced the results from the previous study on urea detection on diffusion.[3] The decrease in current could be fitted with equation 3.3 and gave a comparable effective dif-
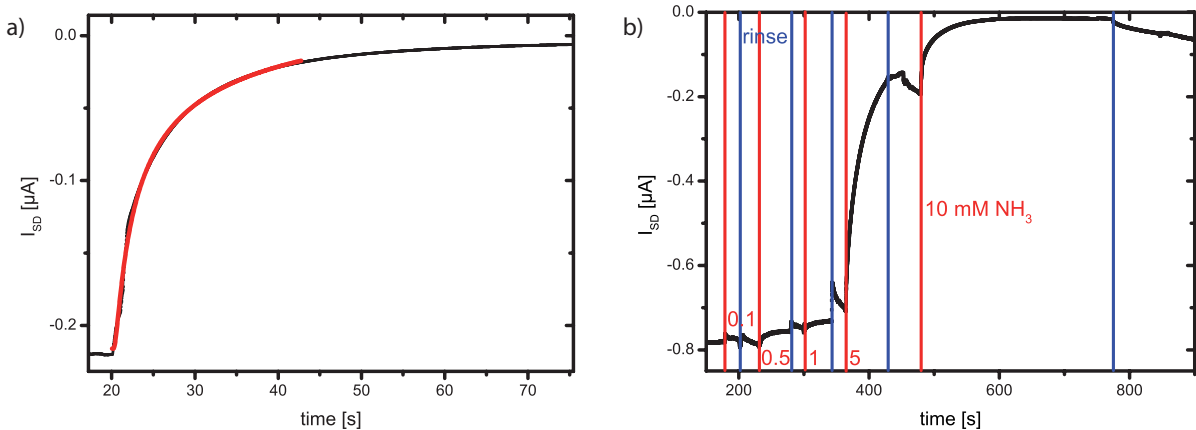
Figure 3.7: *a) Transient response to 10 mM NH$_3$ of a parylene-N capped OFET. b) Transient recording of current responses to consequent ammonia exposures of a OFET as in a).*

fusion constant as in the previous study.[3]

Here, the Volmer-Weber growth gives rise to a high surface to volume ratio and many grain boundaries, which increase adsorption type interactions.[138] Related, the semiconductor film morphology also offers many pathways for diffusion and decreases diffusion distance for effects in the channel.[86] Thus, independent on the precise interaction type, the film morphology yields improved ammonia response. A similar morphology driven enhancement of ammonia response has recently been reported.[137] If an encapsulation is used, the thickness of the encapsulation sets the diffusion distance and is thus another parameter for optimization.[4] Corresponding to this finding, a parylene-N layer thinner than the previously used parylene-C layers deposited onto DNTT based OFETs gave rise to a reduced response time of 20 s (see Fig. 3.7 a)). However, the thickness of the parylene-N layer on the DNTT could not be measured with sufficient accuracy to extract the diffusion time. These encapsulation layer also enabled recording the injection of 0.5 mM NH$_3$, due to the stabilization of the OFET current versus drift (see Fig. 3.7 b)). However, in line with the earlier findings,[1] these parylene-N encapsulation layers supported only a limited time of operation of a few hours at best, which is not sufficient to apply these layers for measurement series.

Further, the morphologies, which give faster response times, are typically correlated to higher sensitivity.[86] This can be qualitatively understood by the fact that faster response is bound to more interaction site or easier access of molecules to interaction sites. In order to test this, OFET response was recorded for different ammonia exposures. Indeed, unambiguous response can be recorded for ammonia exposures ($\leq 0.5\,mM\,NH_3$), which are smaller than for the previous architecture ($1\,mM\,NH_3$).[3] However, limited stability of the OFET characteristics poses at the moment the boundary condition for sensitivity. This could be addressed in the future by better encapsulation layers, different organic semiconductors, and more refined OFET fabrication protocols.

CONCLUSION AND OUTLOOK

In this work, parylenes were demonstrated as feasible substrates and dielectrics for fabrication of micro-patterned, mechanical flexible OFETs. Such OFETs could be operated in solution.[1] Further, sub-monolayer percolation of pentacene in OFETs on the rough parylene dielectrics was observed and the subsequent evolution of the OFET performance evaluated.[2] These projects set the stage for the application of such OFETs for urea detection. Urease was co-valently bound to the OFET and physiological urea concentrations in buffer solutions were detected via the resultant ammonia.[3] Ammonia detection was interpreted as the diffusion of ammonia molecules from solution into or to the OFET channel. This detection was as in gas sensors, however with a slow response time due to slow diffusion pathways. Omitting the parylene-C dielectric layer gave rise to a improvement in response time of up to two orders on magnitude.[4] However, for stable OFET operation, an encapsulation layer is beneficial. A possible solution would be to use very thin encapsulation, e.g. lipid bilayers.[147] Another possibility to improve stability are organic semiconductors with ordered alkyl side chains at the semiconductor-electrolyte interface.[148] A DNTT derivative could be suitable here, such as C10-DNTT.[149]

Interestingly, the ammonia seems to remain in the DNTT layer after exposure in solution. The OFETs can be regenerated in vacuum and potentially in air, thus the ammonia is not covalently bound. Possibly, the holes in an OFET in operation give rise to a strong interaction with the ammonia. Here, it could be possible to drive regeneration by injection of (minority carrier) electrons into the channel.[52, 150] The interaction between ammonia and electrons would not be as favorable as with holes, and release of ammonia could be activated.

The demonstration of ammonia detection in solution via OFETs has several important implications. Ammonia detection can be the dominant detection signal, which relaxes the necessity of reference electrodes often employed in pH-sensitive transducers. Further, ammonia detection can be improved by applying knowledge gained from optimization of gas sensors. Since ammonia/ammonium is often a byproduct of enzymatic reactions,[60, 151] its presence can disturb the output of OFETs applied in biological environments. Interestingly, OECTs seem to be rather insensitive to this effect,[60] potentially due to their degenerative doping.
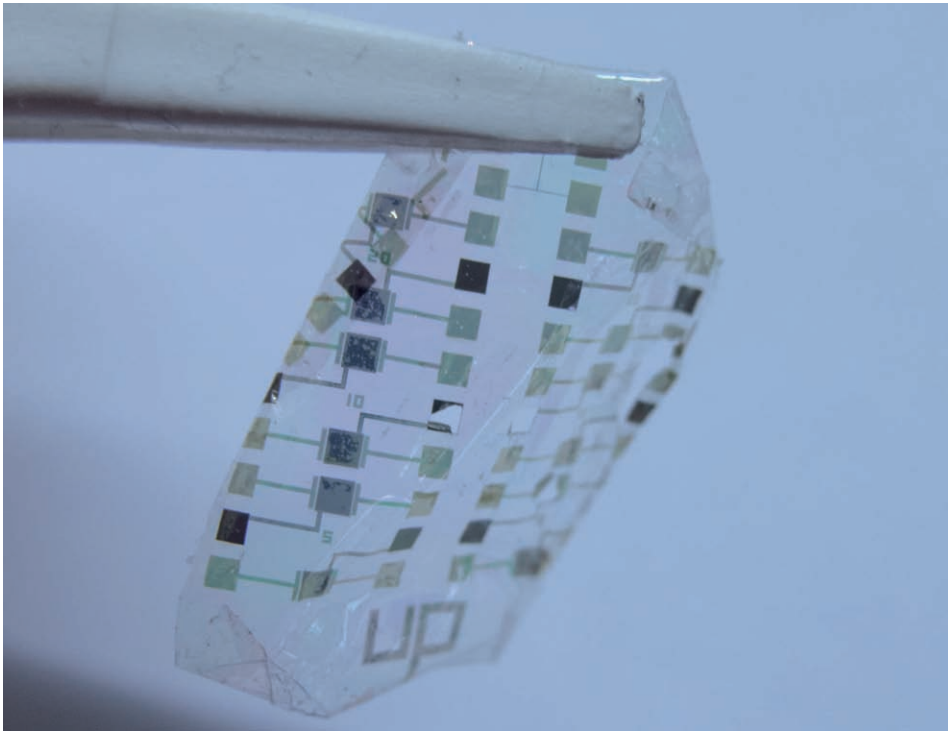
Figure 4.1: *Photograph of a OFET with a parylene-C foil substrate. The OFET architecture is the same as for the reported sensors.[3, 4]*

 Some enzymatic reactions, which produce ammonia, are involved in transport of neurotransmitters. Namely, glutamate and glutamine couple via a enzymatic pathway in neurotransmitter transport and neuronal excitation.[152] The ammonia waste of neurons has been determined to activate surrounding astrocytes.[152] If neurons and astrocytes are both present, their cooperative behavior modifies enzymatic activity.[153] Here, the developed ammonia detection scheme could be employed to monitor ammonia levels in conjunction with neuronal activity measurements. The parylene-C in contact with the neuronal tissue/cell culture have been demonstrated to be biocompatible in reports in the literature.[28] Furthermore, mechanical flexible OFET sensor configurations are possible (see Fig. 4.1), which can be adjusted to more complex sample environments than typical fluorescence microscopy.

Another neurotransmitter, nitric oxide has been reported to function as a switch for neuronal remodeling.[154] Interestingly, nitric oxide and nitric dioxide gas sensors based on OFETs have been developed for potential application in breath analysis.[155, 156] Consequently, it should be possible to extend the proposed ammonia detection in cellular signaling to other molecules. As a long term vision, the differential sensor arrays already realized for detection of several gases[157, 158] could be transferred to a system in solution. This would enable multi-analyte measurements in the same array with spatial resolution.

On SU-8 DNTT grows in Volmer-Weber instead of Stranski-Krastanov growth mode induced by the photolithography fabrication steps. For pentacene, this transition is typically associated with better charge transport as reported in the literature.[90][141] This improved charge transport is explained by a more dense morphology of the organic semiconductor grains.[159]

However, for Stranski-Krastanov growth only the first monolayers are reported to contribute to charge transport and these layers grow in a 2D layer-by-layer fashion.[160, 161] For SU-8 surfaces, it should be possible to change the growth mode by substrate temperature alone after correct surface treatment.[141] In future, this can be an interesting system to study the structural changes due to growth mode and link them to the charge transport properties.

Growth on dielectric interface becomes more difficult to study on rough dielectrics. Here, our In-Situ measurements revealed sub-monolayer percolation of pentacene thin films on parylene-C dielectrics. Furthermore, OFET formation was identical to the situation on smooth dielectrics. The used parylene-C dielectrics display a high surface roughness, however with a rather long spatial correlation length. This situation should be similar in many commercial available plastic foils, which also are expected to be applied in potential mass-production. Our results imply that knowledge from research on model systems with smooth dielectric surfaces can be directly transferred to these more practical substrates.

Appendix A

Publications

Overview Publications

[1] - **F. Werkmeister**, B. Nickel, *Towards flexible organic thin film transistors (OTFTs) for biosensing*, Journal of Materials Chemistry B, 2013.

[2] - **F. X. Werkmeister**[1], S. J. Noever[1], B. A. Nickel, *Sub-Monolayer Percolation of Pentacene on Rough Parylene-C Dielectrics*, Organic Electronics, 2015, [1](shared first authorship).

[3] - **F. X. Werkmeister**, T. Koide, B. A. Nickel, *Ammonia sensing for enzymatic urea detection with organic field effect transistors and a semipermeable membrane*, Journal of Materials Chemistry B, 2016.

[4] - **Franz X. Werkmeister**, Bert A. Nickel, *Fast detection of blood gases by solution gated organic field effect transistors*, Organic Electronics, 2016.

Following, the attached manuscripts appear in chronological order.

A.1   TOWARDS FLEXIBLE ORGANIC THIN FILM TRANSISTORS (OTFTs) FOR BIOSENSING

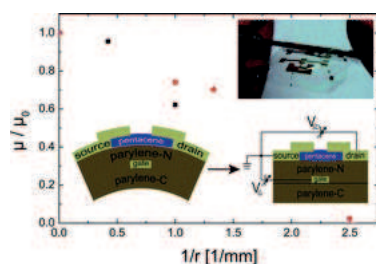Franz Werkmeister, Bert Nickel

Abstract

We have studied parylene-N and parylene-C for their use as substrates and gate dielectrics in OTFTs. Parylene-N films with a thickness of 300 nm show the required dielectric properties, as verified by breakthrough-voltage measurements. The surface roughness measured for 300 nm thick parylene-N films is 4-5 nm. However, initial growth of parylene depends on the subjacent surface. This results in different thicknesses on Au electrodes and substrate materials for thin films. Capping of micropatterned Au-electrodes with a thin Al layer via lift-off results in homogenous parylene film thickness on the whole sample surface. OTFTs are fabricated on glass with parylene-N as a gate dielectric and pentacene as a semiconductor. The electrodes are patterned by photolithography enabling micrometer sized features. The contact resistance is extracted by variation of the channel length. Modification of the parylene dielectric layer surface by plasma treatment with oxygen after deposition allows shifting of the threshold voltage to more positive values, however at the cost of increasing hysteresis. OTFTs fabricated on thin parylene-C films can be peeled off and could result in flexible devices employing parylene-C foil as a substrate. For a foil thickness of 3-4 μm, operational devices can be bent down to radii less than 1 mm, e.g. in the range of cannulas. Operation of such OTFTs with parylene-C as a gate dielectric in liquids is demonstrated. The OTFT current can be modulated by the potential in the electrolyte as well as by the bottom gate potential. This allows for application of such OTFTs as sensors in medical devices.

My Contribution

I produced the samples, performed the experiments and the data evaluation. Furthermore, I wrote the manuscript and designed the figures.

Table of contents graphic

Journal of
Materials Chemistry B

PAPER

Towards flexible organic thin film transistors (OTFTs) for biosensing

Franz Werkmeister and Bert Nickel*

We have studied parylene-N and parylene-C for their use as substrates and gate dielectrics in OTFTs. Parylene-N films with a thickness of 300 nm show the required dielectric properties, as verified by breakthrough-voltage measurements. The surface roughness measured for 300 nm thick parylene-N films is 4–5 nm. However, initial growth of parylene depends on the subjacent surface. This results in different thicknesses on Au electrodes and substrate materials for thin films. Capping of micro-patterned Au-electrodes with a thin Al layer *via* lift-off results in homogenous parylene film thickness on the whole sample surface. OTFTs are fabricated on glass with parylene-N as a gate dielectric and pentacene as a semiconductor. The electrodes are patterned by photolithography enabling micrometer sized features. The contact resistance is extracted by variation of the channel length. Modification of the parylene dielectric layer surface by plasma treatment with oxygen after deposition allows shifting of the threshold voltage to more positive values, however at the cost of increasing hysteresis. OTFTs fabricated on thin parylene-C films can be peeled off and could result in flexible devices employing parylene-C foil as a substrate. For a foil thickness of 3–4 μm, operational devices can be bent down to radii less than 1 mm, *e.g.* in the range of cannulas. Operation of such OTFTs with parylene-C as a gate dielectric in liquids is demonstrated. The OTFT current can be modulated by the potential in the electrolyte as well as by the bottom gate potential. This allows for application of such OTFTs as sensors in medical devices.

Introduction

Application of organic materials as active materials in sensors is an emerging field of research. Here, especially the possibility to choose biocompatible materials and to construct mechanical flexible devices allows us to potentially outperform the established inorganic semiconductor technology for practical applications, for example in medical applications.[1] The organic semiconductor pentacene is known to support the growth of neural networks, thus it can be considered biocompatible for at least several days.[2] Parylene, another commonly employed material in organic electronics, is FDA approved for implants. Furthermore, it offers good dielectric properties and can be deposited *via* chemical vapour deposition (CVD) at room temperature forming insulating layers for *e.g.* gate dielectrics. By careful choice of the employed materials biodegradable devices could be achieved.[3] The low energy cost for production is another advantage of organic materials.

A number of sensors utilising organic semiconductors have been demonstrated.[4] One architecture family is the organic electrochemical transistor (OECT), which can be used for enzymatic sensing[5] and barrier tissue evaluation.[6] The sensing relies on a dedoping mechanism of the active material. Another principle is based on the classical field effect transistor.[7] Here, charge carrier accumulation is controlled *via* a gate field. The accumulated charge carriers are transported through the channel *via* an additional source–drain voltage, resulting in an on-state current. Detection of targets relies on the shift of the threshold voltage induced by adsorption of charged particles or by changes of the chemical potential at the transistor–sample interface. These principles have been developed for CMOS technology,[8] and have also been successfully applied to other materials *e.g.* diamond.[9] Similarly, sensors of this type based on organic semiconductors are able to detect pH,[10] penicillin,[11] biotin,[12] trimethylamine[13] and DNA.[14,15] In the later case, the probes were covalently bound to the organic semiconductor, highlighting the advantage of easy ways to functionalise the sensor surface.[15] Another interesting approach is the formation of a lipid bilayer on the sensor, which allows the incorporation of biological receptors at the sensor surface.[16] In the line of sensors employing organic semiconductors, we demonstrated a transducer resembling the architecture of conventional double-gate thin film transistors (DGTFTs).[17] To realise this experiment, it was essential to identify tetratetracontane (TTC) as a top gate dielectric.[18]

Our transducers are able to detect the adsorption of fatty acids onto the sensor *via* a threshold-voltage shift both in top gate as well as in bottom gate sweeps. A main drawback of our

Ludwig-Maximilians-Universität München, Fakultät für Physik & CeNS, Geschwister-Scholl-Platz 1, 80539 München, Germany. E-mail: bert.nickel@physik. lmu.de

previous work is that it still utilises a silicon chip for the bottom gate and the bottom gate dielectric. Although tissue is soft, Si is brittle, so interfaces between biological samples and the sensor pose sources of inflammation due to mechanical stress.[19]

Furthermore, in setups with optical microscopes working in transmission, a transparent device is mandatory.

Here, we report our progress on the fabrication of flexible and micro-patterned OTFTs for biosensors based on pentacene as a organic semiconductor.

Experimental results

Parylene, a widely used dielectric in organic electronics,[20,21] is chosen as the dielectric. It offers many advantages, such as high dielectric strength, mechanical flexibility and good optical transparency. It can be easily deposited on glass slides for transparent devices. Peeled off, parylene itself can also serve as the substrate. This results in flexible devices, which are already used for fabrication of electrode arrays for *in vivo* recordings.[22] It has also been shown that one can conduct photolithography on parylene, which enables the fabrication of micro-patterned electrode structures on parylene.[23]

Growth study of parylene

The gate dielectric is a critical part of the device;[24] here, thin films with good dielectric properties are required.[25] Consequently the dielectric materials, namely two variants of parylene, parylene-N and parylene-C, are studied first. Both are deposited *via* CVD at temperatures ranging from 8 °C to 15 °C.

A capacitor structure with an area of 2 mm × 2 mm and the dielectric layer in between Au electrodes was used to test for stability against breakthrough due to the applied voltages. The parylene film thickness was evaluated with a DekTak 6M. Parylene-N films of a thickness of 400 nm withstand an applied voltage of at least 60 V. Working OTFTs can be fabricated with dielectric layers from 300 nm onwards. In contrast, parylene-C films of a thickness of 600 nm withstand only 20 V or less. Thus parylene-N was chosen, since it allows for thinner dielectric layers.

A surface roughness (rms) of less than 1 nm is preferable for the preferred pentacene thin-film phase growth. Thus parylene-N and -C films are evaluated for their surface roughness using a Veeco Dimension 3100 AFM. The AFM micrographs were evaluated using the WSxM software.[26] For parylene-N, a surface roughness of 4–6 nm is typical for a 300 nm thick film.

Evaluation of the dielectric layer surfaces by AFM shows that the thickness of the parylene-N layer is significantly lower on the Au electrodes than on the surrounding parylene substrate (see Fig. 1). The same result is observed for different substrates like borosilicate-glass or silicon-oxide. Since the Au electrodes are higher than the surrounding substrate surface, one would expect the parylene surface to appear higher on the Au electrodes than on the substrate. This is in contrast to the measured lower height on the Au electrodes. Once 6 nm of Al is evaporated on top of a 25 nm Au electrode, patterned by photolithography, the grown parylene film is homogenous on the whole sample.
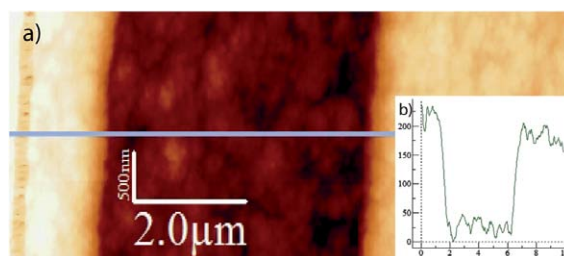

Fig. 1 Parylene-N on Au. (a) AFM micrograph of parylene-N grown on a 4 µm Au electrode on silicon dioxide. (b) Height profile extracted from the line indicated in (a).

Such parylene-N films are employed as gate dielectrics for the fabrication of OTFTs.

OTFT fabrication and characterisation

OTFTs are fabricated on thin parylene-C foils as well as on glass slides. The later offer a smooth substrate surface, which is beneficial for AFM studies. Furthermore, some OTFTs are fabricated with electrodes defined by shadow masks and photolithography. While photolithography allows for micro-patterned electrode structures, shadow masks have restrictions in feature size and obtained structures. However, patterning by shadow masks is a solvent free process and it features faster fabrication compared to photolithography.

The substrates (glass slides) are cleaned in acetone, iso-propanol and purified water in an ultrasound bath for 10 min each. For flexible device configurations, a parylene-C (Plasma-Parylene Systems GmbH) layer with a thickness of 2–4 µm is deposited onto glass substrates *via* CVD in a home-built CVD-chamber (Fig. 2a I). For the gate, 30 nm of Au and 6 nm of Al are deposited using an e-beam UHV evaporation system. The gate is patterned either by a lift-off process (II) or by evaporation through a shadow mask. For micro-patterned gates, the Al-capping ensures homogenous parylene film growth on the whole sample surface. A 3 nm Ti sticking layer is added for samples produced directly on the glass slides. Parylene-N is deposited to a thickness of 400 nm as a gate dielectric (III). For micro-patterned OTFTs, 30 nm of Au is patterned as the source and drain electrodes *via* a subsequent lift-off process (IV). This is followed by the deposition of 30 nm of pentacene (Sigma Aldrich, triple sublimed grade) (V). This results in micro-patterned, bottom contact OTFTs. Alternatively, 30 nm of pentacene is deposited first, and the source and drain electrodes (30 nm of Au) are evaporated through a shadow mask (see Fig. 2b). This way, top contact OTFTs are fabricated.

The OTFTs are measured under ambient conditions employing a Keithley 2612 Source Measure Unit. In general, they show saturation mobility on the order of 10^{-3} cm^2 V^{-1} s^{-1}, extracted from the slope of the square root of the current *versus* the gate voltage in the saturation regime. Since the saturation mobility is directly proportional to the current, it must be as high as possible for good signal strength. Among different devices the threshold voltage varies from 0 V to −15 V. The
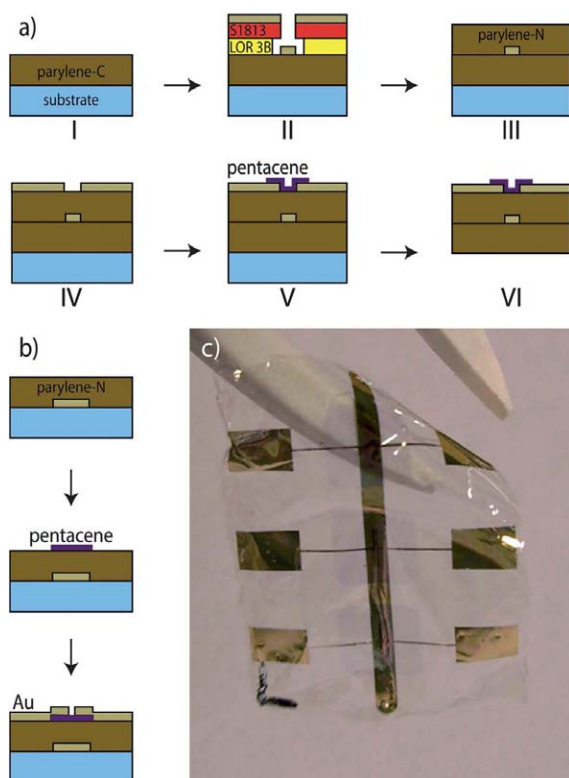
Fig. 2 Fabrication pathways. (a) Processing steps for bottom contact OTFTs with electrode structures patterned by photolithography. For the lift-off process a bilayer photoresist with LOR-3B and S1813G2 was spun onto the samples. (b) Processing steps for the production of top contact OTFTs. (c) Photograph of three top contact OTFTs fabricated on a thin parylene-C foil.

Fig. 3 Transistor characteristics. (a) Gate sweeps of a transistor fabricated on a thin parylene-C foil. The black (squares) and red (circles) lines are the forward and backward sweeps before taking the OTFT off the rigid support, the blue and magenta ones are the corresponding sweeps of the flexible device after peeling off. The black curves belonging to the logarithmic scale give the situation before the peel off. (b) Source–drain voltage sweeps of the transistor in the rigid situation.

threshold voltage should be close to 0 V, because the threshold voltage has to be compensated by the voltage applied to the bottom gate in our DGTFT sensors. This was achieved in some devices. For the previously demonstrated Si-oxide based transducers, the threshold voltage was always more negative with values between −14 V and −30 V.[17] The hysteresis can be as small as 1 V ranging up to 10 V. A typical device example is given in Fig. 3. The threshold voltage can be moved towards positive threshold voltages by modifying the parylene surface with oxygen groups. We use an oxygen plasma treatment, which replaces the previously reported UV-treatment.[28] The samples are subjected to an oxygen plasma treatment in a LabAsh 100 at 2 torr oxygen pressure and 53 W incident power before deposition of pentacene. An increasing shift of the threshold voltage towards more positive voltages with increasing treatment times is observed. However, any plasma treatment increases the hysteresis (see Table 1).

When different channel lengths are fabricated in one step, one can extract the contact resistance. The contact resistance can limit the current through the channel resulting in a lower saturation mobility of the device. For the electrode structures, patterned by photolithography, different channel lengths at a co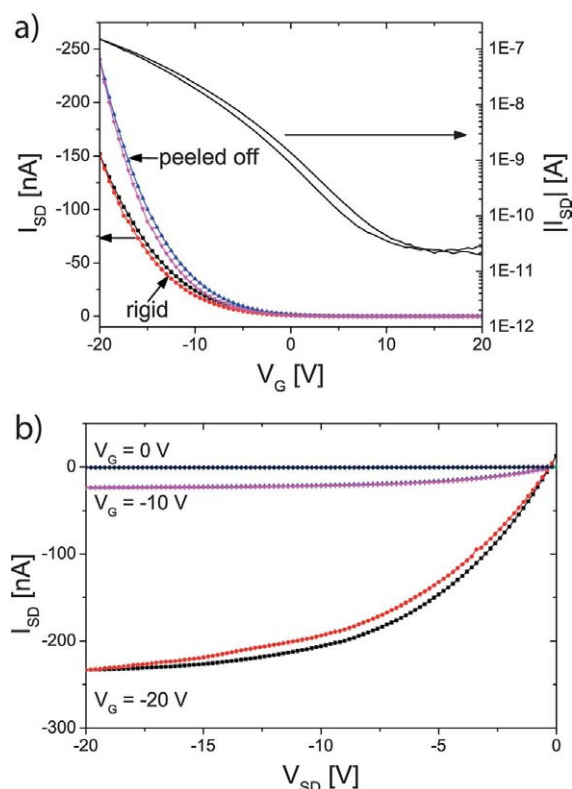nstant channel width of 1 mm are realised. 10 μm, 6 μm, 4 μm and 2 μm are chosen as channel lengths. These dimensions allow for a high number of individual sensors on a small area. The resistance for the different channel lengths can be obtained from the linear slopes of the conductance in source–drain

Table 1 Threshold voltage shift upon functionalisation of the dielectric surface by an oxygen plasma treatment (before deposition of the pentacene). The threshold voltage is extracted from the backward sweeps at a source–drain voltage of −20 V and a gate voltage of up to −32 V. The extracted data for two batches are shown. On parylene-N, hole mobilities of pentacene of 0.55 cm^2 V^{-1} s^{-1} have been reported, which have been measured at higher voltages[27]

Treatment time [s]	Saturation mobility [cm^2 V^{-1} s^{-1}]	Threshold voltage [V]	Hysteresis [V]
0	1.3×10^{-3}	−4.0	7.1
3	0.2×10^{-3}	−1.8	22.0
6	1.3×10^{-3}	2.7	20.8
9	1.6×10^{-3}	7.9	11.3
0	8.8×10^{-4}	−1.3	2.6
2	9.1×10^{-4}	9.5	17.0
4	1.9×10^{-4}	3.7	19.3
6	2.2×10^{-4}	7.3	22.0

voltage sweeps. Extrapolation to zero channel length allows us to obtain the contact resistance.[29] This results in a contact resistance of 3 GΩ for a 1 mm wide channel. A pronounced nonlinearity at low source–drain voltages is observed (see Fig. 4).

For the flexible configuration the finished devices produced on a parylene-C film are placed in a water bath. After soaking for 1 to 3 hours, the adhesion of the parylene films is reduced and the OTFTs are peeled off (Fig. 2a VI and c).

The electrical characteristics are recorded before and after they were stripped off their rigid support. All device characteristics change after the transistor is peeled off the rigid support, presumably due to the mechanical stress. Remarkably, in some cases some or all of the figures of merit are better after the transistor is peeled off. For the OTFT shown in Fig. 3, the saturation mobility increased from 7×10^{-3} cm^2 V^{-1} s^{-1} to 1×10^{-2} cm^2 V^{-1} s^{-1}, when the OTFT was peeled off.

Once the devices are bent to a radius of a few mm, a decrease of the electrical properties can be observed. In terms of saturation mobility the transistors retain above 60% of their original performance for a bending radius of 1 mm. For a sample of a thickness of 3 μm, the transistor can be bent around a cannula with a radius of 800 μm, still showing transistor behaviour at a decreased performance afterwards. In contrast, if wrapped around a cannula with a radius of 400 μm, the transistor still shows an on- and off-state, but the electrical characteristics of a gate sweep deviate from the standard curve. Thus, one can expect the devices to stay operational if wrapped around a cannula with a radius of 800 μm (see Fig. 5). This would allow for the intended use in medical treatment, for example for medication triggered by transducer signals.

To demonstrate that such a device will be applicable as a biosensor, operation with the OTFT channel immersed in 10 mM PBS buffer is tested. While in initial tests the parylene-N layers have shown good dielectric properties immersed in electrolytes, the parylene-N layer is found to have an insufficient reliability in longer measurements. Thus we use parylene-C as the dielectric for the sensing devices. While the film thickness
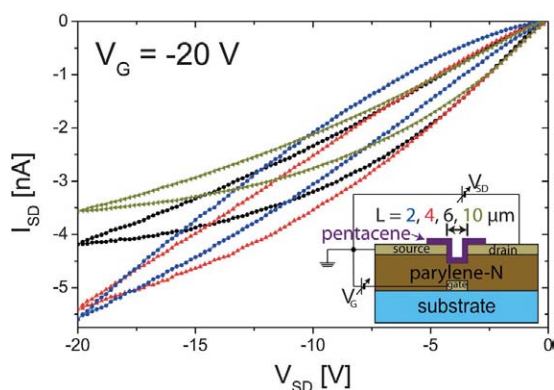

Fig. 5 Bending of the flexible transistors. Decrease of the saturation mobility after bending the OTFT to small radii. The inset shows an OTFT wrapped around a cannula.

of the dielectric layer has to be increased with respect to parylene-N, the results of processing and OTFT performance can be transferred. A 2 μm thick parylene-C layer serves as the bottom gate dielectric. To cap the source and drain contacts, a photoresist with good dielectric properties (S1813G2) is spun onto the finished micro-patterned OTFTs and baked at 120 °C for 10 min. It is patterned using photolithography, such that only the channel region is reopened again. A layer of 50 nm of TTC is deposited on the top. This leaves the pentacene in the channel region capped with 50 nm of TTC.

A droplet of 10 mM PBS buffer (degassed) is put on the transistor and is brought into contact with a Pt–Ir wire, which is glowed out with a Bunsen burner before the measurement. Gate sweeps with both bottom and top gate are performed at different fixed potentials of the other electrode. The

Fig. 4 Source–drain voltage sweeps for different channel lengths. The curves are colored in blue (circles) for the 2 μm, in red (upward facing triangles) for the 4 μm, in black (squares) for the 6 μm and in yellow (sideward facing triangles) for the 10 μm long channel.
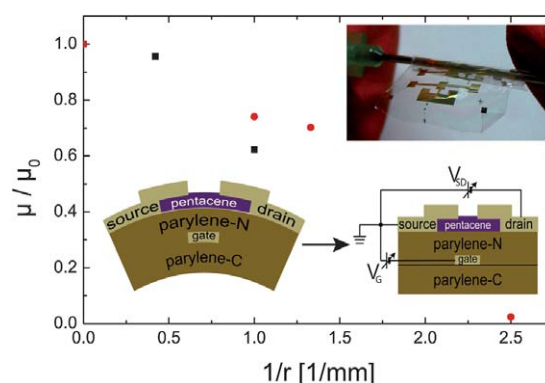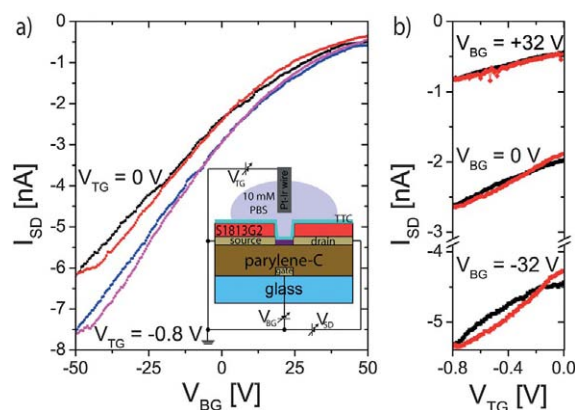

Fig. 6 Transistor operation in 10 mM PBS buffer solution. (a) Bottom gate sweeps at fixed top gate potential. For a more negative top gate potential, additional charge carriers are accumulated, resulting in an increase in the current. (b) Top gate sweeps at fixed bottom gate potential. The response of the top gate is modulated by the bottom gate. For positive bottom gate potentials, the semiconductor gets more depleted reducing the response to the top gate voltage and conversely for more negative bottom gate voltages. Thus, the sensitivity of the device can be tuned by the bottom gate.

source–drain voltage is set to −0.6 V. The leakage current through the bottom gate dielectric is negligible and for the top gate dielectric, the source–drain current is corrected for the gate leakage current, as previously reported.[17] The transistors can be measured several hours, until finally breakdown of the top gate dielectric occurs.

The transistor current can be clearly modulated by the bottom as well as the top gate potential (see Fig. 6). The extracted transconductance from the bottom gate sweeps is 4.0×10^{-11} A V^{-1}, 8.0×10^{-11} A V^{-1} and 9.0×10^{-11} A V^{-1} for +32 V, 0 V and −32 V bottom gate potential, respectively. For the top gate it is 4.5×10^{-10} A V^{-1}, 8.0×10^{-10} A V^{-1} and 10.0×10^{-10} A V^{-1} at +32 V, 0 V and −32 V bottom gate potential, respectively. The ratio of the top gate to the bottom gate transconductance calculated from these values is *ca.* 11.

Discussion

The disturbed growth of parylene films on the bare Au electrodes gives rise to sharp flanks at the rims of the underlying electrodes at least for thin films. This distorted growth of parylene on certain metals is described in the literature. Inhibition of parylene growth on Au seems to be dependent on the precise Au surface, since inhibition has not been reported in at least one case.[30] A capping of the Au electrode surface with a thin Al layer gives rise to homogenous parylene film growth on the whole sample surface for micro-patterned devices. For thin dielectric layers (300 nm), the thin Al top layer in the micro-patterned gate electrode is necessary to avoid the distorted parylene growth on the gate. For thicker layers (μm), these deviations may not be relevant.

The shift of the threshold voltage to more positive values and increase of the hysteresis due to the addition of oxygen groups to the surface are established effects.[28] The oxygen plasma treatment instead of UV-ozone assisted reactions may further roughen the surface in comparison. Since parylene is known to degrade under UV irradiation, the plasma approach may be more gentle, since the UV degradation weakens the dielectric properties of parylene.[31] Both treatments can also be used as a starting step for introducing functionality to the surface.[32]

The contact resistance of 3 GΩ extracted for our devices is high in comparison with values found in the literature. While contact resistance is reported to decrease with increasing gate voltages,[29] this may not be feasible in every application. A Schottky barrier can give rise to the observed nonlinearity in conductance at low source–drain voltages. Also trap states may give rise to such effects.[33] A decrease can be expected if the electrode surface is treated with a functional layer.[34,35]

When the transistors are peeled off, some devices improve while some degrade. This is encouraging since it indicates that a controlled peel-off process may result in devices as good as on solid support. The mechanism that changes the performance is complex and may range from loss of material up to strain induced phase transitions.[36]

Degradation of OTFTs at controlled bending radii is a well-known effect, which is attributed to the displacement of molecules within the thin film.[37] The degradation can be averted if the organic semiconductor is placed in a neutral strain position. This reduces the strain acting on the thin film.[38] However, this may not be possible in sensor applications. Here, the organic semiconductor is separated from the test sample only by a thin capping layer, or it is even in direct contact with the sample.

In liquids, the OTFTs show stable performance for several cycles and the gate leakage current in the case of the bottom gate dielectric is negligible. The transconductance extracted for the sweep of the bottom and the top gate at +32 V, 0 V and −32 V differ by a factor of 11. The expected factor is given by the ratio of the capacitances of the top-gate dielectric (50 nm of TTC; ε_r = 1.3) and the bottom gate dielectric (2 μm parylene-C; ε_r = 2.95). This ratio is calculated to $C_{TTC}/C_{parylene-C} = 17.7$ and fits reasonably well to the extracted ratio of the top- and bottom-gate's transconductances, as deduced from the theory of DGTFTs. The modulation of the current by the top gate is the principle of our sensor mechanism.[17]

Conclusions

The use of parylene as a substrate and dielectric enables the production of flexible OTFTs of just a few μm thickness. The electrodes can be micro-patterned by lift-off, which is a parallelisable technique that allows for high throughput processing. The materials utilized in production of the devices are all biocompatible. This is mandatory for interfacing with tissue. Especially the possibility of wrapping the OTFTs around cannulas, with the transistors staying operational, already shows possible future applications. The processes involved in the change of the device characteristics upon taking the OTFTs off the rigid support are certainly worth further attention. Operation of such devices fabricated on glass in PBS buffer solution is demonstrated. This further points to future applications of such devices as biosensors. The presented devices serve as the starting point for our ongoing work to realise flexible and optical transparent biosensors.

Acknowledgements

Notes and references

1 M. Muskovich and C. J. Bettinger, *Adv. Healthcare Mater.*, 2012, **1**, 248–266.

2 E. Bystrenova, M. Jelitai, I. Tonazzini, A. N. Lazar, M. Huth, P. Stoliar, C. Dionigi, M. G. Cacace, B. Nickel, E. Madarasz and F. Biscarini, *Adv. Funct. Mater.*, 2008, **18**, 1751–1756.

3 M. Irimia-Vladu, N. S. Sariciftci and S. Bauer, *J. Mater. Chem.*, 2011, **21**, 1350–1361.

4 L. Kergoat, B. Piro, M. Berggren, G. Horowitz and M. C. Pham, *Anal. Bioanal. Chem.*, 2012, **402**, 1813–1826.

3834 | *J. Mater. Chem. B*, 2013, **1**, 3830–3835

This journal is © The Royal Society of Chemistry 2013

5 D. A. Bernards, D. J. Macaya, M. Nikolou, J. A. DeFranco, S. Takamatsu and G. G. Malliaras, *J. Mater. Chem.*, 2008, **18**, 116–120.

6 L. H. Jimison, S. A. Tria, D. Khodagholy, M. Gurfinkel, E. Lanzarini, A. Hama, G. G. Malliaras and R. M. Owens, *Adv. Mater.*, 2012, **24**, 5919–5923.

7 G. Horowitz, *Adv. Mater.*, 1998, **10**, 365–377.

8 A. Lambacher, M. Jenkner, M. Merz, B. Eversmann, R. A. Kaul, F. Hofmann, R. Thewes and P. Fromherz, *Appl. Phys. A: Mater. Sci. Process.*, 2004, **79**, 1607–1611.

9 M. Dankerl, M. V. Hauf, M. Stutzmann and J. A. Garrido, *Phys. Status Solidi A*, 2012, **209**, 1631–1642.

10 F. Buth, D. Kumar, M. Stutzmann and J. A. Garrido, *Appl. Phys. Lett.*, 2011, **98**, 153302.

11 F. Buth, A. Donner, M. Sachsenhauser, M. Stutzmann and J. A. Garrido, *Adv. Mater.*, 2012, **24**, 4511–4517.

12 H. U. Khan, M. E. Roberts, W. Knoll and Z. A. Bao, *Chem. Mater.*, 2011, **23**, 1946–1953.

13 A. K. Diallo, J. Tardy, Z. Q. Zhang, F. Bessueille, N. Jaffrezic-Renault and M. Lemiti, *Appl. Phys. Lett.*, 2009, **94**, 263302.

14 S. Lai, M. Demelas, G. Casula, P. Cosseddu, M. Barbaro and A. Bonfiglio, *Adv. Mater.*, 2013, **25**, 103–107.

15 L. Kergoat, B. Piro, M. Berggren, M. C. Pham, A. Yassar and G. Horowitz, *Org. Electron.*, 2012, **13**, 1–6.

16 M. Magliulo, A. Mallardi, M. Y. Mulla, S. Cotrone, B. R. Pistillo, P. Favia, I. Vikholm-Lundin, G. Palazzo and L. Torsi, *Adv. Mater.*, 2013, 2090–2094.

17 M. Göllner, G. Glasbrenner and B. Nickel, *Electroanalysis*, 2012, **24**, 214–218.

18 M. Göllner, M. Huth and B. Nickel, *Adv. Mater.*, 2010, **22**, 4350–4354.

19 P. Klimach, A. Richter, S. Danner, C. Kruse, V. Tronnier and U. G. Hofmann, *Biomed. Tech.*, 2012, **57**(suppl. 1), 481–484.

20 A. F. Stassen, R. W. I. de Boer, N. N. Iosad and A. F. Morpurgo, *Appl. Phys. Lett.*, 2004, **85**, 3899–3901.

21 Y. Kubozono, S. Haas, W. L. Kalb, P. Joris, F. Meng, A. Fujiwara and B. Batlogg, *Appl. Phys. Lett.*, 2008, **93**, 033316.

22 D. Khodagholy, T. Doublet, M. Gurfinkel, P. Quilichini, E. Ismailova, P. Leleux, T. Herve, S. Sanaur, C. Bernard and G. G. Malliaras, *Adv. Mater.*, 2011, **23**, H268–H272.

23 D. Khodagholy, M. Gurfinkel, E. Stavrinidou, P. Leleux, T. Herve, S. Sanaur and G. G. Malliaras, *Appl. Phys. Lett.*, 2011, **99**, 163304.

24 D. Knipp, P. Kumar, A. R. Völkel and R. A. Street, *Synth. Met.*, 2005, **155**, 485–489.

25 A. Facchetti, M. H. Yoon and T. J. Marks, *Adv. Mater.*, 2005, **17**, 1705–1725.

26 I. Horcas, R. Fernandez, J. M. Gomez-Rodriguez, J. Colchero, J. Gomez-Herrero and A. M. Baro, *Rev. Sci. Instrum.*, 2007, **78**, 013705.

27 T. Yasuda, K. Fujita, H. Nakashima and T. Tsutsui, *Jpn. J. Appl. Phys., Part 1*, 2003, **42**, 6614–6618.

28 A. Wang, I. Kymissis, V. Bulovic and A. I. Akinwande, *Appl. Phys. Lett.*, 2006, **89**, 112109.

29 D. J. Gundlach, L. Zhou, J. A. Nichols, T. N. Jackson, P. V. Necliudov and M. S. Shur, *J. Appl. Phys.*, 2006, **100**, 024509.

30 H. Y. Chen, J. H. Lai, X. Jiang and J. Lahann, *Adv. Mater.*, 2008, **20**, 3474–3480.

31 J. B. Fortin and T. M. Lu, *Thin Solid Films*, 2001, **397**, 223–228.

32 K. Länge, S. Grimm and M. Rapp, *Sens. Actuators, B*, 2007, **125**, 441–446.

33 S. Scheinert and G. Paasch, *Phys. Status Solidi A*, 2004, **201**, 1263–1301.

34 R. Winter, M. S. Hammer, C. Deibel and J. Pflaum, *Appl. Phys. Lett.*, 2009, **95**, 263313.

35 C. L. Fan, T. H. Yang and P. C. Chiu, *Appl. Phys. Lett.*, 2010, **97**, 143306.

36 C. Yang, J. Yoon, S. H. Kim, K. Hong, D. S. Chung, K. Heo, C. E. Park and M. Ree, *Appl. Phys. Lett.*, 2008, **92**, 243305.

37 T. Sekitani, Y. Kato, S. Iba, H. Shinaoka, T. Someya, T. Sakurai and S. Takagi, *Appl. Phys. Lett.*, 2005, **86**, 073511.

38 T. Sekitani, S. Iba, Y. Kato, Y. Noguchi, T. Someya and T. Sakurai, *Appl. Phys. Lett.*, 2005, **87**, 173502.

A.2 SUB-MONOLAYER PERCOLATION OF PENTACENE ON ROUGH PARYLENE-C DIELECTRICS

Franz X. Werkmeister[1], Simon J. Noever[1], Bert A. Nickel
Organic Electronics 2015, Vol. 26, 439-442 [2]
DOI: 10.1016/j.orgel.2015.08.009

[1]These authors contributed equally.

Abstract

We determine the evolution of electrical characteristics of pentacene transistors on rough parylene-C substrates during the physical vapor deposition of pentacene. Here, the changing field effect transistor characteristics are recorded in real time. The root mean square (rms) roughness of the parylene-C dielectric is 7 nm, which is much larger than the size of the pentacene molecule (1.5 nm). In spite of this huge roughness, we observe a source-drain current before nominal film thickness of a monolayer equivalent, i.e. pentacene is able to percolate for sub-monolayers, as in the case for very smooth substrates. This suggests that the pentacene film is able to conformally cover the rough substrate.

My Contribution

I prepared the transistor substrates with the parylene-C dielectrics. Further, Simon Noever and myself carried out all experiments on the parylene-C samples together. I wrote the manuscript draft and contributed significantly to the preparation of the final manuscript.

Table of contents graphic
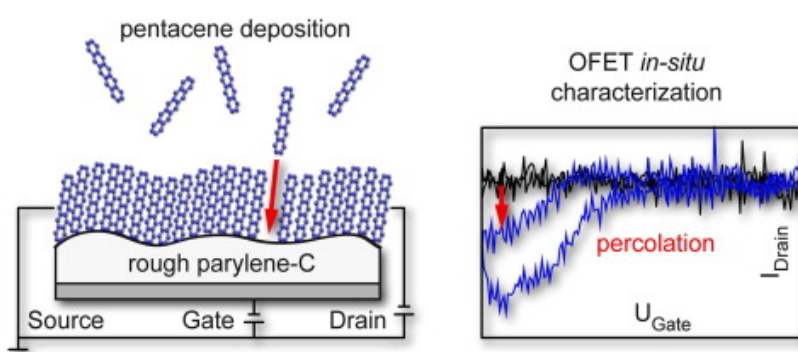
Contents lists available at ScienceDirect

Organic Electronics

journal homepage: www.elsevier.com/locate/orgel

Sub-monolayer percolation of pentacene on rough parylene-C dielectrics

CrossMark

Franz X. Werkmeister [a,1], Simon J. Noever [a,b,1], Bert A. Nickel [a,b,*]

[a] *Fakultät für Physik & CeNS, Ludwig-Maximilians-Universität München, Munich D-80539, Germany*
[b] *Nanosystems Initiative Munich (NIM), D-80799 Munich, Germany*

ARTICLE INFO

ABSTRACT

We determine the evolution of electrical characteristics of pentacene transistors on rough parylene-C substrates during the physical vapor deposition of pentacene. Here, the changing field effect transistor characteristics are recorded in real time. The root mean square (rms) roughness of the parylene-C dielectric is 7 nm, which is much larger than the size of the pentacene molecule (1.5 nm). In spite of this huge roughness, we observe a source-drain current before nominal film thickness of a monolayer equivalent, i. e. pentacene is able to percolate for sub-monolayers, as in the case for very smooth substrates. This suggests that the pentacene film is able to conformally cover the rough substrate.

© 2015 Published by Elsevier B.V.

1. Introduction

In organic electronics, it is well known that the gate dielectric has a huge influence on the growth mode of semiconducting thin films and on device performance [1]. Consequently, organic semiconductor film formation has been studied extensively for a large number of gate dielectric materials [2,3]. In this context, the role of surface roughness of the dielectric is not very clear. Rough dielectric surfaces often impair the performance of organic transistors; this has been observed for inorganic [4] as well as organic dielectrics [5]. However, some studies also report that increasing roughness does not degrade transport properties [6]. Resolving these conflicting reports is of special interest from a technological point of view, since utilizing rough substrates holds various industrial benefits like the lack of need for smoothing- and contact adhesion layers [7]. Most authors report the rms roughness σ, i.e. the variance of the height fluctuations, to quantify the corrugation of surfaces. Strictly speaking, this rms roughness describes the height variations between two surface positions in the limit of large lateral separation R. However, height changes occurring at larger lateral length scale (e.g. waviness) have been found not to impair device performance, in contrast to those at short lateral length scale [8]. The explanation for this very likely originates in the growth mode of the first molecular layers of the semiconducting layer. Typically, transistor performance is investigated for complete devices with rather thick films. However, the charge carrying layer is situated at the dielectric – semiconductor interface within the first few monolayers [9]. Optimization of organic transistors is therefore strongly dependent on insight on early stage thin film formation. Experimental evaluation of such thin layers via AFM is limited by tip quality and tip size and therefore is restricted to feature sizes of several nm up to microns [10,11]. Diffuse X-ray scattering techniques on the other hand allow to study lateral height variations from Angstroms to nm scale [12]. However, most studies focus on surface roughening of films with increasing thickness rather than roughness of ultrathin films on a rough substrate [10]. Especially, sub-monolayer studies of organic semiconductor thin film growth are generally restricted to smooth surfaces such as SiO_2 [13].

A second aspect of the evolution of a conduction channel is, that some organic semiconductors form a non conductive dead layer in presence of highly disturbed electrostatic landscapes [14]. This disturbance can be effected by a rough topography or open binding sites on the dielectric surfaces. In that case the onset of charge transport is delayed. To gain insight into the percolation behavior of semiconducting thin films and thereby the formation of active layers in deposition grown electronic devices, it is advantageous to measure percolation by the onset of device performance.

Here, we explore the influence of the roughness of chemical vapor deposition (CVD) grown parylene-C on OFET performance. The roughness is intrinsic due to the CVD growth of parylene-C [15]. Parylene-C is an FDA approved polymer, which is heavily used as dielectric layer in sensors based on organic semiconductors [16,17]. Parylene, deposited as gate dielectric on organic single crystals, forms a trap free interface enabling record devices [18].

---

* Corresponding author at: Fakultät für Physik & CeNS, Ludwig-Maximilians-Universität München, Munich D-80539, Germany.
    E-mail address: nickel@lmu.de (B.A. Nickel).
[1] These authors contributed equally.

Furthermore, thin films deposited on parylene-C dielectrics, have resulted in high performance organic transistors [19]. Interestingly, intrinsic charge carrier mobility in pentacene thin films has been found to be as high as 20 cm^2/Vs, on parylene-N [20], which has a similarly rough surface as parylene-C.

Several studies address the morphology and crystallinity of pentacene film on parylene-C by X-ray diffraction [21], micro-Raman spectroscopy [22] and AFM studies [23]. These studies show crystallinity of pentacene films on rough parylene-C surfaces and a characteristic grainy, 3-D like morphology. However, no conclusions were presented about the nature of the first monolayers, which form the accumulation channel in field effect transistors [9].

The *in-situ* deposition experiment here provides experimental access to the growth behavior of the first few monolayers with sub-monolayer precision; we record trans-conductance characteristics of an OFET in real time during deposition of the active material [24,25]. The evolution of the electronic properties of the OFET could thus be studied in dependence of the nominal film thickness.

2. Experiment and discussion

In detail, bottom gate, bottom contact samples were prepared by depositing nominally 1.6 μm parylene-C as gate dielectric on a glass slide with an Au gate. Next, 30 nm of Au were patterned by shadow mask onto the parylene-C to yield source and drain contacts with a channel width W of 2 mm and a channel length L of 50 μm.

In the experiment, pentacene was deposited at a rate of ca. 0.01 nm/s onto the sample, which was held at room temperature. Before deposition, a gate sweep was recorded as baseline, then the sample was exposed to the molecular beam and gate sweeps were recorded continuously during the deposition (Fig. 1). The applied source drain voltage (V_{SD}) was held at −20 V for all shown transport measurements. The film thickness was recorded by a quartz crystal microbalance. The resulting dataset included the film thickness, applied gate voltage, and source-drain current for each voltage step in the gate sweeps. Each dataset was completed by the measured source-gate current, to probe for leakage currents through the dielectric, which however were within the noise limit.

The onset of the source-drain current is observed for a nominal pentacene thickness of 1.2 nm, i.e. below the equivalent of a complete monolayer. This onset and the corresponding baseline before deposition are shown in Fig. 1a. The corresponding gate currents after percolation (red curve in Fig. 1b) exhibits no deviation from the sweep prior to drain-current onset (black curve). To demonstrate the early stage evolution of the transistor characteristics, the first five gate voltage sweeps, i.e. *in-situ* measurements to a film thickness of about 5 nm, are depicted in Fig. 1c. The source-drain current increases supralinearly with film thickness. These results were reproducible for different batches of samples and for different deposition rates of 0.01 and 0.02 nm/s.

While the evaluation of the electrical measurements reveal the nature of early stage thin film growth, AFM shows no clear signature from the pentacene layer after percolation (Fig. 2) [26]. The AFM micrograph at nominally 1.37 nm of pentacene (Fig. 2b) looks very similar to the pristine parylene-C surface with an rms roughness of ca. 7 nm rms on-top the Au gate (Fig. 2a), i.e. it is not possible to draw any conclusions about the early growth mode from topography, because the sub-monolayer pentacene film cannot be imaged, a common problem for rough substrates. The combination of both studies suggests that the first layer coated the substrate conformally. Pentacene thin films at higher thicknesses, here a nominal thickness of 12 nm and 57 nm, respectively, exhibit granular topographies with grain sizes <300 nm (Fig. 2c and d) [23]. This subsequent island growth for thicker films allows to
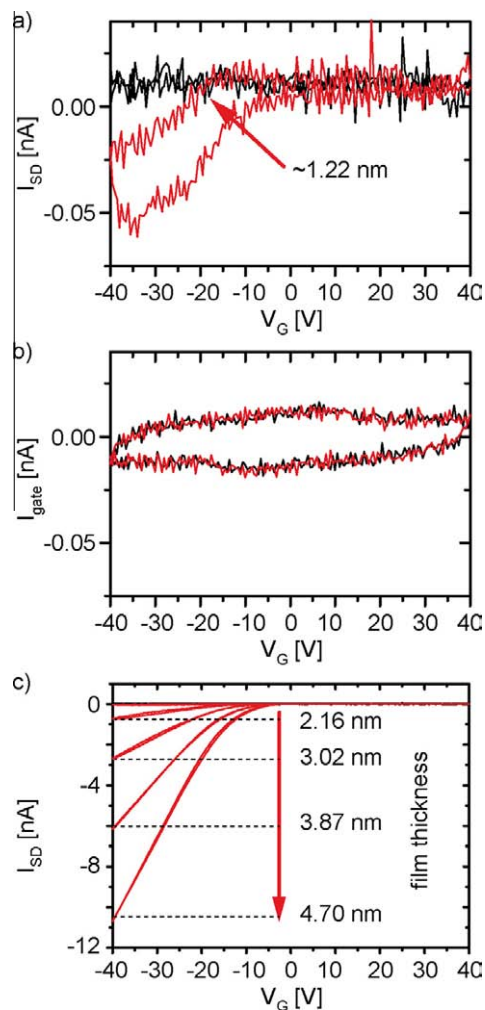

Fig. 1. Early growth stage *in-situ* measurement. (a) Transfer measurements of early-stage pentacene deposition (forward and backward sweeps). First drain currents occur at film thickness of ~1.22 nm (0.8 ML). (b) Corresponding gate current measurements. Here, the gate sweeps do not indicate any change after percolation. (c) Transfer measurements of the first five gate voltage sweeps during film deposition after drain current onset.

classify the growth mode of pentacene on parylene-C as the Stranski–Krastanov (layer plus island) mode [25].

To understand how charge transport can occur on a sub-monolayer scale on rough surfaces, it is necessary to estimate the influence of height fluctuations at distances matching the unit cell dimensions of organic semiconductors, i.e. distances of the order 1 nm, on the pi-system overlap. As the height difference correlation function approaches zero for separation much smaller than the correlation length ξ [10,12], i.e. it is quite possible that the height difference at unit cell dimensions (lattice distortion) can be very small, even for large rms σ values. This implies that as long as the lateral correlation length is large enough, a rather large rms is tolerable.

Besides the influence of roughness on percolation, it is also important to verify its influence on channel completion, which should, from an electrostatic point of view, occur within the Debye length. However, channel completion could be delayed due to defects and other impurities. To answer this, we evaluate the evolution of mobility, threshold and hysteresis of the OFETs from the current in the saturation regime: $I_{SD} = W/2L * \mu * C_i * (V_G − V_T)^2$.
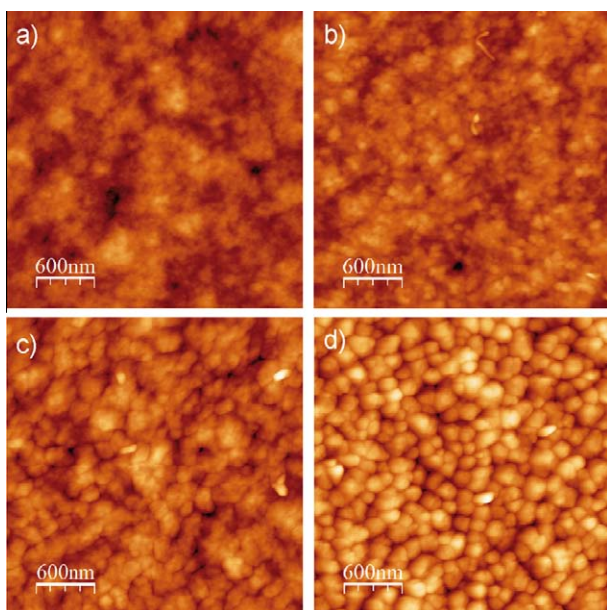
Fig. 2. AFM micrographs of parylene-C covered by different thicknesses of pentacene. (a) Pristine parylene-C surface. (b) 0.9 ML pentacene (1.37 nm) on parylene-C; the film is percolated, i.e. conductive. (c) 12 nm pentacene on parylene-C. (d) 57 nm pentacene on parylene-C. The z-scale is 77.7 nm for all micrographs.

Here, W is the channel width and L is the channel length, μ is the effective charge carrier mobility, C_i the capacitance of the dielectric per area, V_G the applied gate voltage and V_T the threshold voltage. For any given thickness interval, whose range is determined by the sweep speed, the corresponding gate sweeps are shown in Fig. 3a. To clarify the evolution of the device performance, mobility and threshold voltage is extracted from the forward and backward sweeps of the OFETs in the saturation regime from every sweep (Fig. 3b and c, mobility shown for forward sweep direction). The nominal film thickness is chosen as the value at the end of the sweep, and assumed to be constant during the sweep.

During deposition of the first 3 monolayers (ML) the threshold voltage experiences a steep shift of more than 15 V (Fig. 3b). Within the same nominal thickness, the hysteresis, i.e. the difference between forward and backward sweep threshold voltage, decreases rapidly from about 16 V to a value smaller than 1 V. Similar behavior has been observed for pentacene OFETs on SiO$_2$ [24]. The threshold voltage shift can be explained by an increase of deep electron volume traps with increasing film thickness. Until a film thickness of 3 ML, these traps are within the Debye length of the transistor channel and consequently lay within the accumulation layer. The hysteresis on the other hand arises due to traps at the pentacene surface, which quickly grow out of the OFET channel region. These traps are energetically shallower than the deep traps that cause the threshold shift, since they can be filled and depleted at room temperature. Beyond 3 ML the shifts saturate, because further thickness increase occurs outside of the accumulation channel of the transistor.

On the other hand, saturation mobility reproducibly continues to increase up to a thickness of ca. 20 nm (Fig. 3c), which is far beyond the Debye length. Investigation of the topography of pentacene at the electrode edge reveals small grained pentacene topography with deep valleys (Fig. 4). Such dewetting of pentacene in the vicinity of gold is in fact a well known problem for bottom contact geometry [27]. This suggests that also here, especially for early stage film growth, the impaired film formation near and on the gold contacts disturbs charge injection. Hence, the extracted
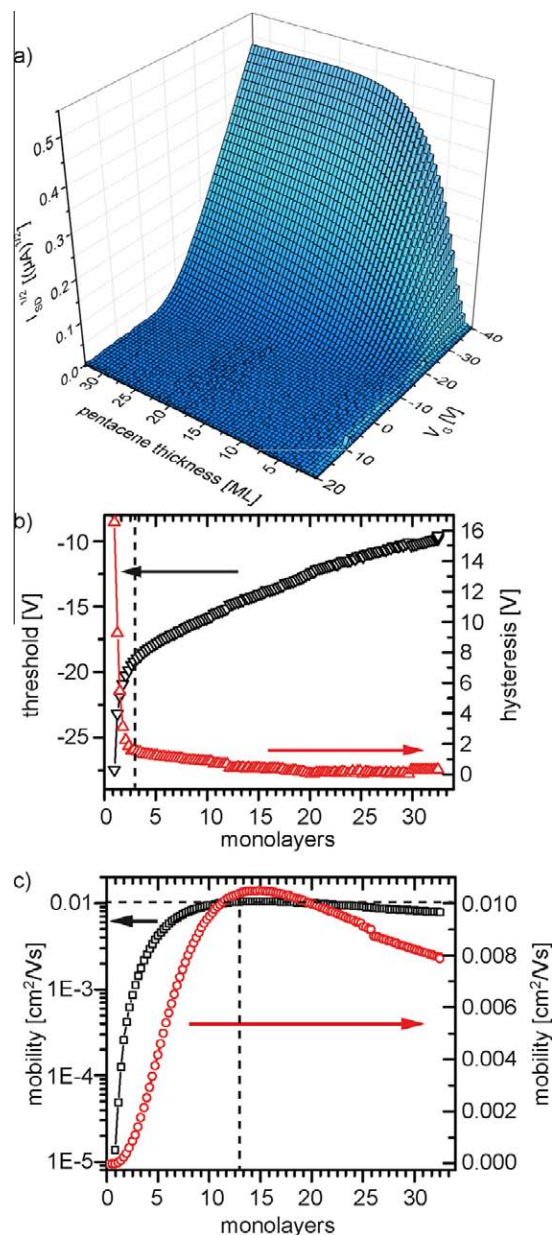
Fig. 3. Electronic data from one *in-situ* growth measurement. (a) Gate voltage (V_G) sweeps, plotted against the nominal pentacene film thickness and the square root of the source drain current I_{SD}. For clarity, only every second sweep and every second gate voltage data point is shown. (b) Threshold voltage (black downward facing triangles) and hysteresis (red upward facing triangles). The vertical dashed line at ~3 MLs indicates the region, where the threshold shift turns from rapid to slow. (c) Mobility in linear (red circles) and logarithmic plot (black squares) in dependence of the film thickness (extracted from forward sweeps). The vertical line indicates saturation of the mobility at ~13 MLs. (For interpretation of the references to color in this figure legend, the reader is referred to the web version of this article.)

mobilities at early growth might be influenced by poor charge injection and extraction, and therefore may not represent intrinsic charge carrier mobility within the film. The ongoing increase in measured mobility is likely to be caused by the improvement of charge injection with film thickness. The final mobility is probably not limited by the rough dielectric surface, but due to the overall device preparation, which was adapted to the presented *in-situ* study, using bottom contact geometry and pristine surfaces with-
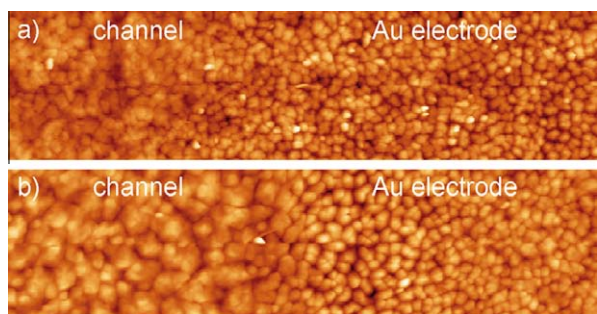
Fig. 4. AFM height micrographs of the OFET channel/Au electrode interface (10 μm × 2.5 μm). The growth differences of pentacene on parylene-C and gold, i. e. smaller grain size and deeper grain gaps on Au are clearly visible. (a) 12 nm thick pentacene film. (b) 57 nm thick pentacene film.

out modifications. In fact, using an optimized device geometry, a mobility of 0.81 cm^2/Vs was reported for transistors with top contact geometry on parylene-C dielectrics [28].

3. Conclusion

In conclusion, we performed *in-situ* deposition of pentacene on a rough parylene-C dielectric and observed sub-monolayer percolation of the pentacene film. This initial closed layer of pentacene points to a Stranski–Krastanov growth mode. This demonstrates that conformal monolayer growth is possible on rough substrates. Like in the case of smooth dielectrics, subsequent transistor channel formation is dominated by electrostatic and charge injection phenomena. In fact, saturation of electrical properties is observed for the same film thickness as on smooth substrates. These findings imply that, as long as conformal growth of the organic semiconductor is possible, high surface roughness does not cause impaired device performance. Consequently, one should explore rough substrates as the choice for dielectric material more systematically.

Acknowledgments

Appendix A. Supplementary data

Supplementary data associated with this article can be found, in the online version, at http://dx.doi.org/10.1016/j.orgel.2015.08.009.

References

[1] A. Facchetti, M.H. Yoon, T.J. Marks, Gate dielectrics for organic field-effect transistors: new opportunities for organic electronics, Adv. Mater. 17 (2005) 1705–1725.
[2] J. Wunsche, G. Tarabella, S. Bertolazzi, M. Bocoum, N. Coppede, L. Barba, G. Arrighetti, L. Lutterotti, S. Iannotta, F. Cicoira, C. Santato, The correlation between gate dielectric, film growth, and charge transport in organic thin film transistors: the case of vacuum-sublimed tetracene thin films, J. Mater. Chem. C 1 (2013) 967–976.
[3] C. Kim, A. Facchetti, T.J. Marks, Gate dielectric microstructural control of pentacene film growth mode and field-effect transistor performance, Adv. Mater. 19 (2007) 2561–2566.
[4] S. Steudel, S. De Vusser, S. De Jonge, D. Janssen, S. Verlaak, J. Genoe, P. Heremans, Influence of the dielectric roughness on the performance of pentacene transistors, Appl. Phys. Lett. 85 (2004) 4400.
[5] H.-G. Min, E. Seo, J. Lee, N. Park, H.S. Lee, Behavior of pentacene molecules deposited onto roughness-controlled polymer dielectrics films and its effect on FET performance, Synth. Met. 163 (2013) 7–12.
[6] K. Shin, C. Yang, S.Y. Yang, H. Jeon, C.E. Park, Effects of polymer gate dielectrics roughness on pentacene field-effect transistors, Appl. Phys. Lett. 88 (2006) 072109.
[7] M. Kaltenbrunner, T. Sekitani, J. Reeder, T. Yokota, K. Kuribara, T. Tokuhara, M. Drack, R. Schwodiauer, I. Graz, S. Bauer-Gogonea, S. Bauer, T. Someya, An ultra-lightweight design for imperceptible plastic electronics, Nature 499 (2013) 458–463.
[8] G. Lin, Q. Wang, L. Peng, M. Wang, H. Lu, G. Zhang, G. Lv, L. Qiu, Impact of the lateral length scales of dielectric roughness on pentacene organic field-effect transistors, J. Phys. D Appl. Phys. 48 (2015) 105103.
[9] A. Dodabalapur, L. Torsi, H.E. Katz, Organic transistors: two-dimensional transport and improved electrical characteristics, Science 268 (1995) 270–271.
[10] A.C. Dürr, F. Schreiber, K.A. Ritley, V. Kruppa, J. Krug, H. Dosch, B. Struth, Rapid roughening in thin film growth of an organic semiconductor (Diindenoperylene), Phys. Rev. Lett. 90 (2003).
[11] T. Gredig, E.A. Silverstein, M.P. Byrne, Iop, Height–height correlation function to determine grain size in iron phthalocyanine thin films, 15th International Conference on Thin Films (Ictf-15), 417 (2013).
[12] S.K. Sinha, E.B. Sirota, S. Garoff, H.B. Stanley, X-ray and neutron-scattering from rough surfaces, Phys. Rev. B 38 (1988) 2297–2311.
[13] R. Ruiz, B. Nickel, N. Koch, L.C. Feldman, R.F. Haglund, A. Kahn, F. Family, G. Scoles, Dynamic scaling, island size distribution, and morphology in the aggregation regime of submonolayer pentacene films, Phys. Rev. Lett. 91 (2003).
[14] K.P. Weidkamp, C.A. Hacker, M.P. Schwartz, X.P. Cao, R.M. Tromp, R.J. Hamers, Interfacial chemistry of pentacene on clean and chemically modified silicon (0 0 1) surfaces, J. Phys. Chem. B 107 (2003) 11142–11148.
[15] J.B. Fortin, T.-M. Lu, Chemical Vapor Deposition Polymerization – The Growth and Properties of Parylene Thin Films, Springer Science & Business Media, 2003.
[16] A.K. Diallo, J. Tardy, Z.Q. Zhang, F. Bessueille, N. Jaffrezic-Renault, M. Lemiti, Trimethylamine biosensor based on pentacene enzymatic organic field effect transistor, Appl. Phys. Lett. 94 (2009) 263302.
[17] D. Khodagholy, T. Doublet, M. Gurfinkel, P. Quilichini, E. Ismailova, P. Leleux, T. Herve, S. Sanaur, C. Bernard, G.G. Malliaras, Highly conformable conducting polymer electrodes for in vivo recordings, Adv. Mater. 23 (2011) H268–H272.
[18] V. Podzorov, S.E. Sysoev, E. Loginova, V.M. Pudalov, M.E. Gershenson, Single-crystal organic field effect transistors with the hole mobility similar to 8 cm (2)/V s, Appl. Phys. Lett. 83 (2003) 3504–3506.
[19] C.D. Dimitrakopoulos, B.K. Furman, T. Graham, S. Hegde, S. Purushothaman, Field-effect transistors comprising molecular beam deposited alpha, omega-di-hexyl-hexathienylene and polymeric insulator, Synth. Met. 92 (1998) 47–52.
[20] S.G. Engelbrecht, M. Prinz, T.R. Arend, R. Kersting, Terahertz spectroscopy on hole transport in pentacene thin films, Appl. Phys. Lett. 105 (2014) 012101.
[21] A. Moser, H.G. Flesch, A. Neuhold, M. Marchl, S.J. Ausserlechner, M. Edler, T. Griesser, A. Haase, D.M. Smilgies, J. Jakabovic, R. Resel, Crystallization of pentacene thin films on polymeric dielectrics, Synth. Met. 161 (2012) 2598–2602.
[22] A. Vincze, J. Jakabovic, R. Srnanek, A. Satka, J. Kovac, J. Kovac, Surface and interface properties of thin pentacene and parylene layers, Cent. Eur. J. Phys. 7 (2009) 270–278.
[23] V.A. Skryshevsky, J. Tardy, M. Phaner-Goutorbe, E. Souteyrand, R. Villey, M. Erouel, M. Iazykov, An Afm investigation of surface energy of pentacene films on parylene-C and benzocyclobutene, Funct. Mater. Lett. 05 (2012) 1250016.
[24] M. Fiebig, D. Beckmeier, B. Nickel, Thickness-dependent in situ studies of trap states in pentacene thin film transistors, Appl. Phys. Lett. 96 (2010) 083304.
[25] S.-W. Liu, C.-C. Lee, H.-L. Tai, J.-M. Wen, J.-H. Lee, C.-T. Chen, In situ electrical characterization of the thickness dependence of organic field-effect transistors with 1–20 molecular monolayer of pentacene, ACS Appl. Mater. Interfaces 2 (2010) 2282–2288.
[26] I. Horcas, R. Fernandez, J.M. Gomez-Rodriguez, J. Colchero, J. Gomez-Herrero, A.M. Baro, WSXM: a software for scanning probe microscopy and a tool for nanotechnology, Rev. Sci. Instrum. 78 (2007) 013705.
[27] Y. Tsuruma, A. Al-Mahboob, S. Ikeda, J.T. Sadowski, G. Yoshikawa, Y. Fujikawa, T. Sakurai, K. Saiki, Real-time observation and control of pentacene film growth on an artificially structured substrate, Adv. Mater. 21 (2009) 4996.
[28] T. Yasuda, K. Fujita, H. Nakashima, T. Tsutsui, Organic field-effect transistors with gate dielectric films of poly-p-xylylene derivatives prepared by chemical vapor deposition, Jpn. J. Appl. Phys. 1 (42) (2003) 6614–6618.

A.3   AMMONIA SENSING FOR ENZYMATIC UREA DETECTION WITH ORGANIC FIELD EFFECT TRANSISTORS AND A SEMIPERMEABLE MEMBRANE

Franz Werkmeister, Teru Koide, Bert Nickel

Abstract

Organic Field Effect Transistors (OFETs) are used to measure ammonia in solution via ammonia diffusion into the OFET channel. Increases in ammonia concentrations result in a decrease in transistor currents. The regeneration of the OFET current after ammonia uptake is slow, which allows to read out the maximum ammonia dose which was applied. A 100 nm parylene-C layer serves as a semipermeable top gate dielectric. The parylene layer is functionalized with the covalently attached enzyme urease. The enzyme catalyzes the hydrolysis of urea to ammonia and carbon dioxide, i.e. urea can be detected via its hydrolysis product ammonia. The sensitivity covers the range of physiological concentrations of urea, which is several mM.

My Contribution

I produced and prepared the transistor samples, performed the electrical experiments on the transistors and the data evaluation. Teru Koide developed the surface functionalization and validated the urea conversion in test series in solution. Furthermore, I wrote the manuscript draft and designed the figures.

Table of contents graphic

PAPER

Ammonia sensing for enzymatic urea detection using organic field effect transistors and a semipermeable membrane†
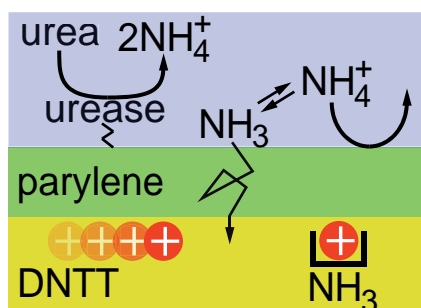
F. X. Werkmeister,[a] T. Koide[ab] and B. A. Nickel*[ac]

Organic Field Effect Transistors (OFETs) are used to measure ammonia in solution *via* ammonia diffusion into the OFET channel. An increase in ammonia concentrations results in a decrease in transistor currents. The regeneration of the OFET current after ammonia uptake is slow, which allows us to read out the maximum ammonia dose which was applied. A 100 nm parylene-C layer serves as a semipermeable top gate dielectric. The parylene layer is functionalized with the covalently attached enzyme urease. The enzyme catalyses the hydrolysis of urea to ammonia and carbon dioxide, *i.e.* urea can be detected *via* its hydrolysis product ammonia. The sensitivity covers a range of physiological concentrations of urea, which are several mM.

Introduction

Ammonia, the end product of amino acid metabolism, is highly toxic. Therefore, ammonia is circulated only in low concentrations in body fluids, and most of it is first converted into urea in a cycle of biochemical reactions known as the urea cycle. Urea is present in body fluids in high concentrations; in healthy humans, the normal range of urea concentrations in blood is 2.5–7 mM.[1] The measurement of urea concentrations is important as a marker for *e.g.* potential kidney malfunction.[2,3] Specific detection of urea is possible by the enzyme urease. Urease catalyzes the hydrolysis of urea to ammonium (NH_4^+) and carbon dioxide in water:

$$CO(NH_2)_2 + 3H_2O \xrightarrow{\text{urease}} CO_2 + 2NH_4^+ + 2OH^- \qquad (1)$$
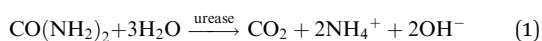
The OH^- production of the reaction shifts the pH value, which has been used to detect urea using silicon transistors.[4] Transistors are especially feasible for the label free measurement of target molecules, because transistors measure and at the same time amplify the signal.[5,6] Organic transistors are appealing alternatives to silicon technology, since organic transistors can be mechanically flexible[7] and biocompatible[8] at low production cost with high throughput, *e.g.* with printing techniques.[9,10] Furthermore, organic semiconductors can be directly functionalized with

e.g. biotin[11] and interfaced with tissue.[12] Organic transistors operate as sensors in liquids by two different main principles. In Organic Electrochemical Transistors (OECTs), ions diffuse into the semiconducting film and dope or de-dope the transistor channel.[13] In Organic Field Effect Transistors (OFETs), the charge carrier concentration in the transistor channel is manipulated *via* capacitive coupling,[14–16] resulting in a change of the current through the device. The source drain current I_{SD} of the transistor in saturation mode is given by:[16]

$$I_{SD} = \frac{W}{2L} \times C \times \mu \times (V_{gate} - V_T)^2, \qquad (2)$$

with W being the channel width, L the channel length, C the dielectric's areal capacitance, μ the mobility of the semiconductor, V_{gate} the applied gate voltage and V_T the threshold voltage. Three parameters can change upon interaction with a substance of interest. First, the threshold voltage V_T may change due to electrostatic field changes, *e.g.* due to different pH values or adsorption of charged molecules.[17] Second, upon binding of a substance, the capacity C of the dielectric can change.[16] Finally, mobility μ can change *e.g.* due to morphological interface effects.[18] In practice, often a combination of these effects occurs. So far, organic transistors have been demonstrated for the measurement of proteins,[9] glucose,[13,19] adrenaline,[20] glutamate[21] and specific ions.[22–24]

For enzymatic urea detection *via* its hydrolysis product ammonium and OH^- (eqn (1)), one could consider a pH based or ion specific detection scheme.[4,23] Here, a shift of the electrochemical potential due to urea hydrolysis is picked up *via* a shift in the electrostatic gate potential, which controls the semiconducting channel.[4] This approach is limited for a weak base as

[a] *Fakultät für Physik & CeNS, Ludwig-Maximilians – Universität München, München, D-80539, Germany. E-mail: nickel@lmu.de*
[b] *Japan Patent Office, 3-4-3 Kasumigaseki, Chiyoda-ku, Tokyo 100-8915, Japan*
[c] *Nanosystems Initiative Munich (NIM), D-80799 Munich, Germany*
† Electronic supplementary information (ESI) available: Evaluation of parylene-C as top-gate dielectric. Urease activity evaluation. OFET current regeneration after exposure to ammonia. See DOI: 10.1039/c5tb02025e

ammonium since ammonium forms in solution a chemical equilibrium between NH_4^+ and ammonia (NH_3):

$$NH_4^+ + H_2O \leftrightarrow NH_3 + H_3O^+ \quad (3)$$
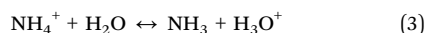
Alternatively, NH_3 is well known to reduce charge transport in organic semiconductors,[25] most likely *via* creation of traps. These traps have been discussed to be caused by the interaction of the holes with the lone electron pair of NH_3, as well as by dipole interaction.[26] A range of ammonia gas sensors were demonstrated based on this principle.[26–29] Other nitrogenous molecules like NO and NO_2, which are biologically relevant, have also been detected in gas.[30] Furthermore, it has been possible to construct arrays, which can differentiate between different vapors by the characteristic response on the organic transistors.[31–33] This gas detection principle works also for organic semiconductors in direct contact with solution, as demonstrated for some molecules, *e.g.* cysteine[34] and melamine.[35]

Note that another reaction product of the hydrolysis (eqn (1)) is CO_2. CO_2, however, is known to have only negligible interactions with organic transistors,[36] and thus not expected to influence device characteristics. It can form a chemical equilibrium with carbonic acid and thus contribute to buffering in solution.

Here, we explore OFETs for the detection of urea. For this purpose, we fabricated a 100 nm parylene-C membrane onto the OFETs and functionalized the parylene-C surface with a covalently attached enzyme, urease. We suggest that urea can be detected *via* its hydrolysis product ammonia. Ammonia should be able to diffuse through the parylene-C membrane and give rise to a response *via* trapping of charge carriers in the organic semiconductor film. To determine the mechanism of sensing, *i.e.* pH *vs.* trapping, the response of the OFETs towards shifts of the pH value as well as NH_3 concentration in solution is tested, with a detailed investigation of the latter. Finally, the urea concentration range, which can be detected, is determined.

Experimental

OFET fabrication

Glass slides (R. Langenbrinck) were cleaned in an ultrasonic bath with acetone, 2-propanol, and Milli-Q water for 10 min each. Next nominally 1.7 µm parylene-C (Plasma Parylene Systems GmbH) was deposited in a homebuilt CVD chamber *via* the Gorham route. Source and drain electrodes were defined from 20 nm of Au using a Lift-Off process: a bilayer of LOR 3B and S1813 G2 was spin coated, illuminated and developed using Microposit 351 Developer. The LOR 3B layer beneath the photoresist gives rise to an undercut in the dual layer during development and avoids fencing at the rims of the patterned metal electrodes after Lift-Off. Lift-Off was performed with 1165 Remover. The electric leads defined on the surface were encapsulated with a layer of SU 8 (Microchem), which was processed as recommended by the fabricant; mr-Dev 600 (Microchemicals GmbH) was used as a developer. 18 nm DNTT (Sigma 767638, purified by one sublimation run by CreaPhys GmbH) was deposited thermally onto the transistor areas

through a shadow mask at a rate of 0.2 Å s^{-1} with the substrates at room temperature and a base pressure of $<10^{-6}$ mbar. The devices were encapsulated by depositing *ca.* 100 nm parylene-C onto the transistor area. The area of parylene-C deposition was defined by a PDMS mask put onto the devices.

Surface treatment and urease attachment

The OFETs were treated with oxygen plasma in a plasma cleaner (50 W power, 2 mbar, 18 s). Immediately afterwards, the OFETs were put into a 1 vol% aqueous solution of APTES (Sigma A3648) for at least 4 h. Subsequently, the OFETs were dried under gentle nitrogen flow and put into a 5% solution of glutaraldehyde (Sigma G6257) for at least 4 hours. After drying under nitrogen flow again, the urease was bound to the surface by putting the OFETs into a solution of urease (Sigma U1500, 75 mg) in PBS buffer (10 mM, 15 ml).

Assembly into the flow chamber

Commercially available sticky slides IV 0.4 (Ibidi GmbH) were modified as follows: the adhesive tape was peeled off from the flow chamber and the holes necessary for the electrical contacts were drilled utilizing a CNC milling machine. After drilling the holes 467 MP adhesive tape (3 M) was applied to the bottom of the slides and patterned according to the holes and the channel. A PtIr (Pt80/Ir20, GoodFellow, PT045110) wire was introduced into each channel after being glowed out using a Bunsen burner to serve as the electrode in the electrolyte. Finally, the OFET was attached to the modified sticky slides and the glue was given one night to obtain a good seal.

Electrical measurements

Measurements were performed using a linked system of a Keithley 2612 and 2602 source measurement unit. The source and drain contacts were hot switched using a Keithley 7072 switching matrix card. The equipment was controlled using custom written LabView programs. The potential in the electrolyte (top gate) was swept down to −0.6 V *versus* the source contact. The source drain bias was −0.3 V *versus* the source. All measurements were performed in ambient at 20–21 °C.

pH measurements in the electrolyte

The solution for any measurement was based on 10 mM Dulbecco's phosphate buffered saline solution without Ca/Mg (Biochrom L 182-50, powder dissolved in Milli-Q water). Urea (Sigma U0631) and ammonia (Carl Roth 5460.1) were dissolved/ pipetted into 10 mM DPBS solution. A HANNA 213 pH meter was used for the pH measurements and calibrated before each use.

AFM measurements

AFM micrographs were recorded using a Veeco Dimension 3100 AFM in tapping mode. The software Gwyddion 2.40 was used for evaluation.
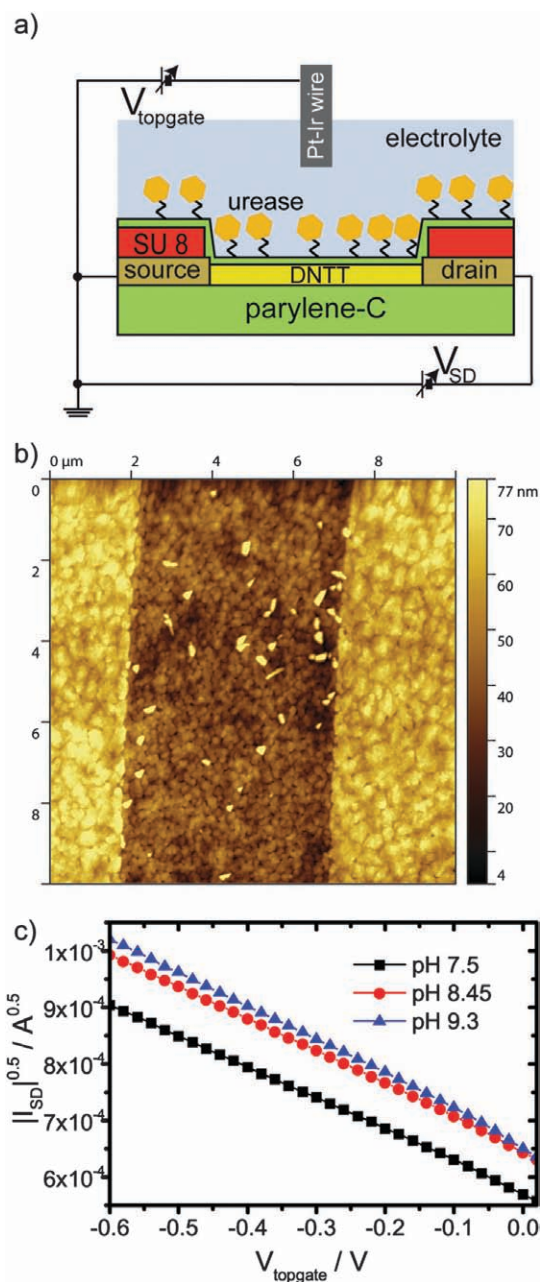
Fig. 1 (a) Schematic of the OFET device architecture and measurement scheme in solution. (b) AFM micrograph of the DNTT film in an OFET channel of length 5 μm. The source–drain electrodes are visible to the left and the right. (c) pH effect on the transconductance curve of an OFET.

Results and discussion

We designed an OFET gated *via* a Pt/Ir wire in solution (Fig. 1a). A parylene-C layer with source and drain electrodes patterned by photolithography for bottom contact served as a substrate.[37] Dinaphtho[2,3-*b*:2′,3′-*f*]thieno[3,2-*b*]thiophene (DNTT) was chosen as the organic semiconductor for its stability[38] and thermally deposited onto the substrate to form the organic semiconducting channel (Fig. 1b). Onto the semiconductor channel, we deposited a 100 nm thick parylene-C layer, which served as the top gate dielectric (ESI†). Furthermore, parylene-C dielectric's surface can be functionalized by a silane coupling reaction. The functionalization procedure was based on a silane coupling reaction adapted from the functionalization of silicon dioxide dielectrics of inorganic silicon biosensors.[4] To activate the parylene-C surface, it was treated with an oxygen plasma for 18 s.[39] Here, the stability of DNTT *versus* oxidation was necessary to maintain transistor operation after the oxygen treatment. Less stable organic semiconductors might be employable, if parylene derivatives are employed, which facilitate function-alization procedures avoiding plasma activation.[40] Oxygen plasma treated parylene-C surfaces were silanized by 3-amino-propyltriethoxysilane (APTES). Subsequently, glutaraldehyde and urease were bound to this surface. To verify the function of bound urease, the catalysis of urea was tested. Urea was dissolved in Milli-Q water to a concentration of 10 mM. This solution was added into a beaker together with dissolved urease or a treated parylene-C surface on glass. The pH value of the solution was measured against the time using a digital pH meter (ESI,† Fig. S5). The maximum value of pH attainable was 9.3, likely the urease degraded at this pH value. For the lower amount of urease, the pH value saturated at decreasing values. This implied a limited total number of catalyses sustainable for an individual urease enzyme. We found that the pH response for the bound urease was comparable to a concentration above 10 μg ml^{-1} of free urease in solution, albeit slower. The slower response of bound urease is likely due to mass transport from and to the surface and a larger distance of the pH meter from the reaction.

First, we tested the pH response of our OFET. The pH value of 10 mM Dulbecco's phosphate buffered saline (DPBS) solution was adjusted by HCl and NaOH. Increasing the pH value from 7.5 to 8.5 results in a positive threshold voltage shift (Fig. 1c). This shift exceeds the Nernstian limit for a single type of charged surface group.[41] Most likely, the enzyme layer is responsible for this behavior. A further increase of the pH values from 8.45 to 9.3 and above results in small threshold voltage shifts only. Likely, the enzyme degraded (see S5, ESI†) and the functionalization layer covering the transistor changed its properties. Similarly, the small increase in transconductance observed with increasing pH value may result from conformational changes of the urease layer. Consequently, we conclude that the bound enzyme layer is responsible for the observed pH response, which gives rise to an overall increase of transistor current with increasing pH.

Second, we tested the response and sensitivity of our OFET towards ammonia in solution. Ammonia was dissolved in DPBS solution with concentrations of 0.1 mM, 1 mM and 10 mM. For 0.1 mM solution, no change was observed, see Fig. 2a, red circles and black squares, while for a 1 mM solution, a small change was observed (Fig. 2a, blue triangles). For an ammonia concentration of 10 mM, the transistor current reduced to half of the initial value in a matter of tens of seconds (Fig. 2b).
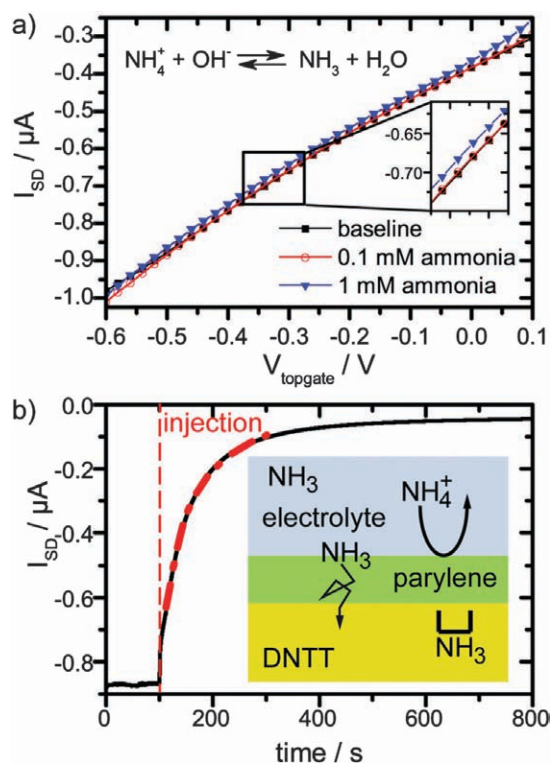
Fig. 2 (a) Effect of small ammonia concentrations (0 mM, 0.1 mM, and 1 mM) in 10 mM DPBS buffer on the transconductance, shown as black, red, and blue curves, respectively. (b) Time resolved OFET current upon addition of 10 mM ammonia solution with $V_{topgate}$ = −0.4 V. The scheme shows the proposed interaction mechanism of ammonia with the organic semiconductor. All data were recorded at V_{SD} = −0.3 V.
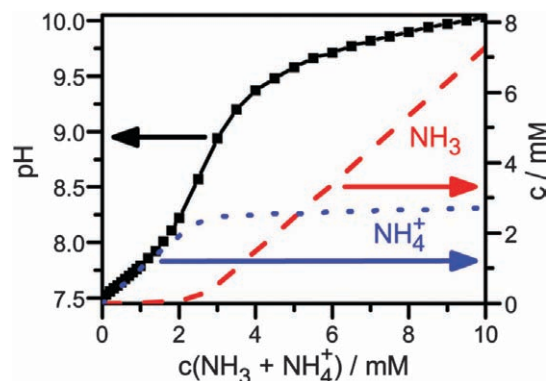

Fig. 3 pH value and ratio of NH_3 vs. NH_4^+ depending on ammonia concentration in 10 mM DPBS. The ratio was calculated assuming a K_a of ammonia of 9.6, since the literature value of 9.4[42] for ammonia in water leads to unphysical results.

This is encouraging, because the ammonia concentrations that cause this strong response are comparable to the relevant urea concentrations in body fluids of 2.5 to 7 mM.[1]

Remarkably, the reduction of current with increasing ammonia and pH is opposite to the pure pH effect. This suggests that the current reduction dominated from NH_3 passing the encapsulation layer and diffusing into the semiconductor. In order to quantify this argument, we estimate the amount of NH_3 for a 1 mM ammonia solution at the pH of 7.75 and for a 10 mM solution at a pH of 10.17. The ratio of NH_3 and NH_4^+ depending on the pH is given by the Henderson–Hasselbach equation:

$$\frac{c(NH_3)}{c(NH_4^+)} = 10^{pH-pK_a} \quad (4)$$

here, pK_a is the acid dissociation constant of NH_4^+.[42] The interplay between pH and the ratio of NH_3 and NH_4^+ can be found in Fig. 3; there is a rather sharp transition at pH values of ∼8. Below pH 8, there is an almost linear relationship between NH_4^+ and pH, i.e. one could use the pH value to determine the NH_4^+ concentration, which in this case is also similar to the total concentration (NH_4^+ and NH_3). However, beyond this pH, i.e. at NH_4^+ concentration beyond 2 mM, a

pronounced increase of NH_3 concentration occurs, while the NH_4^+ concentration saturates (Fig. 3). Thus, the NH_3 concentration is a better indicator at high concentrations, while pH or NH_4^+ is better suited at low concentrations.

We find that the NH_3 concentration is increased by a factor of ca. 1000 between ammonia concentrations of 1 and 10 mM, which suggest that indeed NH_3 causes the transistor current drop. In fact, detection of ammonia in solution, as demonstrated here, is interesting itself, because it is an indicator of a range of diseases.[43]

The device response towards an increase of ammonia concentration occurs within seconds (Fig. 2b). Since our analysis suggested that the diffusion of NH_3 into the semiconductor layer dominates the response, we assume that the NH_3 profile is described by a 1D solution of Fick's 2nd law of diffusion:[19]

$$n(x,t) = n_0 \, \mathrm{erfc}\left(\frac{x}{2\sqrt{Dt}}\right) \quad (5)$$

here, $n(x,t)$ is the concentration of the diffusing species at time t in distance x from the reservoir with constant concentration n_0 in a material with diffusion constant D. We modeled the decrease of the current with this equation excluding the initial response in the first few seconds, since it includes effects from mixing.[44] The fit to the data was reproducing the experimental curve well (Fig. 2b), with an extracted diffusion constant D = 1.4×10^{-12} cm^2 s^{-1}. This diffusion constant is three orders of magnitude lower than the diffusion constants for molecular oxygen and nitrogen in parylene,[45] which should be similar to the one for NH_3. On the other hand, the response time corresponds well to those of bare pentacene films sensing ammonia gas.[28,29] This suggests that the organic semiconductor film, which is poly-crystalline (Fig. 1b), and not the parylene layer, is the dominant diffusion barrier. Therefore, improvements on response time are more likely to be achievable by thinning or patterning engineering the organic semiconducting layer.[26]

While parylene is apparently no diffusion barrier for neutral NH_3, it is very efficient in suppressing diffusion of charged ions (Na^+ and Cl^-) to the channel region. This is because the movement

of an ion (with radius a and valency Z) from water into an nonpolar medium with dielectric constant ε is prohibited by a high energy barrier, the Born charging energy $(Ze)^2/8\pi\varepsilon_0\varepsilon a$.[46] This effect gives rise to the high resistance of lipid bilayers.[47] This principle also applies to the case of an nonpolar organic semiconductor ($\varepsilon \approx 80$ for water[46] and $\varepsilon \approx 3$ for pentacene[14]) or nonpolar encapsulation layers such as parylene. In practice, defects, *e.g.* pores, in nonpolar layers can lower the energy barrier,[46] thus materials and processing have to be carefully chosen.[10,48] In summary, the parylene acts here as a semipermeable membrane which blocks ions, while charge neutral NH_3 molecules pass through rapidly. Diffusion speed in parylene decreases with the molecule size,[49] therefore larger molecules will also be blocked.

Upon rinsing with fresh DPBS buffer after application of 10 mM ammonia solution, the current of the transistor recovers slowly (ESI,† Fig. S6). Apparently, the process of loading NH_3 into the semiconducting layer was much faster than the unloading process. This is reasonable, since the NH_3 gradient driving the diffusion from 10 mM ammonia solution to the pristine semiconducting film is much steeper than the one from the NH_3 loaded semiconducting film to the bare DPBS solution. Additionally, during exposure to the ammonia solution, ammonia may pass the semiconducting layer and diffuse into the parylene layer beneath the organic semiconductor. Subsequent release would take place *via* diffusion through the organic semiconductor with a very low rate, *i.e.* the parylene layer beneath the organic semiconductor acts as a reservoir.

Finally, the urea sensing of OFETs with bound urease was evaluated. Different concentrations of DPBS solutions with urea were prepared and pipetted into the flow channel of the sensor after completion of the first gate sweep. Gate sweeps were recorded continuously and the change of the transconductance curve after fixed time (5 min) was evaluated (Fig. 4, red data points). The first
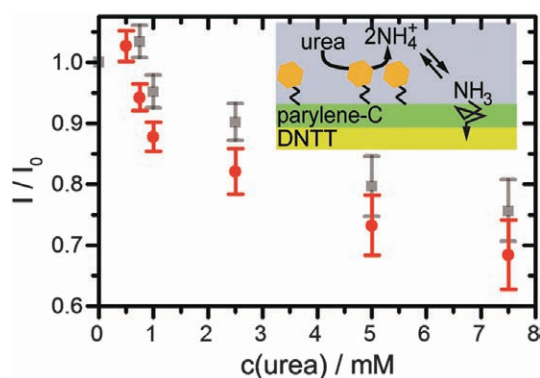

Fig. 4 Influence of increasing urea concentrations on transistor current. The first source–drain current I_{SD} at $V_{SD} = -0.3$ V and $V_{topgate} = -0.3$ V (without urea) is used as reference current I_0 (grey data point). The resultant ratio I_{SD}/I_0 (red dots) is displayed as recorded after 5 min exposure to a given urea concentration. After each exposure, and prior to the next exposure the OFETs are rinsed with fresh buffer by exchanging the liquid volume 5 times. The ratio I_{SD}/I_0 prior to each urea exposure is shown after rinsing with buffer as grey squares. The data points are an average of the data of 3 different OFETs with the error bars giving the standard deviation.

response was detected for a urea concentration of 0.75 mM. Between the different urea concentrations, we rinsed the flow channel with fresh DPBS buffer by replacing the complete liquid volume 5 times with fresh buffer. Due to the slow recovery, the transistor current stayed at the low level (Fig. 4, gray data points) suggesting that the device is best suited to monitor the maximal dose that the semiconductor film has seen. We observed a systematic decrease of the current up to a urea concentration of 7.5 mM, *i.e.* the device covers the full urea range in a healthy patient. In comparing the response in Fig. 4 to the ammonia concentration dependence in Fig. 3 one may note that the response starts before the pronounced increase in NH_3 in Fig. 3. Already below the pronounced increase in NH_3 at 2 mM in Fig. 3 the NH_3 concentration is nonzero and linearly increasing. Organic transistors are sensitive to small amounts of NH_3,[29,50] as also observed here in the detection of 1 mM ammonia (Fig. 2a). Furthermore, the response of organic transistors with increasing NH_3 tends to saturate,[50] which is also seen here for higher urea/ammonia concentrations (Fig. 4). After some measurement cycles, our OFETs did not react any more to the addition of urea, even after long times of regeneration. This is not unexpected, since urease was expected to sustain only a limited number of reactions before degradation. Hence, the device is best used as a disposable (use once) sensor, very much in agreement with what is needed in typical healthcare applications.

Now, we compare the sensitivity of our device with other detection schemes. In electrochemical detection, the reaction is coupled to a redox species and the corresponding charge transfer is recorded. This way a detection range of 0.8–16.6 mM could be realized.[51] Another transduction mechanism is to record the potential shift of a pH sensitive device due to the change of the pH value by the hydrolysis of urea in solution.[4] A detection range of 0.05–10 mM was reported for urease functionalized polymer membranes coupled to an external FET.[52] Both schemes used Ag/AgCl reference electrodes, which are hard to miniaturize[53] and integrate into fabrication schemes. Here, we propose a detection scheme, which covers the urea range of medical samples. Our detection scheme relies on NH_3 concentration. Since the NH_3 interaction dominates electrochemical effects, it is less affected by potential changes. This makes it possible to use a simple Pt/Ir wire as a gate electrode in the electrolyte. A Pt electrode[13] can be included as a planar electrode on top of the device during fabrication of the OFET.

Conclusions

In conclusion, we demonstrated an OFET configuration, which allows the measurement of NH_3 in aqueous solution. The OFET shows a rapid current decrease within seconds due to the diffusion of NH_3 through a semipermeable parylene membrane into the organic semiconducting layer. Therefore, in applications where organic electronic devices are to work in a biological environment, undesired influences of NH_3 should be taken into account. Furthermore, such OFETs can detect physiologically relevant urea concentrations of 0.75 mM to 7.5 mM due to urea

hydrolysis into NH_3 by anchoring urease to the membrane. Regeneration of transistor current is slow, thus the device is well suited for the readout of the maximal urea dose that the device has been exposed to. In turn, the readout may be performed after exposure to *e.g.* body fluids, which may be interesting for diagnosis purposes. We expect that OFETs with thin and micro-/nanopatterned organic semiconductor layers will show improved sensitivity as well as faster response and recovery times. This case study shows that gas sensing of partial pressure[32] and sensing of molar concentration in solution are similar. In liquid, a non-polar semipermeable membrane allows us to separate neutral molecules from the charged species and stabilizes the device. This opens up interesting avenues for design of biosensors utilizing organic semiconductors.

Acknowledgements

References

1 I. Gotsman, D. Zwas, D. Planer, D. Admon, C. Lotan and A. Keren, *Medicine*, 2010, **89**, 197–203.

2 M. Singh, N. Verma, A. K. Garg and N. Redhu, *Sens. Actuators, B*, 2008, **134**, 345–351.

3 G. Dhawan, G. Sumana and B. D. Malhotra, *Biochem. Eng. J.*, 2009, **44**, 42–52.

4 D. Niwa, K. Omichi, N. Motohashi, T. Homma and T. Osaka, *Sens. Actuators, B*, 2005, **108**, 721–726.

5 A. Poghossian and M. J. Schöning, *Electroanalysis*, 2014, **26**, 1197–1213.

6 D. Khodagholy, J. Rivnay, M. Sessolo, M. Gurfinkel, P. Leleux, L. H. Jimison, E. Stavrinidou, T. Herve, S. Sanaur, R. M. Owens and G. G. Malliaras, *Nat. Commun.*, 2013, **4**, 2133.

7 P. Leleux, C. Johnson, X. Strakosas, J. Rivnay, T. Hervé, R. M. Owens and G. G. Malliaras, *Adv. Healthcare Mater.*, 2014, **3**, 1377–1380.

8 G. Scarpa, A. L. Idzko, S. Götz and S. Thalhammer, *Macromol. Biosci.*, 2010, **10**, 378–383.

9 M. L. Hammock, O. Knopfmacher, T. N. Ng, J. B. H. Tok and Z. Bao, *Adv. Mater.*, 2014, **26**, 6138–6144.

10 M. Medina-Sánchez, C. Martínez-Domingo, E. Ramon and A. Merkoçi, *Adv. Funct. Mater.*, 2014, **24**, 6291–6302.

11 E. D. Glowacki, R. R. Tangorra, H. Coskun, D. Farka, A. Operamolla, Y. Kanbur, F. Milano, L. Giotta, G. M. Farinola and N. S. Sariciftci, *J. Mater. Chem. C*, 2015, **3**, 6554–6564.

12 S. Loffler, B. Libberton and A. Richter-Dahlfors, *J. Mater. Chem. B*, 2015, **3**, 4979–4992.

13 D. A. Bernards, D. J. Macaya, M. Nikolou, J. A. DeFranco, S. Takamatsu and G. G. Malliaras, *J. Mater. Chem.*, 2008, **18**, 116–120.

14 M. Göllner, G. Glasbrenner and B. Nickel, *Electroanalysis*, 2012, **24**, 214–218.

15 F. Buth, D. Kumar, M. Stutzmann and J. A. Garrido, *Appl. Phys. Lett.*, 2011, **98**, 153302.

16 G. Palazzo, D. De Tullio, M. Magliulo, A. Mallardi, F. Intranuovo, M. Y. Mulla, P. Favia, I. Vikholm-Lundin and L. Torsi, *Adv. Mater.*, 2014, **27**, 911–916.

17 M. Demelas, S. Lai, A. Spanu, S. Martinoia, P. Cosseddu, M. Barbaro and A. Bonfiglio, *J. Mater. Chem. B*, 2013, **1**, 3811–3819.

18 M. Magliulo, K. Manoli, E. Macchia, G. Palazzo and L. Torsi, *Adv. Mater.*, 2014, DOI: 10.1002/adma.201403477.

19 D. Elkington, W. J. Belcher, P. C. Dastoor and X. J. Zhou, *Appl. Phys. Lett.*, 2014, **105**, 043303.

20 N. Coppede, G. Tarabella, M. Villani, D. Calestani, S. Iannotta and A. Zappettini, *J. Mater. Chem. B*, 2014, **2**, 5620–5626.

21 L. Kergoat, B. Piro, D. T. Simon, M.-C. Pham, V. Noël and M. Berggren, *Adv. Mater.*, 2014, **26**, 5658–5664.

22 M. Sessolo, J. Rivnay, E. Bandiello, G. G. Malliaras and H. J. Bolink, *Adv. Mater.*, 2014, **26**, 4803–4807.

23 K. Melzer, A. M. Münzer, E. Jaworska, K. Maksymiuk, A. Michalska and G. Scarpa, *Org. Electron.*, 2014, **15**, 595–601.

24 T. Minami, T. Minamiki and S. Tokito, *Chem. Commun.*, 2015, **51**, 9491–9494.

25 A. Assadi, G. Gustafsson, M. Willander, C. Svensson and O. Inganäs, *Synth. Met.*, 1990, **37**, 123–130.

26 L. Li, P. Gao, M. Baumgarten, K. Müllen, N. Lu, H. Fuchs and L. Chi, *Adv. Mater.*, 2013, **25**, 3419–3425.

27 J. W. Jeong, Y. D. Lee, Y. M. Kim, Y. W. Park, J. H. Choi, T. H. Park, C. D. Soo, S. M. Won, I. K. Han and B. K. Ju, *Sens. Actuators, B*, 2010, **146**, 40–45.

28 J. S. Yu, X. G. Yu, L. Zhang and H. J. Zeng, *Sens. Actuators, B*, 2012, **173**, 133–138.

29 X. Yu, N. Zhou, S. Han, H. Lin, D. B. Buchholz, J. Yu, R. P. H. Chang, T. J. Marks and A. Facchetti, *J. Mater. Chem. C*, 2013, **1**, 6532–6535.

30 F. Marinelli, A. Dell'Aquila, L. Torsi, J. Tey, G. P. Suranna, P. Mastrorilli, G. Romanazzi, C. F. Nobile, S. G. Mhaisalkar, N. Cioffi and F. Palmisano, *Sens. Actuators, B*, 2009, **140**, 445–450.

31 L. Torsi, A. Dodabalapur, L. Sabbatini and P. G. Zambonin, *Sens. Actuators, B*, 2000, **67**, 312–316.

32 B. Crone, A. Dodabalapur, A. Gelperin, L. Torsi, H. E. Katz, A. J. Lovinger and Z. Bao, *Appl. Phys. Lett.*, 2001, **78**, 2229.

33 W. Huang, J. Sinha, M.-L. Yeh, J. F. M. Hardigree, R. LeCover, K. Besar, A. M. Rule, P. N. Breysse and H. E. Katz, *Adv. Funct. Mater.*, 2013, **23**, 4094–4104.

34 M. E. Roberts, S. C. Mannsfeld, N. Queralto, C. Reese, J. Locklin, W. Knoll and Z. Bao, *Proc. Natl. Acad. Sci. U. S. A.*, 2008, **105**, 12134–12139.

35 H. Chen, S. Dong, M. Bai, N. Cheng, H. Wang, M. Li, H. Du, S. Hu, Y. Yang, T. Yang, F. Zhang, L. Gu, S. Meng, S. Hou and X. Guo, *Adv. Mater.*, 2015, **27**, 2113–2120.

36 M. Mirza, J. Wang, L. Wang, J. He and C. Jiang, *Org. Electron.*, 2015, **24**, 96–100.

37 F. Werkmeister and B. Nickel, *J. Mater. Chem. B*, 2013, **1**, 3830–3835.

38 T. Yamamoto and K. Takimiya, *J. Am. Chem. Soc.*, 2007, **129**, 2224–2225.

39 K. Länge, S. Grimm and M. Rapp, *Sens. Actuators, B*, 2007, **125**, 441–446.

40 C.-H. Chang, S.-Y. Yeh, B.-H. Lee, C.-W. Hsu, Y.-C. Chen, C.-J. Chen, T.-J. Lin, M. Hung-Chih Chen, C.-T. Huang and H.-Y. Chen, *J. Mater. Chem. B*, 2014, **2**, 8496–8503.

41 P. Bergveld, *ISFET, Theory and Practice*, Toronto, 2003.

42 R. G. Bates and G. D. Pinching, *J. Res. Natl. Bur. Stand.*, 1949, **42**, 419–430.

43 T. A. Kumar, E. Capua, M. Tkachev, S. N. Adler and R. Naaman, *Adv. Funct. Mater.*, 2014, **24**, 5833–5840.

44 M. L. Hammock, O. Knopfmacher, B. D. Naab, J. B. H. Tok and Z. Bao, *ACS Nano*, 2013, **7**, 3970–3980.

45 Y. S. Yeh, W. J. James and H. Yasuda, *J. Polym. Sci., Part B: Polym. Phys.*, 1990, **28**, 545–568.

46 A. Parsegian, *Nature*, 1969, **221**, 844–846.

47 S. Gritsch, P. Nollert, F. Jahnig and E. Sackmann, *Langmuir*, 1998, **14**, 3118–3125.

48 M. Göllner, M. Huth and B. Nickel, *Adv. Mater.*, 2010, **22**, 4350–4354.

49 S. C. George and S. Thomas, *Prog. Polym. Sci.*, 2001, **26**, 985–1017.

50 M. Mirza, J. Wang, D. Li, S. A. Arabi and C. Jiang, *ACS Appl. Mater. Interfaces*, 2014, **6**, 5679–5684.

51 M. Tak, V. Gupta and M. Tomar, *J. Mater. Chem. B*, 2013, **1**, 6392–6401.

52 N. C. S. Vieira, A. Figueiredo, E. G. R. Fernandes, F. E. G. Guimaraes and V. Zucolotto, *Synth. Met.*, 2013, **175**, 108–111.

53 A. W. Hassel, K. Fushimi and M. Seo, *Electrochem. Commun.*, 1999, **1**, 180–183.

59

A.4   FAST DETECTION OF BLOOD GASES BY SOLUTION GATED ORGANIC FIELD EFFECT TRANSISTORS
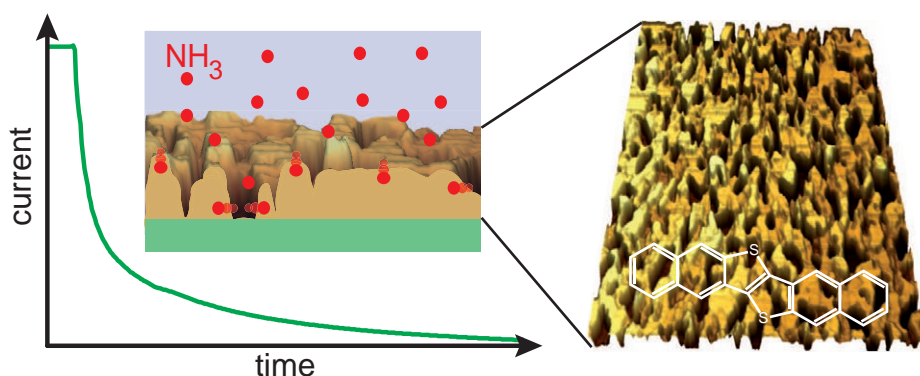
Franz X. Werkmeister, Bert A. Nickel

Abstract

We characterize the electrochemical stability of the organic semiconductor Dinaphtho[2,3-b:2',3'-f]thieno[3,2-b]thiophene (DNTT) in aqueous solutions. Electrochemical stability of DNTT in solution is validated by cyclic voltammetry and demonstrated by solution gating of DNTT organic field effect transistors (OFETs). Then, we investigate the response time of DNTT OFETs to ammonia, a common blood gas. For bare OFETs, the response time to ammonia is 1 to 2s only. The exact response time depends on the DNTT film morphology; the fastest response is obtained for pronounced 3D (Volmer-Weber) growth. By comparing OFETs with and without a semipermeable parylene-C encapsulation layer, the influence of the capping on the response time is investigated. An encapsulation layer of 86 nm prolongs the response time to 100s, indicating that parylene-C acts as an efficient diffusion barrier for ammonia.

My Contribution

I produced the samples, performed the measurements on the samples and the data evaluation. Furthermore, I wrote the manuscript draft.

Table of contents graphic

Contents lists available at ScienceDirect

Organic Electronics

journal homepage: www.elsevier.com/locate/orgel

CrossMark

Fast detection of blood gases by solution gated organic field effect transistors

Franz X. Werkmeister [a], Bert A. Nickel [a, b, *]

[a] Fakultät für Physik & CeNS, Ludwig-Maximilians-Universität München, Munich, D-80539, Germany
[b] Nanosystems Initiative Munich (NIM), D-80799, Munich, Germany

ARTICLE INFO

ABSTRACT

We characterize the electrochemical stability of the organic semiconductor Dinaphtho[2,3-b:2′,3′-f] thieno[3,2-b]thiophene (DNTT) in aqueous solutions. Electrochemical stability of DNTT in solution is validated by cyclic voltammetry and demonstrated by solution gating of DNTT organic field effect transistors (OFETs). Then, we investigate the response time of DNTT OFETs to ammonia, a common blood gas. For bare OFETs, the response time to ammonia is 1—2s only. The exact response time depends on the DNTT film morphology; the fastest response is obtained for pronounced 3D (Volmer-Weber) growth. By comparing OFETs with and without a semipermeable parylene-C encapsulation layer, the influence of the capping on the response time is investigated. An encapsulation layer of 86 nm prolongs the response time to 100s, indicating that parylene-C acts as an efficient diffusion barrier for ammonia.

1. Introduction

Due to the possibility to fabricate mechanically flexible devices [1—3], e.g. by printing techniques [1], organic transistors are heavily investigated as biosensors. Sensors are based on two different device architectures, the organic field effect transistor (OFET) and the organic electrochemical transistor (OECT). For OFETs, a charge sheet accumulates in the semiconducting channel. Detection of substances is possible via capacitive coupling of charges at the gate [4], semiconductor [5,6], or dielectric interface [7,8] or by modification of the capacitance at the interfaces [9], similar to inorganic semiconductors [10,11]. Furthermore, the mobility of charge carriers in the semiconducting layer can change [12]. OECTs operate via a gate potential mediated drift diffusion of ions into the hygroscopic semiconducting film. The ions modulate the doping and, consequently, the conductivity, and set the relevant timescale for detection [13]. As such, OECTs can translate ionic currents into electronic ones and have also found applications in e.g.

measurement of neuronal activity [14] and, with modified architectures, as ion pumps [15].

Recently, we have demonstrated an OFET based detection scheme for urea [16]. The detection relies on the enzymatic hydrolysis of urea. Urea binds to urease and hydrolyses into ammonia. Ammonia passes a semipermeable parylene-C layer and diffuses into the OFET channel, a Dinaphtho[2,3-b:2′,3′-f]thieno[3,2-b] thiophene (DNTT) [17,18] film. In the OFET channel, ammonia reduces the transistor current due to charge trapping, similar to the case of OFET ammonia gas sensors [16,19,20]. The response time of our devices was in the order of 100 s. Since transport of molecules, as well as reaction kinetics govern the response time and performance of biosensors [21], optimization of the detection time is possible by providing the analyte, here ammonia, faster access to the OFET channel. Optimal device architectures known from OFET gas sensors are laterally patterned thin films [19,22,23]; a large number of grain boundaries is also beneficial [24]. Here, we evaluate experimentally the influence of the DNTT film morphology and of the parylene-C membrane on the sensor response time. We find that Volmer-Weber growth mode of DNTT allows for a response time of bare DNTT device on the order of 1 s. Even a rather thin (86 nm) parylene-C encapsulation increases the response time considerably.

* Corresponding author. Fakultät für Physik & CeNS, Ludwig-Maximilians-Universität München, Munich, D-80539, Germany.
E-mail address: nickel@lmu.de (B.A. Nickel).

2. Materials and methods

2.1. Sample fabrication

Microscope cover slip glass slides (R. Langenbrinck) of thickness 0.2 mm were cleaned by sonication for 10 min each in aceton, isopropanol (IPA) and pure water, and used as substrates. Gate electrodes were patterned via Lift-Off process: A photo-resist bilayer of LOR 3B (4000 rpm, 40s, softbake 3 min @ 150 °C) and AZ 701 MIR (6000 rpm, 40s, softbake 1 min @ 90 °C) were formed via spin coating, patterned in a MJB 3 Maskaligner and postbaked for 1 min @ 110 °C. Development was carried out with AZ 726 MIF and subsequently 3 nm Ti and 15 nm Au deposited via E-Beam evaporation in an UHV-chamber. Lift-Off was performed by sonication in mr-Rem 400, and after Lift-Off the samples were cleaned by sonication in fresh mr-Rem 400 and IPA. SU-8 2000.5 (Micro-Chem) was patterned as the dielectric: The resist was spincoated (5000 rpm, 40s, softbake 2 min @ 95 °C), illuminated with an excessive dose (ca. 8—10 times optimal illumination dose) to create an abundance of photo activated crosslinker and postbaked 10 min at 95 °C. A second layer was patterned on top with the same parameters to reduce electrical leakage and both layers developed in mr-Dev 600. The SU-8 was then cured at 280 °C under vacuum. Source and Drain electrodes (1 nm Ti, 15 nm Au) were patterned by the same Lift-Off process as the gates and encapsulated by a thin layer of SU-8 outside of the transistor field and the contact pads. 23 nm DNTT were deposited in High Vacuum ($<10^{-6}$ mbar) through shadow masks at a deposition rate of 0.2 Å/s. OFET performance can now be checked via the bottom gate architecture. Optionally, an encapsulation layer of parylene-C can be deposited with Chemical Vapor Deposition via the Gorham route onto the OFETs.

The reference OFETs on parylene-C substrates were fabricated as previously reported [16]. Parylene-C was deposited via chemical vapor deposition in a SCS PDS 2010 labcoater.

The prepared OFETs are glued to a prepared Ibidi flow-chamber with a Pt wire (PT005127, GoodFellow) as previously reported [16].

2.2. Measurements

AFM micrographs were recorded with a Veeco Dimension 3100 AFM in tapping mode and evaluated with Gwyddion.

Electrical measurements were performed with two Keithley 2612 SMUs and a Keithley 7072 switching matrix card. The OFETs were operated with common gates, while source and drains were hot-switched through. Typical Source-Drain Voltages are −0.3 V and Source-electrolyte voltages in the range −0.6 V to 0.2 V, depending on device architecture. Measurements were done in ambient at 20 °C. Transistor parameters were extracted from the transistor behavior in the saturation regime, which is described by the equation:

$$I_{SD} = \frac{W}{2L} * C * \mu * (V_{Gate} - V_T)^2, \qquad (1)$$

W is the channel width, L the channel length, C the areal capacitance coupling the gate to the channel, μ the mobility of the organic semiconductor, V_{Gate} the applied gate voltage, and V_T the threshold voltage.

Electrochemical measurements were performed with a three electrode setup with a Pt-counter electrode and a leakage-free Ag/AgCl reference electrode (Warner instruments). An Ivium CompactStat was used for the cyclic voltammetry and impedance spectroscopy. For the later, the oscillation amplitude was 10 mV. The data was evaluated with the software IviumSoft.

3. Results and discussion

Electrolyte gated organic field effect transistors (EGOFETs) are appealing, because the electrical double layers at the gate to electrolyte and electrolyte to semiconductor interface exhibit high capacitances [25—28]. Furthermore, it seems favorable for the response time of the device to have the sensitive region, i.e. the conducting channel, at the sensor's interface. Electrolyte gated OFETs (EGOFETs) [25] are feasible, if the electrochemical stability of the organic semiconductor permits to apply the gate potential *via* the electrolyte without driving chemical reactions at the semiconductor interface [29,30]. Here we test the operation of DNTT OFETs in electrolyte without additional parylene-C encapsulation. For this purpose, we investigate first the electrochemical stability of DNTT films on Au electrodes by cyclic voltammetry (CV) [31]. Cyclic voltammetry measurements were performed with a three electrode setup. An Ag/AgCl was used as reference electrode in combination with a Pt counter electrode. The working electrode was a 30 nm DNTT layer on an Au film. In order to facilitate DNTT growth, the Au layer was coated with SU-8, baked, and subsequently SU-8 was removed with solvent before deposition of DNTT. The DNTT working electrode was exposed to the electrolyte with an area of 16 mm². The electrolyte was a 1 mM NaCl solution, which was degassed before the experiment. The resulting cyclic voltammogram displays a set of peaks at 0.38 V and 0.63 V vs. Ag/AgCl (Fig. 1 a). These peaks could be measured for several cycles with different scan rates (supporting info Fig. S1), indicating a reversible oxidation of this molecular energy
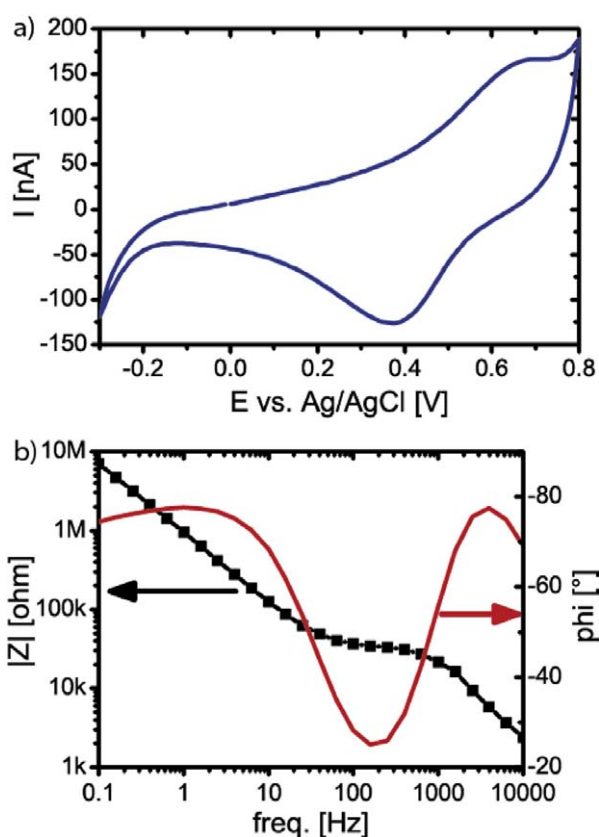

Fig. 1. a) Cyclic voltammegram of a DNTT film coated onto the working electrode at a sweeping rate of 10 mV/s in 1 mM NaCl. b) Impedance spectrum recorded on the same sample as in a) with 10 mV amplitude.

level. The corresponding energy level on absolute scale, i.e. against vacuum level, is −5.2 eV ± 0.05 eV. This energy level can be interpreted as the hole transport level of the DNTT thin film [32] in good agreement with frontier level calculations of −5.19 eV [17]. Previously, a slightly different experimental value of −5.44 eV was measured using an anhydrous electrolyte [17]. Capacitive coupling can be inferred from the impedance spectrum recorded at 0 V potential offset, which displayed a phase angle of close to −80° at frequencies below 100 Hz (Fig. 1 b) [33]. From the CV measurements, we estimate that an electrolyte gate potential of up to −0.5 V can be applied to DNTT based OFETs via a Pt gate electrode, which is set off by ca. 0.2 V from the Ag/AgCl reference electrode used for the CV measurements [31].

Next, we gate DNTT based OFETs via the electrolyte. First, we fabricated bottom-gate, bottom-contact OFETs. The additional bottom gate enabled us to test and optimize fabrication yield before operation in electrolyte. The negative-tone photoresist SU-8 (2000.5) served as gate insulator layer. SU-8 was reported before to provide a dielectric layer suitable for fabrication of OFETs and application of photolithography steps for pattern definition [34]. The Au gate as well as source and drain electrodes were patterned by photolithography via a lift-off process. The electrical leads were passivated against the electrolyte by an additional SU-8 layer. The organic semiconductor DNTT was physical vapor deposited to a thickness of ca. 23 nm. A capping layer on the DNTT was omitted, i.e. the electrolyte, a 10 mM Dulbecco's Phosphate Buffered Saline Solution (DPBS), was in direct contact with DNTT surface. We restrict the gate voltage to a maximum potential of −0.5 V applied via a Pt-wire. A Pt-wire was chosen, since Pt could be easily implemented as a planar Pt-electrode. In this configuration, we observed typical OFET behavior, see Fig. 2. Since the EGOFETs displayed sufficient drain current at gate potentials lower than −0.4 V, we further limited the gate voltage window to this value for subsequent measurements (Fig. 2 a). As visible from the data, peak current decreased slightly from −8.58 μA to −8.37 μA, while the hysteresis increased. Drift of EGOFETs in solutions of physiological strength is a known issue, which can be solved by application of a thin capping layer [35].

Since high ammonia concentrations shift the pH value of the electrolyte, we tested the pH response of the DNTT EGOFETs. A pH value of 10 mM DPBS solution was adjusted with NaOH and HCl, and the transconductance curve of the EGOFETs was recorded (supporting info Fig. S2). The threshold voltage shifted 14 mV per decade pH for pH values between 5.5 and 10.3; a steeper shift was observed towards a pH value of 3.65 (Fig. 2b). The sign of the threshold voltage shift per pH points towards the Pt electrode-electrolyte as the pH sensitive interface. That is, the surface groups at the polarizable Pt electrodes dominate the pH response [36]. Correlated with the threshold voltage shifts, the slope of the transfer curves shifts (supporting info Fig. S3). For lower pH values, the slope increases and thus the charge carrier density or mobility. This could originate from protonic doping of the hole conducting organic semiconductor DNTT [37]. Another potential reason could be gate potential dependent mobility [38]. The data also reveal that the DNTT based EGOFETs operate stable in a wide range of acidic (pH = 3.65) to basic (pH = 10.3) conditions. A similar stability for OFETs operated in solution has so far been demonstrated only for few examples, namely for epindolidiones and α-sexithiophene (6T). Epindolidione based OFETs were operated in direct contact with the electrolyte at pH values ranging of 3–10, however these OFETS were gated via back gate [39] while 6T based OEFTs were solution gated in a pH range of ca. 2–10 [40].

The pH stability allows us to determine the time response of bare DNTT FETs to ammonia exposure. For this purpose, the EGOFETs were exposed to a 10 mM ammonia solution. Upon
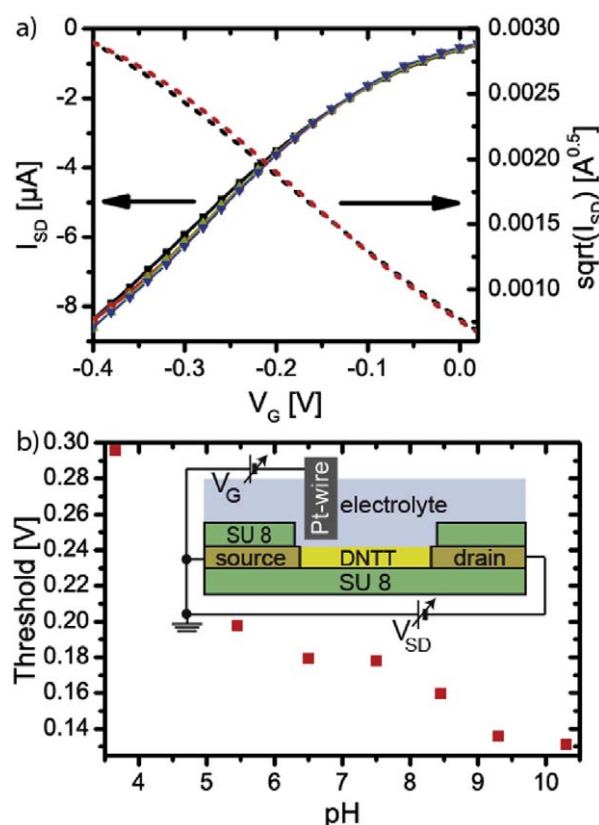

Fig. 2. a) Transconductance curves of a solution gated DNTT based OFET with $V_{SD} = -0.3$ V. Green upward facing triangles give the forward sweep direction and blue downward facing triangles the backward sweep direction. Data for transconductance after 30 min of operation is given by black (squares) for the forward sweep direction, and red (circles) for the backward sweep direction. b) Dependence of the threshold voltage on pH of the solution. (For interpretation of the references to colour in this figure legend, the reader is referred to the web version of this article.)

injection of the ammonia into the buffer solution, the drain current dropped rapidly within 1 s, and stabilized within several seconds (Fig. 3 a). This response is orders of magnitude faster than our previous devices that used a parylene-C encapsulation. Since our previous design uses also a parylene-C gate dielectric, we fabricated for comparison a device that has a parylene-C gate dielectric omitting the parylene-C capping. This device does not perform as good as the SU-8 device, i.e. the reduction in drain current is less pronounced and the response time is slower (Fig. 3 a). We observed that the lift-off process used promotes a pronounced DNTT film morphology of discrete islands of typically 100 nm lateral size on SU-8 (Fig. 3 b, supporting info Fig. S4). These islands percolate only rather late during growth, similar to growth of pentacene on low surface-energy polyimides [41]. In turn, the DNTT film on SU-8 has a rather open surface structure compared to DNTT films on parylene, which show a dense grainy texture (Fig. 3 c). A large surface is beneficial for OFET based gas sensors, and methods to increase the surface artificially by lateral structuring have been developed [19]. Here, the DNTT growth was apparently optimized by the surface modification during lift off, which favored Vollmer Weber (3D) growth and boosts response behavior.

Next, we test the influence of a thin parylene-C encapsulation on response time. For this purpose, a transistor with an 86 nm parylene-C encapsulation layer was fabricated. For this device, the
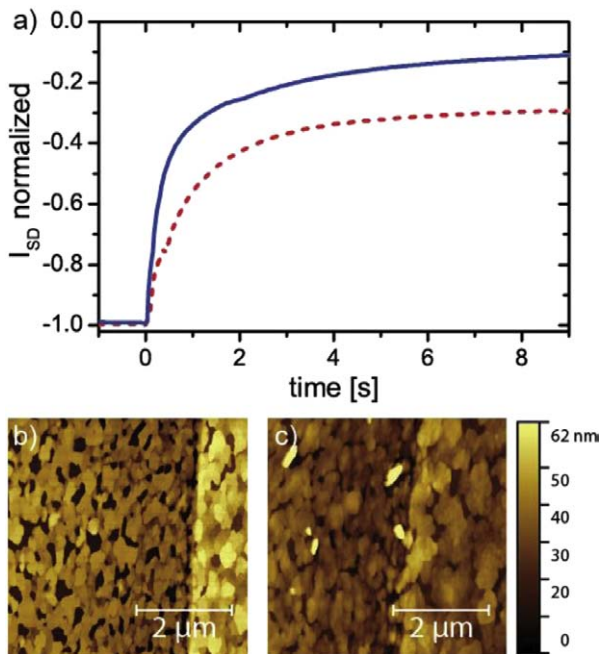
Fig. 3. a) Time trace of solution gated OFET current reduction upon injection of 10 mM ammonia. $V_{SD} = -0.3$ V and $V_{gate} = -0.3$ V. The curve in blue is for the presented OFETs on SU-8, the red dashed curve displays the response of OFETs fabricated on parylene-C substrate as in Ref. [16]. b) AFM micrograph of DNTT grown on SU-8 dielectric and c) of DNTT grown on parylene-C dielectric. To the left is the transistor channel, to the right the Au source/drain electrode. The z-scale applies to both AFM micrographs. (For interpretation of the references to colour in this figure legend, the reader is referred to the web version of this article.)

drain current reduction after ammonia injection occurs on two timescales, initially a fast drop within 1 s as observed for the bare device and subsequently a much slower response (Fig. 4). The initial fast response may be due to pinholes in the parylene-C film. The slow response with a characteristic timescale of several 100 s is apparently caused by the encapsulation layer acting like a barrier. The passage of the ammonia through the parylene-C layer can be modeled by a 1D diffusion process [16,37].
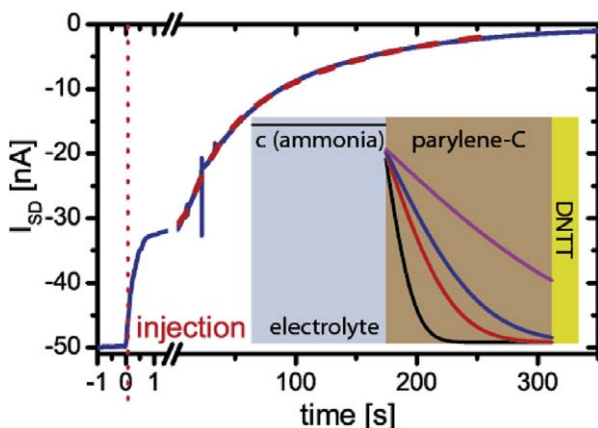

Fig. 4. b) Time trace of current reduction of a parylene-C encapsulated OFET upon injection of 10 mM ammonia. $V_{SD} = -0.3$ V and $V_{gate} = -0.6$ V. The inset displays the evolution of ammonia concentrations within a 100 nm parylene-C layer according to eq. (2). The black trace is for a time of 1s, the red trace for 5s, the blue trace for 10s, and the magenta trace for 50 s. (For interpretation of the references to colour in this figure legend, the reader is referred to the web version of this article.)

$$n(x,t) = n_0 \, erfc\left(\frac{x}{2\sqrt{Dt}}\right) \tag{2}$$

Here, the ammonia concentration profile $n(x,t)$ propagates from a constant reservoir with concentration n_0 into the material layer. The diffusion in the parylene-C layer after time t and depth x is controlled by the diffusion constant D according to relation (2). For the data analysis in Fig. 3b, the assumption is made that the OFET current reduction $n(L,t)$ scales with the concentration of ammonia at the organic semiconductor interface $(x = L)$, according to the idea that current reduction is caused by hole trapping due to ammonia intercalation. Thus, the drain current $I(t)$ is given by $I(t) = I_0 - n(L,t)$. Within this model, the slow response time for the thin capping device can be explained by an diffusion constant of $D = 9 \cdot 10^{-13}$ cm^2/s for ammonia in parylene-C, which is in agreement with our previous results [16]. This confirms that even a thin film of parylene-C acts as an efficient diffusion barrier for ammonia slowing down the response time considerably.

In previous experiments, the regeneration of the OFETs after ammonia exposure was rather slow. We tested if the improved response time is accompanied by a faster recovery; we find that this is not the case (supporting info Fig. S5). Upon rinsing the device with buffer solution, part of the drain current recovers rapidly, while most of the effect prevails. This suggests that the slow recovery is mainly due to absorption and binding of ammonia to the DNTT film. The OEFTs could be regenerated in a desiccator, thus the binding appears to be reversible. On the other hand, the sensitivity of the bare DNTT device is clearly improved. Previously, the ammonia detection limit was at 1 mM [16]. With the improved morphology, and without parylene-C encapsulation, a 1 mM concentration of ammonia induces still a pronounced drain current reduction, cf. supporting info Fig. S5 b. Noise upon solution flow, an issue reported in literature [5], prevented examination of transient current response for lower ammonia concentrations. Interestingly, such effects are less pronounced during active gate voltage sweeps. For transfer curves, the effect of ammonia down to ammonia concentrations of 0.1 mM can be measured (supporting info Fig. S6). A level of 0.1 mM ammonia in blood is indicative of acute disease, normal concentrations are below 0.05 mM [42]. With further improvements, organic transistors may be able to provide a point-of-care measurement platform for this blood gas, if reliable control of drift is obtained.

Initially, our intention was to employ the parylene-C encapsulation as a semipermeable hydrophobic membrane keeping ions away from the semiconductor surface while neutral ammonia can pass. In view of the electrochemical stability of DNTT, this seems obsolete, since the DNTT layer itself is hydrophobic enough to exclude the ions from the semiconducting layer. Another benefit of the parylene-C layer is that it can be plasma activated in order to covalently bind urease for enzymatic detection of urea. Further, encapsulation helps to stabilize EGOFETs output in solutions of physiological strength [35]. Given the observation that the parylene-C coating slows down detection, other ultrathin hydrophobic barriers, such as lipid bilayers, should be explored for surface functionalization [35,43,44].

4. Conclusion

DNTT based OFETs are electrochemically stable for solution gating. The response time of solution-gated DNTT OFETs for ammonia concentrations down to 1 mM OFETS is as low as 1s. A less than 100 nm thin parylene-C encapsulation layer delays the response time to 100 s by acting as a diffusion barrier. Consequently, thinner encapsulation layers such as lipid bilayers are

desirable for functionalization of OFET sensors. Next, the regeneration of the OFETs after ammonia exposure requires attention. If the regeneration can be accelerated, such OFETs will be interesting to measure cellular signaling.

Acknowledgements

Appendix A. Supplementary data

Supplementary data related to this article can be found at http://dx.doi.org/10.1016/j.orgel.2016.09.025.

References

[1] M. Medina-Sánchez, C. Martínez-Domingo, E. Ramon, A. Merkoçi, An inkjet-printed field-effect transistor for label-free biosensing, Adv. Funct. Mater. 24 (2014) 6291–6302.

[2] F. Werkmeister, B. Nickel, Towards flexible organic thin film transistors (OTFTs) for biosensing, J. Mater. Chem. B 1 (2013) 3830–3835.

[3] K. Manoli, M. Magliulo, M.Y. Mulla, M. Singh, L. Sabbatini, G. Palazzo, L. Torsi, Printable bioelectronics to investigate functional biological interfaces, Angew. Chem. Int. Ed. 54 (2015) 12562–12576.

[4] M. Demelas, S. Lai, A. Spanu, S. Martinoia, P. Cosseddu, M. Barbaro, A. Bonfiglio, Charge sensing by organic charge-modulated field effect transistors: application to the detection of bio-related effects, J. Mater. Chem. B 1 (2013) 3811–3819.

[5] M.L. Hammock, O. Knopfmacher, B.D. Naab, J.B.H. Tok, Z. Bao, Investigation of protein detection parameters using nanofunctionalized organic field-effect transistors, ACS Nano 7 (2013) 3970–3980.

[6] L. Kergoat, B. Piro, M. Berggren, M.C. Pham, A. Yassar, G. Horowitz, DNA detection with a water-gated organic field-effect transistor, Org. Electron. 13 (2012) 1–6.

[7] L. Göllner, G. Glasbrenner, B. Nickel, An electrochemical transducer based on a pentacene double-gate thin-film transistor, Electroanalysis 24 (2012) 214–218.

[8] H.U. Khan, M.E. Roberts, W. Knoll, Z.A. Bao, Pentacene based organic thin film transistors as the transducer for biochemical sensing in aqueous media, Chem. Mater. 23 (2011) 1946–1953.

[9] G. Palazzo, D. De Tullio, M. Magliulo, A. Mallardi, F. Intranuovo, M.Y. Mulla, P. Favia, I. Vikholm-Lundin, L. Torsi, Detection beyond Debye's length with an electrolyte-gated organic field-effect transistor, Adv. Mater. 27 (2014) 911–916.

[10] A. Poghossian, M.J. Schöning, Label-free sensing of biomolecules with field-effect devices for clinical applications, Electroanalysis 26 (2014) 1197–1213.

[11] E. Bandiello, M. Sessolo, H.J. Bolink, Electrolyte-gated nanostructured ZnO transistors for environmental and biological sensing, J. Mater. Chem. C 2 (48) (2014) 10277–10281.

[12] M. Magliulo, K. Manoli, E. Macchia, G. Palazzo, L. Torsi, Tailoring functional interlayers in organic field-effect transistor biosensors, Adv. Mater. 27 (2015) 7528–7551.

[13] D.A. Bernards, D.J. Macaya, M. Nikolou, J.A. DeFranco, S. Takamatsu, G.G. Malliaras, Enzymatic sensing with organic electrochemical transistors, J. Mater. Chem. 18 (2008) 116–120.

[14] D. Khodagholy, T. Doublet, M. Gurfinkel, P. Quilichini, E. Ismailova, P. Leleux, T. Herve, S. Sanaur, C. Bernard, G.G. Malliaras, Highly conformable conducting polymer electrodes for in vivo recordings, Adv. Mater. 23 (2011) H268–H272.

[15] A. Jonsson, Z. Song, D. Nilsson, B.A. Meyerson, D.T. Simon, B. Linderoth, M. Berggren, Therapy using implanted organic bioelectronics, Sci. Adv. 1 (2015).

[16] F.X. Werkmeister, T. Koide, B.A. Nickel, Ammonia sensing for enzymatic urea detection with organic field effect transistors and a semipermeable membrane, J. Mater. Chem. B 4 (2016) 162–168.

[17] T. Yamamoto, K. Takimiya, Facile synthesis of highly pi-extended heteroarenes, dinaphtho[2,3-b:2',3'-f]chalcogenopheno[3,2-b]chalcogenophenes, and their application to field-effect transistors, J. Am. Chem. Soc. 129 (2007) 2224–2225.

[18] U. Zschieschang, F. Ante, D. Kälblein, T. Yamamoto, K. Takimiya, H. Kuwabara, M. Ikeda, T. Sekitani, T. Someya, J.B. Nimoth, H. Klauk, Dinaphtho[2,3-b:2′,3′-f]thieno[3,2-b]thiophene (DNTT) thin-film transistors with improved performance and stability, Org. Electron. 12 (2011) 1370–1375.

[19] L. Li, P. Gao, M. Baumgarten, K. Müllen, N. Lu, H. Fuchs, L. Chi, High

[20] performance field-effect ammonia sensors based on a structured ultrathin organic semiconductor film, Adv. Mater. 25 (2013) 3419–3425.

[20] B. Crone, A. Dodabalapur, A. Gelperin, L. Torsi, H.E. Katz, A.J. Lovinger, Z. Bao, Electronic sensing of vapors with organic transistors, Appl. Phys. Lett. 78 (2001) 2229.

[21] T.M. Squires, R.J. Messinger, S.R. Manalis, Making it stick: convection, reaction and diffusion in surface-based biosensors, Nat. Biotech. 26 (2008) 417–426.

[22] M. Mirza, J. Wang, D. Li, S.A. Arabi, C. Jiang, Novel top-contact monolayer pentacene-based thin-film transistor for ammonia gas detection, ACS Appl. Mater Interfaces 6 (2014) 5679–5684.

[23] A.-M. Andringa, M.-J. Spijkman, E.C.P. Smits, S.G.J. Mathijssen, P.A.V. Hal, S. Setayesh, N.P. Willard, O.V. Borshchev, S.A. Ponomarenko, P.W.M. Blom, D.M. de Leeuw, Gas sensing with self-assembled monolayer field-effect transistors, Org. Electron. 11 (2010) 895–898.

[24] L. Torsi, A.J. Lovinger, B. Crone, T. Someya, A. Dodabalapur, H.E. Katz, A. Gelperin, Correlation between oligothiophene thin film transistor morphology and vapor responses, J. Phys. Chem. B 106 (2002) 12563–12568.

[25] L. Kergoat, L. Herlogsson, D. Braga, B. Piro, M.C. Pham, X. Crispin, M. Berggren, G. Horowitz, A water-gate organic field-effect transistor, Adv. Mater. 22 (2010) 2565–2569.

[26] J. Lee, L.G. Kaake, J.H. Cho, X.Y. Zhu, T.P. Lodge, C.D. Frisbie, Ion gel-gated polymer thin-film transistors: operating mechanism and characterization of gate dielectric capacitance, switching speed, and stability, J. Phys. Chem. C 113 (2009) 8972–8981.

[27] R. Porrazzo, S. Bellani, A. Luzio, E. Lanzarini, M. Caironi, M.R. Antognazza, Improving mobility and electrochemical stability of a water-gated polymer field-effect transistor, Org. Electron. 15 (2014) 2126–2134.

[28] R.F. de Oliveira, L. Merces, T.P. Vello, C.C. Bof Bufon, Water-gated phthalocyanine transistors: operation and transduction of the peptide–enzyme interaction, Org. Electron. 31 (2016) 217–226.

[29] F. Buth, D. Kumar, M. Stutzmann, J.A. Garrido, Electrolyte-gated organic field-effect transistors for sensing applications, Appl. Phys. Lett. 98 (2011) 153302.

[30] T. Cramer, B. Chelli, M. Murgia, M. Barbalinardo, E. Bystrenova, D.M. de Leeuw, F. Biscarini, Organic ultra-thin film transistors with a liquid gate for extracellular stimulation and recording of electric activity of stem cell-derived neuronal networks, Phys. Chem. Chem. Phys. 15 (2013) 3897–3905.

[31] A.J. Bard, L.R. Faulkner, Electrochemical Methods: Fundamentals and Applications, second ed., Wiley, New York, 2001.

[32] A. Kahn, Fermi level, work function and vacuum level, Mater. Horizons 3 (1) (2016) 7–10.

[33] H. Toss, C. Suspène, B. Piro, A. Yassar, X. Crispin, L. Kergoat, M.-C. Pham, M. Berggren, On the mode of operation in electrolyte-gated thin film transistors based on different substituted polythiophenes, Org. Electron. 15 (2014) 2420–2427.

[34] C.H. Kim, D. Tondelier, B. Geffroy, Y. Bonnassieux, G. Horowitz, Characterization of the pentacene thin-film transistors with an epoxy resin-based polymeric gate insulator, Eur. Phys. J. Appl. Phys. 57 (2011) 20201.

[35] M. Magliulo, A. Mallardi, M.Y. Mulla, S. Cotrone, B.R. Pistillo, P. Favia, I. Vikholm-Lundin, G. Palazzo, L. Torsi, Electrolyte-gated organic field-effect transistor sensors based on supported biotinylated phospholipid bilayer, Adv. Mater. 25 (2013) 2090–2094.

[36] S. Park, H. Boo, Y. Kim, J.-H. Han, H.C. Kim, T.D. Chung, pH-sensitive solid-state electrode based on electrodeposited nanoporous platinum, Anal. Chem. 77 (2005) 7695–7701.

[37] D. Elkington, W.J. Belcher, P.C. Dastoor, X.J. Zhou, Detection of saliva-range glucose concentrations using organic thin-film transistors, Appl. Phys. Lett. 105 (2014) 043303.

[38] K. Ryu, I. Kymissis, V. Bulovic, C.G. Sodini, Direct extraction of mobility in pentacene OFETs using C-V and I-V measurements, IEEE Electron Device Lett. 26 (2005) 716–718.

[39] E.D. Głowacki, G. Romanazzi, C. Yumusak, H. Coskun, U. Monkowius, G. Voss, M. Burian, R.T. Lechner, N. Demitri, G.J. Redhammer, N. Sünger, G.P. Suranna, S. Sariciftci, Epindolidiones-versatile and stable hydrogen-bonded pigments for organic field-effect transistors and light-emitting diodes, Adv. Funct. Mater. 25 (2015) 776–787.

[40] F. Buth, A. Donner, M. Sachsenhauser, M. Stutzmann, J.A. Garrido, Biofunctional electrolyte-gated organic field-effect transistors, Adv. Mater. 24 (2012) 4511–4517.

[41] S.Y. Yang, K. Shin, S.H. Kim, H. Jeon, J.H. Kang, H.C. Yang, C.E. Park, Enhanced electrical percolation due to interconnection of three-dimensional pentacene islands in thin films on low surface energy polyimide gate dielectrics, J. Phys. Chem. B 110 (2006) 20302–20307.

[42] H. McCullough, The determination of ammonia in whole blood by a direct colorimetric method, Clin. Chim. Acta 17 (1967) 297–304.

[43] M.Y. Mulla, P. Seshadri, L. Torsi, K. Manoli, A. Mallardi, N. Ditaranto, M.V. Santacroce, C. Di Franco, G. Scamarcio, M. Magliulo, UV crosslinked poly(acrylic acid): a simple method to bio-functionalize electrolyte-gated OFET biosensors, J. Mater. Chem. B 3 (2015) 5049–5057.

[44] S. Cotrone, M. Ambrico, H. Toss, M.D. Angione, M. Magliulo, A. Mallardi, M. Berggren, G. Palazzo, G. Horowitz, T. Ligonzo, L. Torsi, Phospholipid film in electrolyte-gated organic field-effect transistors, Org. Electron. 13 (2012) 638–644.

APPENDIX B

SUPPORTING INFORMATION

B.1 SUPPORTING INFORMATION FOR "SUB-MONOLAYER PERCOLATION OF PENTACENE ON ROUGH PARYLENE-C DIELECTRICS"

[1]These authors contributed equally.

SUPPORTING INFORMATION

1

Figure S1. Height-height-correlation-function (HHCF) analysis of AFM micrographs of different sizes. a) 5x5 µm micrograph and the respective HHCF (black) with Gaussian fit (red). From the fit, the correlation length is 169 nm and the rms 6.0 nm. b) 3x3 µm micrograph and the respective HHCF (black) with Gaussian fit (red). From the fit, the correlation length is 167 nm and the rms 7.2 nm. c) 0.3x0.3 µm micrograph and the respective HHCF (black) with Gaussian fit (red). From the fit, the correlation length is 53 nm and the rms 3.7 nm. The significant drop in rms roughness and correlation length with decreased scan size implies that one would need to measure at even smaller length scales, i.e. beyond the resolution limit of our AFM, to evaluate the surface with respect to molecular ordering. The height scale for all micrographs is 50 nm.
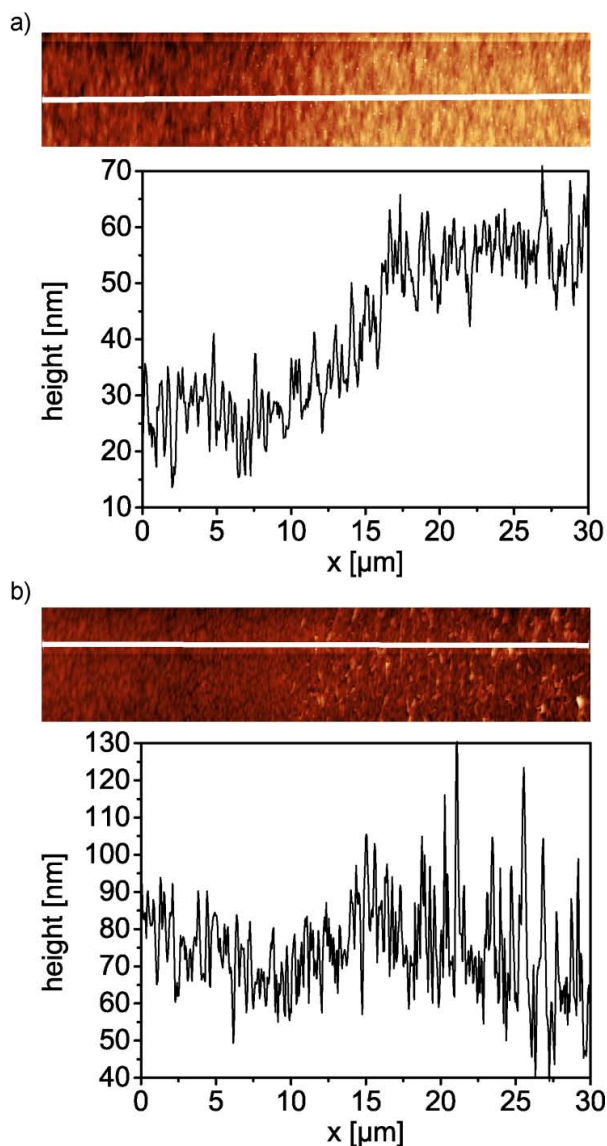
Figure S2. Height profiles of Au electrode edges on parylene-C surface. a) AFM micrograph (length: 30 μm, scale: 80 nm) of the pure gold electrode grown on parylene-C and a profile cut from left to right. The 30 nm Au electrode edge is clearly visible in the profile. b) AFM micrograph (length: 30 μm, scale: 170 nm) of the Au electrode edge topped with a 50 nm layer of pentacene and a profile cut from left to right. The 30 nm Au electrode can be discerned in the profile, while it is difficult to see it beneath the

pentacene layer in the topography image due to plane correction. Only the change in pentacene growth indicates the subjacent electrode. The white lines in the AFM micrographs indicate the profile positions.

4

B.2 SUPPORTING INFORMATION FOR "AMMONIA SENSING FOR ENZYMATIC UREA DETECTION WITH ORGANIC FIELD EFFECT TRANSISTORS AND A SEMIPERMEABLE MEMBRANE"

Electronic Supplementary Information

Urea detection in buffer solution with organic field effect transistors and a semipermeable membrane as top gate dielectric

Franz Werkmeister, Teru Koide, Bert Nickel

Evaluation of parylene-C as top-gate dielectric:

In prior experiments, we have identified tetratetracontane (TTC), a paraffin wax, as possible encapsulation material[1]. The main problem of the wax is that it is rather fragile, thus the long term stability is limited. A polymer layer of cross linked parylene-C has much better mechanical stability.

For this optimization process, double gate OFETs were produced: Gate electrodes were patterned via a Lift-Off process: 15 nm of Au were deposited followed by 6 nm of Al and the Lift-Off was performed with 1165 Remover. An etch stop mask was defined from ma-P 1275 developed with ma-D 331 on the gate contact pads. Subsequently, nominally 1.7 µm parylene-C were deposited as the bottom gate dielectric. The thickness of the parylene layer was measured on glass slides using UV-VIS spectroscopy from the distance of the minima in transmission. An etch mask was fabricated on top of the bottom gate dielectric using again ma-P 1275 and the parylene-C dielectric layer patterned by reactive ion etching (RIE) in a parallel plate RIE chamber with a power of 200 W and 50 sccm O_2. Onto an OFET with pentacene as the organic semiconducting layer (13 nm of pentacene, Sigma 698423, purified by one sublimation run by CreaPhys GmbH), we deposited 100 nm parylene-C. This layer deposition caused some minor damage to the organic semiconducting film[2], see also **Fig. S1.**
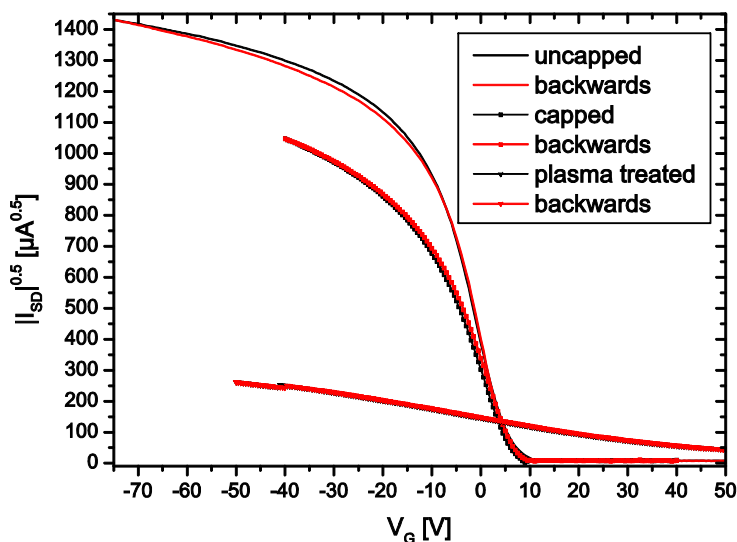
Supporting Figure S1: *Evolution of a pentacene transistor after capping and oxygen plasma treatment. The source drain voltage was -0.3 V.*

To evaluate the sealing properties of the parylene coating, we deposited a 14 nm thick pentacene film onto an Au electrode and encapsulated it with a thin parylene layer. The pentacene oxidation/reduction peak, which is a major contribution to Faradaic currents in bare pentacene films, was absent in cyclic voltammetry experiments with encapsulated films (see **Fig. S2**). This showed that the passivation layer prevents charge transport between pentacene and the electrolyte.
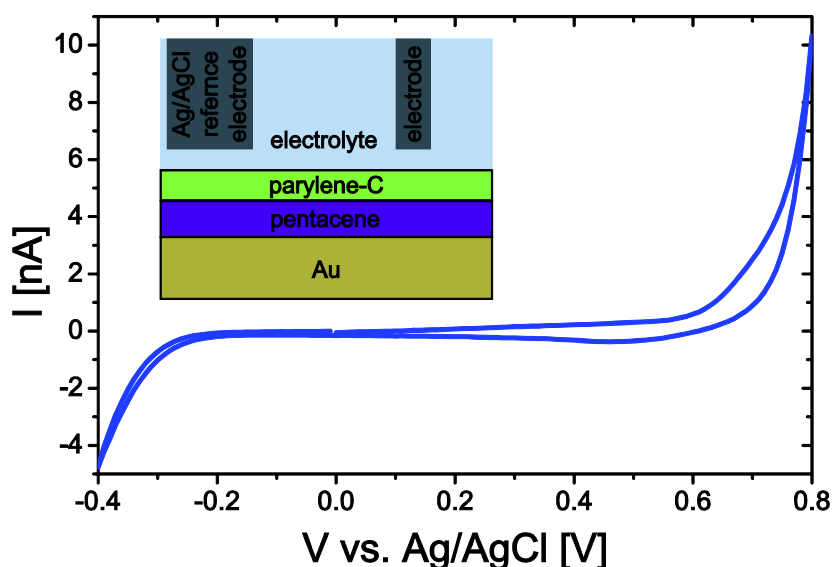
Supporting Figure S2: *Cyclic Voltametry of capped pentacene layer. Cyclic voltametry of a pentacene layer capped with parylene-C on the Au working electrode in a three electrode setup. Ag/AgCl was the reference electrode and a Pt electrode the counter electrode. The electrolyte was 10 mM DPBS. The measurement was performed using an Ivium CompactStat.*

Next, we used a thin parylene-C layer as the top gate dielectric to fabricate Double Gate Organic Field Effect Transistors (DG-OFETs). The top gate was a Pt/Ir wire in 10 mM Dulbecco's phosphate buffered saline (DPBS) electrolyte buffer. For this purpose, the sample was glued in a commercial flow chamber. Since the nominal thickness of the organic semiconductor was below 20 nm, we expected it to be below Debye length.[3] In this case, the advantage of the DG-OFET geometry is that the top gate threshold voltage can be adjusted by the bottom gate voltage in order to maximize the transconductance for the top gate.[4] This behavior is confirmed in **Fig. S3 b**.

Here, the threshold voltage of the top gate was shifted by 0.2 V, when the bottom gate voltage change was 10 V. This proofed that a thin parylene-C layer is suited as a top gate dielectric layer. Pentacene is known to oxidize in the presence of oxygen[5] therefore it is no surprise that the OFETs based on pentacene did not stand oxygen plasma treatment for the attachment of urease (see **Fig. S1**). Therefore we replaced pentacene with Dinaphtho[2,3-b:2',3'-*f*]thieno[3,2-*b*]thiophene (DNTT), an oxygen stable organic semiconductor[6] to maintain transistor performance upon plasma treatment (see **Fig. S4**).
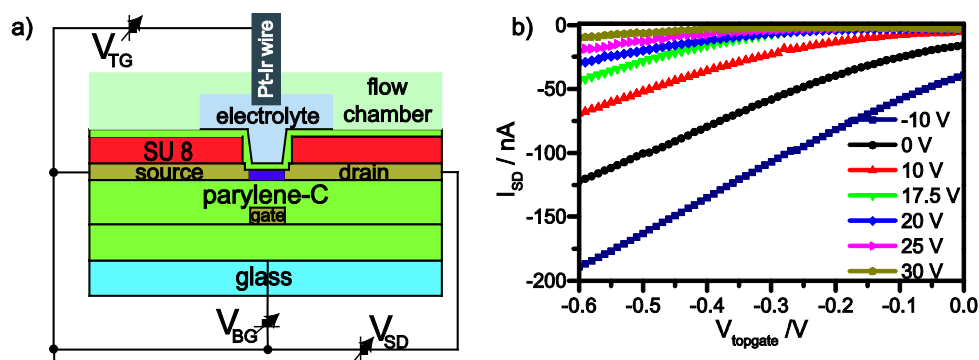
Supporting Figure S3: a) *Schematic of the device architecture and measurement scheme for the characterization of the DG-OFETs in solution.* b) *Top gate transconductance curve with different bottom gate voltages applied as indicated in the graph at V_{SD} = - 0.3 V.*
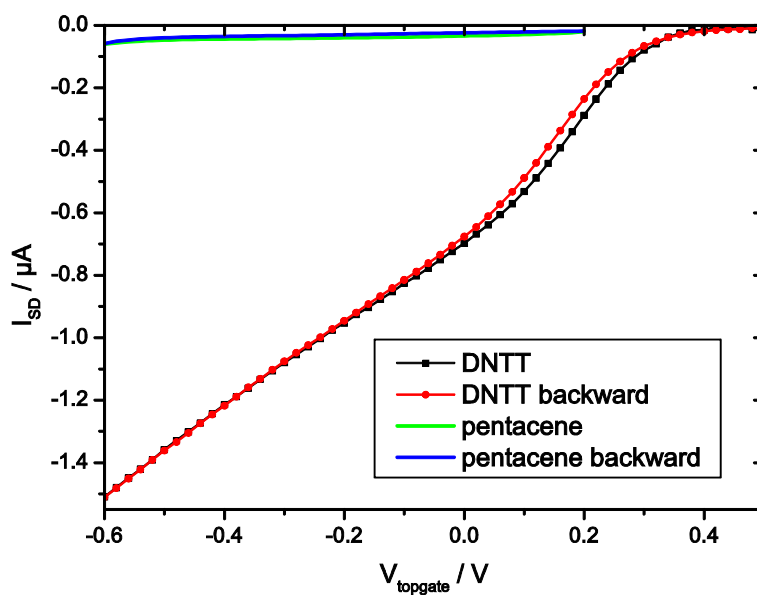
Supporting Figure S4: *Comparison between electrolyte gated sweeps of a plasma treated pentacene transistor and a DNTT based one, which was fully functionalized, at V_{SD} = - 0.3 V. While the degradation of pentacene during the oxygen plasma treatment decreased the performance, the DNTT based transistor showed acceptable performance after the functionalization steps. The source drain current was corrected for leakage current through the electrolyte, which got non-negligible for positive gate voltages, as previously reported[1].*

Urease activity evaluation:
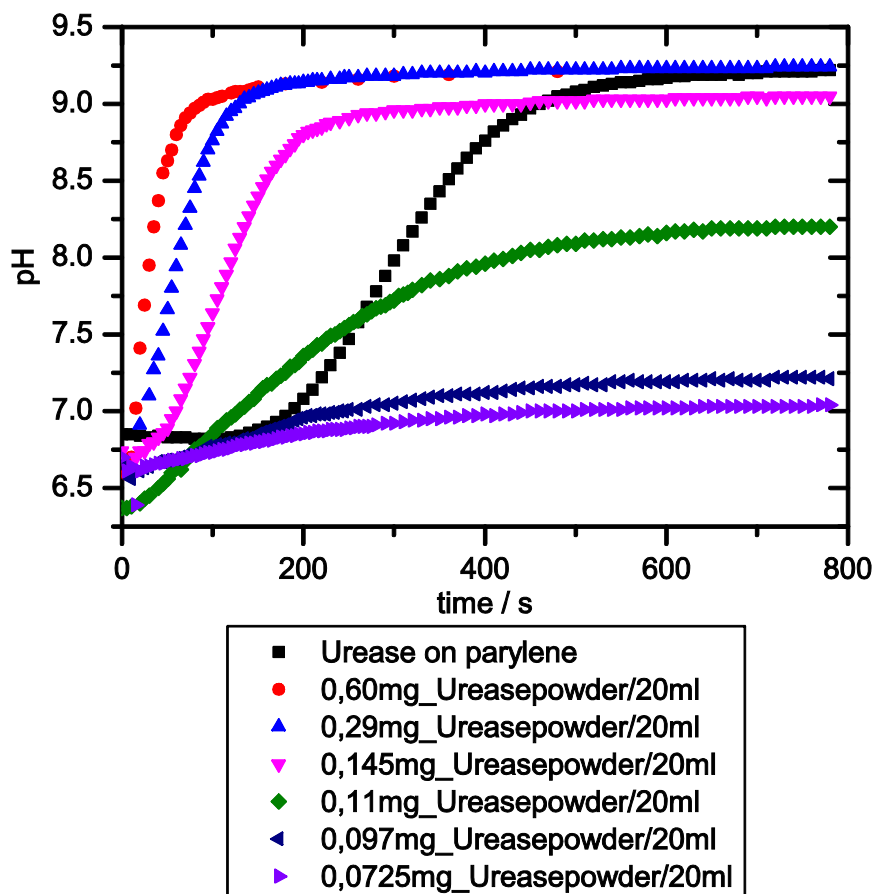
Supporting Figure S5: *pH measurement of urease activity in Milli-Q water without buffer. 20 ml of 10 mM urea solution dissolved in Milli-Q water were left to stabilize the pH value. Then the indicated amount of urease or a functionalized parylene coating were added to the solution and the evolution of the pH value in time was recorded.*

OFET current regeneration after exposure to ammonia:
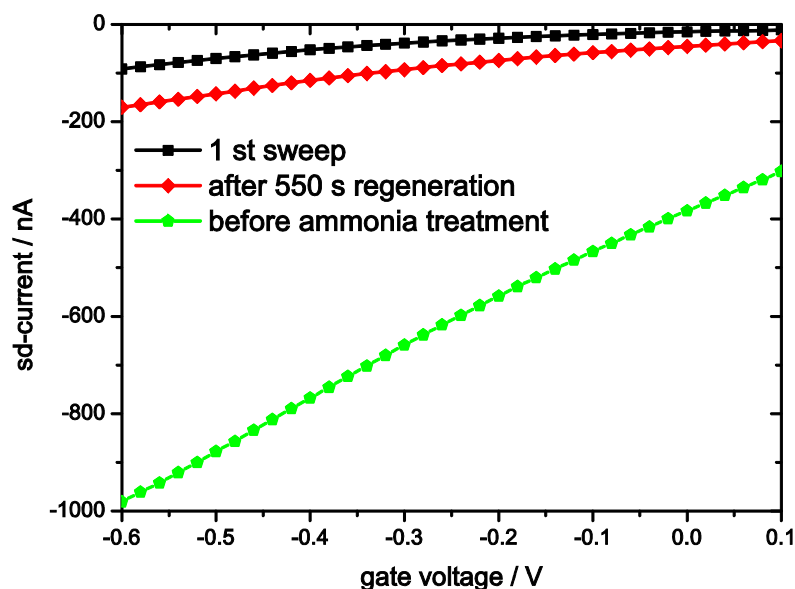
Supporting Figure S6: *Regeneration of transistor current in 10 mM DPBS after ammonia treatment. After exposure to ammonia solution, the electrolyte was replaced with fresh 10 mM DPBS buffer and transistor sweeps recorded at V_{SD} = - 0.3 V and floating bottom gate. For comparison, the original transistor curve is added.*

Supplementary Information References:

1.   M. Göllner, M. Huth and B. Nickel, *Advanced materials*, 2010, **22**, 4350-4354.
2.   J. B. Koo, J. W. Lim, S. H. Kim, C. H. Ku, S. C. Lim, J. H. Lee, S. J. Yun and Y. S. Yang, *Electrochem Solid St*, 2006, **9**, G320-G322.
3.   M. J. Spijkman, K. Myny, E. C. P. Smits, P. Heremans, P. W. M. Blom and D. M. de Leeuw, *Advanced materials*, 2011, **23**, 3231-3242.
4.   H. K. Lim and J. G. Fossum, *Ieee Transactions on Electron Devices*, 1983, **30**, 1244-1251.
5.   M. Yamada, I. Ikemoto and H. Kuroda, *Bulletin of the Chemical Society of Japan*, 1988, **61**, 1057-1062.
6.   T. Yamamoto and K. Takimiya, *Journal of the American Chemical Society*, 2007, **129**, 2224-2225.

B.3   SUPPORTING INFORMATION FOR "FAST DETECTION OF BLOOD GASES BY SOLUTION GATED ORGANIC FIELD EF-FECT TRANSISTORS"

Electronic Supplementary Information

Fast detection of blood gases by solution gated organic field effect transistors

Franz X. Werkmeister, Bert A. Nickel

Cyclic Voltammograms of DNTT
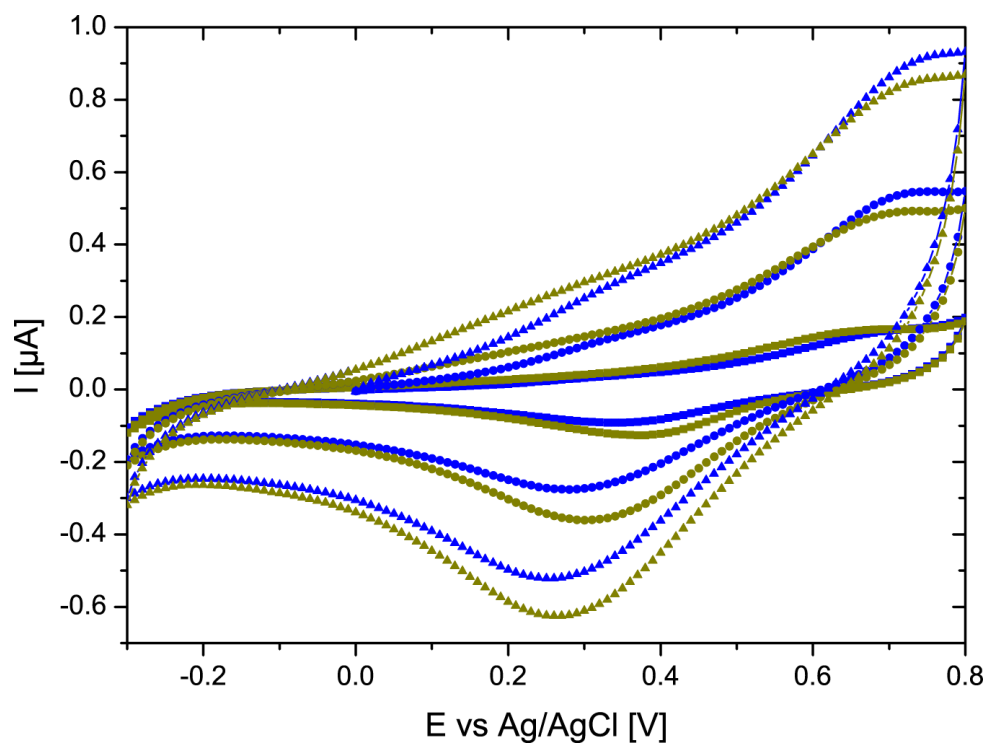
Fig. S1 Cyclic voltammograms with scan rates of 10mV/s (squares), 40 mV/s (circles), and 80 mV/s (triangles). The first cycle for each scan rate is displayed in blue, the second in yellow.

Response of EGOFET at different pH
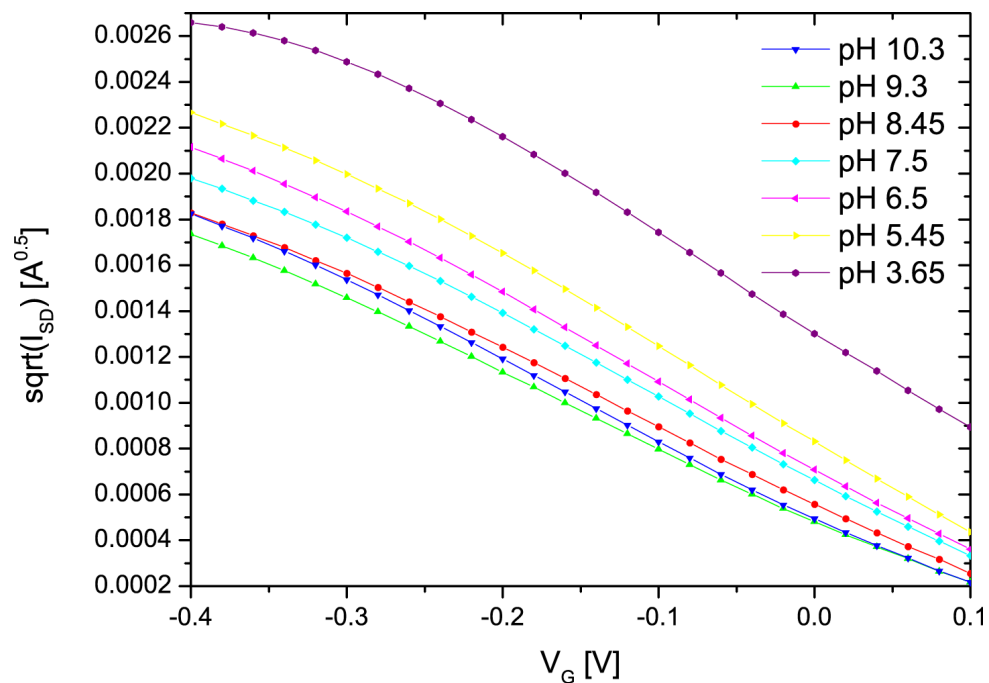
Fig. S2 Transconductance curves at different pH values.
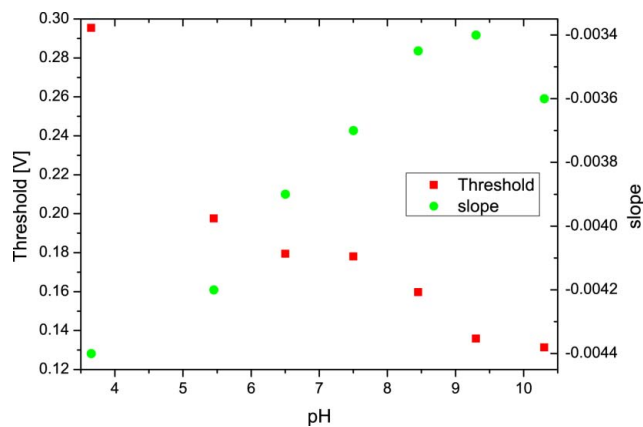
Fig. S3 Threshold voltage and slope of the EGOFET transconductance at different pH values. The slope is direct proportional to the product of areal capacitance C and mobility μ.

SEM image of DNTT on SU-8
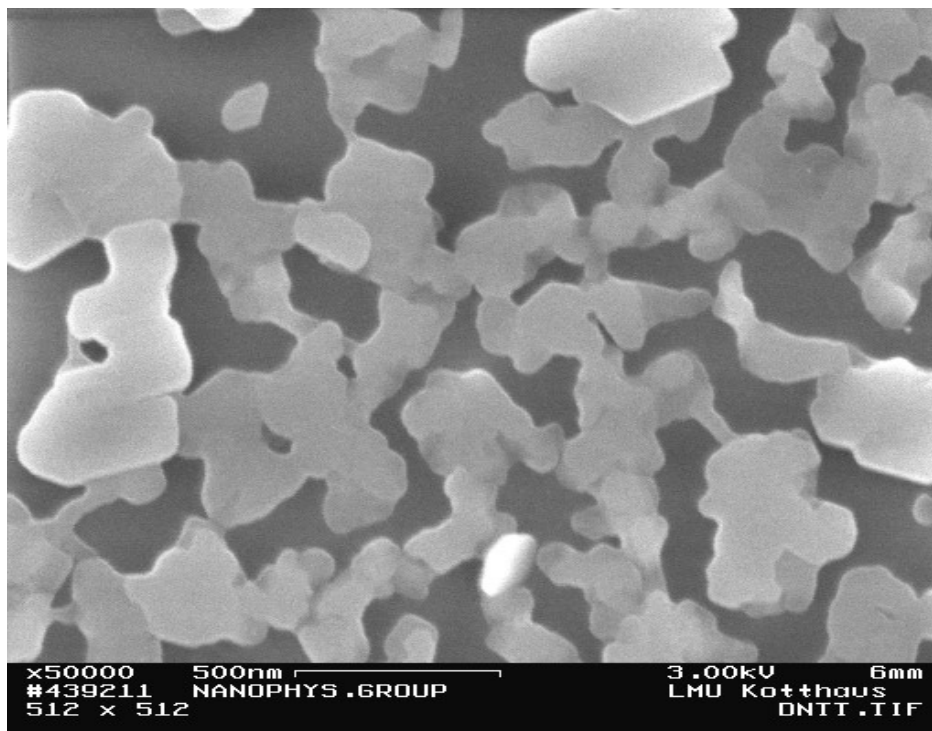
Fig. S4 SEM image of DNTT deposited onto SU-8. The bare SU-8 dielectric surface is visible between the grains. Image recorded with In-lense detector utilizing a LEO-SEM (Gemini 982) equipped with a field-emission cathode. The DNTT film was part of an OFET and connected to ground via a grounded source/drain-electrode.

Regeneration of OFETs upon rinsing after exposure to ammonia and response to 1 mM ammonia concetration
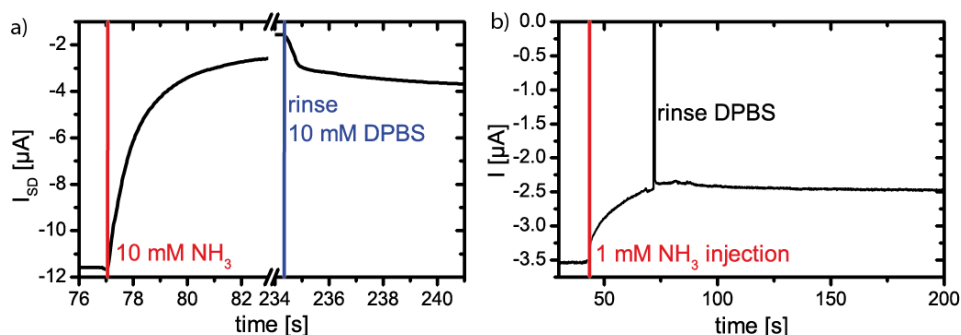
Fig. S5 a) Time trace of Regeneration of transistor current of a solution gated OFET after exposure to 10 mM ammonia. V_{SD} = -0.3V and V_{gate} = -0.3V. b) Time trace of solution gated OFET current reduction upon injection of 1 mM ammonia. V_{SD} = -0.3V and V_{gate} = -0.3V.

Response of OFET to 0.1 mM ammonia exposure
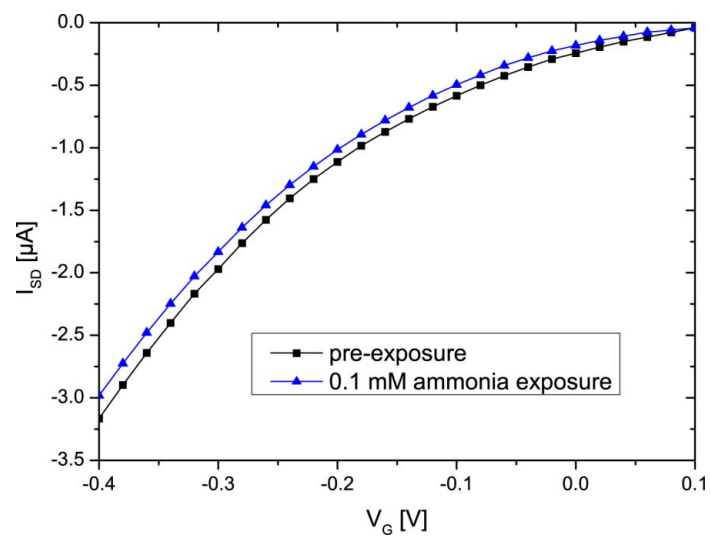
Fig. S6 Transconductance change of an OFET upon 0.1 mM ammonia exposure.

PHOTOLITHOGRAPHY PROTOCOLS

Before use of photolithography chemicals, consult the material safety data sheets, since some process chemicals are toxic and/or harm fertility. Consequently, one should handle these chemicals with care and follow the instructions on safety measures (e.g. use the correct gloves). Please also care for the safety of other persons in the vicinity, e.g. by blocking access to the fume hood during handling the Lift-Off media. Furthermore, one should care about waste disposal before starting the photolithography process.

C.1 LIFT-OFF

A Lift-Off process is one of the possible processes to arrive at photolithographically defined material structures. A pattern gets defined in a layer of photoresist, i.e. the substrate is bare in the pattern region and covered with the photoresist outside of the pattern. Next, the material, often the electrode stacks, get deposited onto the sample. This results in the material deposited onto the substrate in the desired pattern and onto the photoresist outside of the pattern. Last, the photoresist is dissolved in the Lift-Off medium and the material on the photoresist being lifted off the sample, only the desired pattern of material remains.

In practice, one can use either negative-tone or positive-tone photoresists.

In negative-tone photoresists the illuminated areas get crosslinked or polymerized, which has two consequences: First, a wedge structure wider at the bottom is produced, which is beneficial for Lift-Off, since no material gets deposited on the photoresists sidewalls, which would otherwise lead to fencing. Fencing will be discussed below. Second, it can be difficult to completely remove the photoresist[88] or it can bind to the substrate, which can have detrimental consequences for the intended purpose.

In positive-tone photoresists, the illuminated areas get soluble in the developer solution. In contrast to negative-tone photoresists, positive-tone ones do not get crosslinked. However, they display a wedge structure, which is wider at the top of the photoresist layer. This leads to
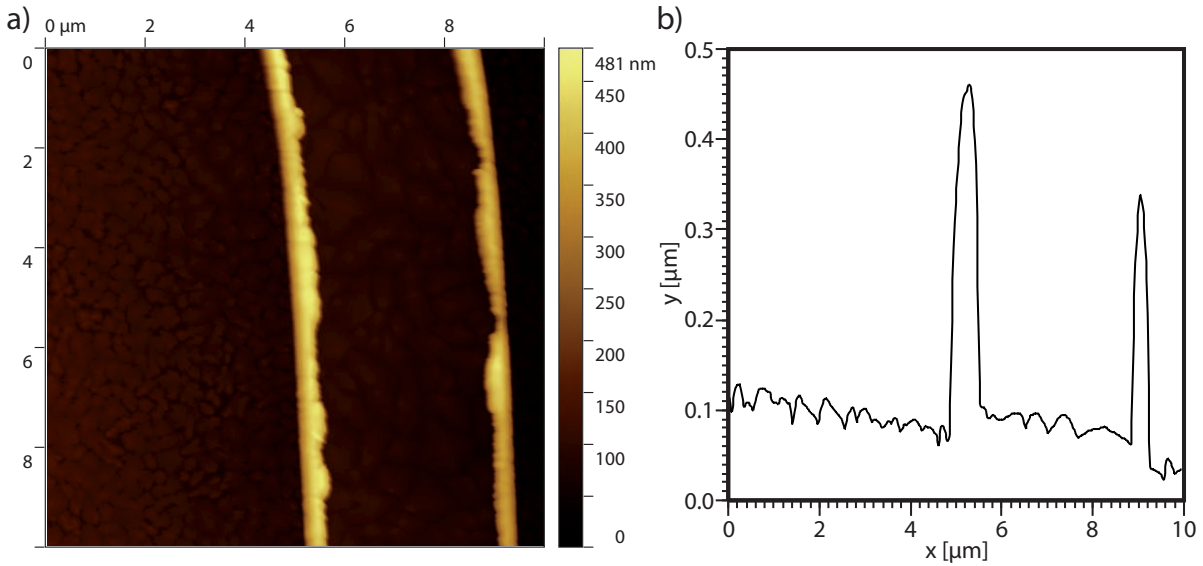
Figure C.1: *a) AFM micrograph of fencing. At the rim of the electrode a fence of material is left after the Lift-Off. Here, only a positive-tone photoresist, AZ 701 MIR, was used for Lift-Off. Further, pentacene is deposited onto the SU-8 dielectric and the electrode. b) Height profile extracted from the AFM micrograph a). The residual fence from material deposited onto the photoresist sidewall can be several 100 nm high.*

a problem called fencing, i.e. material deposited on the sidewalls of the photoresist structures does not get removed, but stays after Lift-Off as a fence at the rim of the defined material patterns (see Fig. C.1). Such structures can decrease transistor performance by their geometrical shadow, which can lead to incomplete coverage of subsequent layers, and impair sample functionality depending on the intended use. To avoid this, a Lift-Off resist can be used, like the LOR 3B employed in this work.

The LOR 3B is applied first and baked. Next a layer of conventional positive-tone photoresist is spincoated on top and processed as usual. During development, first the illuminated photoresist gets dissolved in the developer solution, and then the LOR 3B. The LOR dissolves faster than the unexposed photoresist, which gives rise to an under-etch of the photoresist, i.e. the photoresist flank gets discontinuous and the material film on the photoresist is disconnected from the material in the pattern.[87] It may be necessary to increase the development time upon application of LOR 3B compared to the development time for only the positive photoresist, depending on the dilution of the developer solution and the original developer time. Further, higher bake temperatures will decrease the dissolution rate of the LOR.[87] However, there is a lower limit to the bake temperature, since the LOR layer must withstand attack from the chemicals in the next subsequent coating step. Further processing is the same as for conventional Lift-Off, only the Lift-Off medium has to be chosen compatible with the LOR 3B, which excludes Acetone for this step. Note that there are some typical problems with this process and chemicals, which are discussed in section C.4.

The typical process flow for patterning the Lift-Off resist system is:

coat LOR 3B	40 s @ 4000 rpm	
softbake LOR 3B	3 min @ 150°C	
coat AZ 701 MIR	3 s @ 800 rpm	30 s @ 6000 rpm
softbake AZ 701 MIR	1 min @ 90°C	
illumination	17 s	
postbake AZ 701 MIR	1 min @ 110°C	
development	32 s in AZ MIF 726	rinse DI water
blown-dry		

Table C.1: Lift-Off resist system process parameters for utilization of LOR 3B together with AZ 701 MIR. Note that the illumination time will depend on the current power of the Hg-lamp.

Instead of AZ 701 MIR, also S 1813 G2 can be used as the positive photoresist:

coat LOR 3B	40 s @ 4000 rpm	
softbake LOR 3B	3 min @ 150°C	
coat S 1813 G2	3 s @ 800 rpm	30 s @ 5000 rpm
softbake S 1813 G2	3 min @ 115°C	
illumination	15 s	
development	90 s in Microposit 351 Dev 1:3 in DI water	rinse DI water
blown-dry		

Table C.2: Lift-Off resist system process parameters for utilization of LOR 3B together with S 1813 G2. The Microposit 351 developer is used diluted in DI water in ratio 1:3 by volume. Note that the illumination time will depend on the current power of the Hg-lamp.

Next, the processed samples can be coated with the desired material stack, and afterward the Lift-Off is performed. Here, the Lift-Off medium must be chosen compatible with the material system at hand, which can pose limitations already at the choice of photoresist system. Further, the process flow depends on the resistance of the applied materials with respect to the process conditions, e.g. can the materials withstand sonication in the Lift-Off medium.
Of the dielectrics used in conjunction with Lift-Off, SU-8 is able to stand sonication in Lift-Off medium, while parylene is not. For SU-8 the Lift-Off process flow is:

mr-Rem 400	dwell	5 min
	sonicate	5 min
fresh mr-Rem 400	sonicate	5 min
2-propanol	sonicate	2 min
blown-dry		

Table C.3: Lift-Off process flow on SU-8 dielectrics. The first sonication step can be prolonged, until Lift-Off is complete. Use of a visor during use of the Lift-Off medium is advised.

For parylene dielectrics, sonication is not possible, since the layer will degrade under such harsh treatment before Lift-Off is completed. Here, one can facilitate Lift-Off by bubbling air through the solution near the sample with a syringe. The samples are put into fresh Lift-Off

medium during the process, to reduce the amount of photoresist residuals and particles from the lifted material layers, which are dissolved and present in higher concentration in the first, original Lift-Off medium.

As an alternative to mr-Rem 400, 1165 Remover can be used. However, 1165 Remover is a more health-hazardous Lift-Off medium at present knowledge, so it should be only used if absolutely necessary. After Lift-Off with 1165 Remover, the sample should be rinsed first with Aceton and then with 2-propanol.

C.2 PHOTORESIST ETCH MASKS FOR RIE

Photoresists can be used as etch masks to pattern layers with Reactive-Ion-Etching (RIE). In RIE a layer is ablated by chemical etching by radicals. This happens in concert with activation and weakening of chemical bonds by ions moving onto the sample with preferential movement normal to the surface. RIE is a way to pattern parylene layers.[162] It is applied to open vias in the parylene layer to reach electrode contact pads below the parylene layer.[28][3] The applied photoresist acts as a sacrificial etch stop, i.e. the photoresist is etched instead of the functional dielectric. Consequently, the photoresist has to be chosen thick or resistant enough to remain until the RIE process ends. Note that also so called hardmasks, i.e. other layers such as metals or silicon oxide, are used for such purposes and can be chosen as etch masks if necessary.[162] Patterns are defined in the photoresist as before, so that in the desired regions the sample gets etched. If the layer, at which the etch shall stop, is not inert versus the RIE process, an etch stop mask has to be patterned,[162] to prevent damage to the sample. This can be a photoresist pattern, or a e.g. metal layer patterned precisely for this purpose. Here, a photoresist layer can be patterned as etch stop mask, then the parylene layer gets deposited and last the etch mask, which is inverted with respect to the etch stop mask, gets applied. After the RIE process, the etch mask and the now bare etch stop mask get dissolved in an appropriate solvent, for example a Lift-Off medium (see Fig. C.2).

In principle, any photoresist, which can be dissolved after the etch, can be used as etch masks for RIE, as for example the S 1813 G2. In practice, ma-P 1275 was used. This photoresist is specifically sold for RIE purposes, among others. The advantages are that ma-P dissolves more easily compared to e.g. S 1813 G2 and forms a thick layer. This thick layer has the
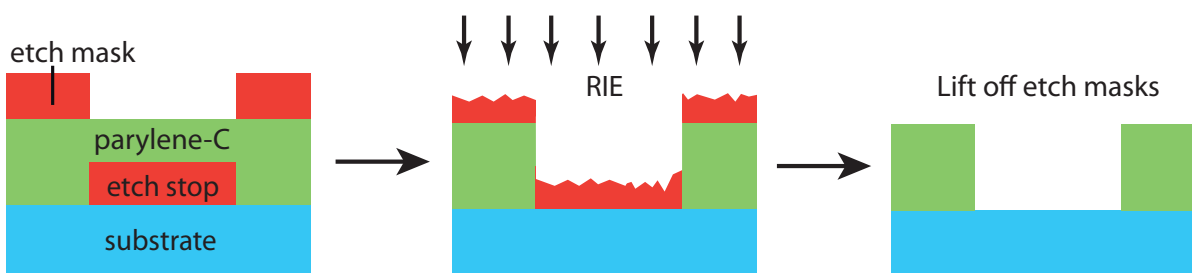
Figure C.2: *Scheme of the process flow of a RIE process with etch mask as well as an etch stop mask.*

consequence that in practical application, i.e. etching of parylene layers of thickness $\leq 2\mu m$, the etch mask poses no limitation in process time.

The patterning parameters for the ma-P 1275 were:

coat ma-P 1275	5 s @ 500 rpm	40 s @ 5000 rpm
wait	5 min	
softbake ma-P 1275	5 min @ 100°C	
illumination	40 s	
development	120 s in ma-D 331	rinse DI water

Table C.4: Parameter set to pattern ma-P 1275 as etch mask.

After RIE, the etch masks are dissolved in Lift-Off medium (1165 Remover or mr-Rem 400). As for Lift-Off, switching to a fresh Lift-Off medium after initial dissolution of layers reduces potential contaminations. For parylene layers, sonication was not used to facilitate dissolution of the etch masks, but gentle mechanical agitation such as bubbling.

C.3   DIELECTRICS FROM SU-8

The commercial photoresist SU-8 from MicroChem can be applied as a dielectric layer for OFETs and allows for further process steps utilizing photolithography and related process chemicals.[141] It can be used as a matrix for nanoparticles to obtain composite materials with desired properties.[163] For more information on SU-8 processes, on can read a recent review on 3D structures patterned from it.[139]

Regarding the photolithography process, SU-8 is a negative-tone photoresist, which means all areas illuminated will get crosslinked and remain after development. In short, the resist is spincoated and then softbaked. Next, the layer gets illuminated in the maskaligner with the appropriate mask, which sets free the chemical agent to facilitate the crosslinking. To thermally drive the catalytic crossling process, a post exposure bake is applied. Afterwards, the resist layer gets developed, in this case the not crosslinked areas of SU-8 are dissolved in the developer, which is an organic solvent such as PGMEA. Optional, the obtained structure can be hardbaked afterward, which completes the crosslinking and increases the chemical resistance of the layer.

C.3.1   FABRICATION OF SU-8 GATE DIELECTRICS

When using SU-8 for OFETs, great care has to be taken to fully crosslink the SU-8 layer, since charge transport organic semiconductors is greatly sensitive to reactive surface groups. The amount of crosslinking in SU-8 can be adjusted/increased by increasing the illumination dose and subsequent postbake time. This is essential for obtaining good charge transport. In

practice, it is necessary to increase the illumination time from the optimum time for patterns as in the data sheet by a factor of 8 to 10 to obtain the OFETs reported on in this thesis.

SU-8 2000.5 was used for the fabrication of the gate dielectrics. SU-8 2000.5 is a formulation of the SU-8 2000 family, which is suited to form ca. 0.5 μm thick layers. To obtain good gate dielectrics without high leakage currents or shorts, 2 layers of SU-8 had to be applied, a problem, which is also reported on in literature.[164]

Following is the set of parameters, which was used to fabricate the layers:

coat SU-8 2000.5	40 s @ 5000 rpm		
softbake SU-8 2000.5	2 min @ 95°C		
illumination	2.5 min		
postbake SU-8 2000.5	10 min @ 95°C		
coat SU-8 2000.5	40 s @ 5000 rpm		
softbake SU-8 2000.5	2 min @ 95°C		
illumination	2.5 min		
postbake SU-8 2000.5	10 min @ 95°C		
development	11 s in mr-Dev 600	11 s in mr-Dev 600	rinse in 2-propanol
blown-dry			

Table C.5: Parameters to fabricate patterned SU-8 gate dielectrics.

The second layer of SU-8 has a tendency to dewet on the first, crosslinked SU-8 layer. Consequently, dirt contamination on the sample will lead to holes in the second SU-8 layer. This matter, which cannot be totally avoided, however typically does not limit the performance of the gate dielectric, if one works fast and clean enough.

The hardbake is performed in the GERO-furnace under vacuum with the following parameters:

PR	PL	PD
240	220	0.5
240	280	0.5
1000	22	End

Table C.6: Parameter set for the hardbake of SU-8 layers in the GERO-furnace. The samples are placed in vacuum, which is generated by a rotary vane pump. In each program step, the PR gives the process ramp in °C/min at which the process level PL in °C is approached and then kept for the process dwell time PD (in h).

These dielectric layers have a total thickness of 630 ± 20 nm, as measured by AFM.

C.3.2   FABRICATION OF SU-8 ENCAPSULATIONS

SU-8 layers can be also used to encapsulate electrical leads, which would be otherwise in contact with electrolyte.[165] For SU-8 layers for this purpose, a simpler protocol is used:

coat SU-8 2000.5	40 s @ 2500 rpm		
softbake SU-8 2000.5	1 min @ 95°C		
illumination	28 s		
postbake SU-8 2000.5	2 min @ 95°C		
development	11 s in mr-Dev 600	11 s in mr-Dev 600	rinse in 2-propanol
blown-dry			
hardbake SU-8 2000.5	ramp up from RT to	15 min @ 150°C	

Table C.7: Parameters to fabricate SU-8 encapsulation for electrical leads.

C.4 TYPICAL PROBLEMS

Some typical problems can occur with photolithography, which are process or equipment related and shall be discussed shortly in the following.

- The maskaligner MJB 3 in the cleanroom is operated with a mercury arc lamp. The emitted illumination power from the lamp will decrease during its lifetime. Consequently the illumination time must be (constantly) adjusted. Typical signs, upon which illumination time needs to be increased, is incomplete development. Often fringes from thin film interference are visible for too low illumination time and thus a good indicator of this problem. Note that with newer equipment this issue might disappear, since here, the illumination power is measured by the tool. The user now chooses the illumination dose instead of time, where the illumination time is adjusted automatically to obtain the desired dose.

- Related to the previous problem, features of the AZ 701 MIR tend to become distorted, if the illumination time is too short. Distorted features means that spaces in the photoresist become too slim, e.g. 3 instead of 5 μm, and photoresist lines too broad, e.g. 7 instead of 5 μm. In this case the illumination dose has to be adjusted to longer illumination times.

- Aging of the photoresist can make Lift-Off impossible. Especially the LOR resist will not dissolve in the development bath, if it is expired. In later exposure to the Lift-Off medium it will dissolve, destroying the electrode structures. A typical sign for this are ruptured holes in the electrodes. Towards the end of the lifetime of the LOR the problem can be addressed by increasing the development time to some extend, however, this will reduce the quality of the photoresist edge of the layer on top of the LOR. Another topic is the aging of the positive photoresist used to define the electrode patterns. Here, longer illumination and development time can become necessary. With some photoresist, e.g. the ma-P 1275, development can become impossible upon expiration. Aging of photoresist can be significantly slowed down, if the photoresist is stored in a refrigerator (when possible).

- The development bath can become saturated with dissolved photoresist. If development appears to slow down or be incomplete after some development processes, refreshing the development solution will be necessary. Likewise, using two development baths, one for initial development and one for completion of the development process, can help to improve photoresist pattern quality. Further, the rinse after development is important to ensure complete removal of the developer (containing dissolved photoresist).

- Development time must be precisely adjusted to the bi-layer photoresist - Lift-Off-Resist system and kept during the process. Too short development time will result in incomplete development of the Lift-Off-Resist. However, for certain combinations of resists, e.g. the LOR 3B and the AZ 701 MIR, the photoresist layer will quickly get under-etched. Consequently, the intended structure will get unstable, since one will arrive at freestanding photoresist areas, which can collapse onto the sample and spoil the formed pattern.

- Dissolving etch masks can become very slow, since the chemical component of the RIE process as well as UV irradiation and heat from the RIE process can crosslink the applied photoresist. Thus, it gets more resistant to the solvent and takes longer to dissolve at the crosslinked top area. Typically, the Lift-Off time of the etch stop masks takes longer, since it is located within the material stack. Mechanical agitation of the Lift-Off medium as well as mechanical, but gentle agitation of the etch stop mask directly (e.g. by tweezers) can help to speed up the process.

- Related to potential aging of the LOR 3B and optimized development times for the bilayer Lift-Off resist system, special care has to taken, if ma-P 1275 is used for etch stop masks for RIE. Since the developer ma-D 331 used for patterning the ma-P 1275 layer is rather strong, any potential LOR 3B residuals below already patterned electrodes or other layers will get dissolved. Consequently, electrodes get damaged by the occurrence of ruptured holes or complete adhesion loss, much like in the case for problems during Lift-Off. However, this effect is more severe for this precise step, than for the Lift-Off step. Consequently, aging of the LOR 3B is a more severe issue, if used in conjunction with RIE patterning of e.g. parylene dielectrics.

- Spincoating of photoresists on not circular substrates will typically give rise to formation of beads at the edges. Later, these beads can set an increased distance between the sample and the mask, reducing the image quality, or lead to attachment of the sample to the mask at the edges, complicating the alignment of the sample and mask structure. Workarounds are, among others, the use of thin photoresists or cutting the edge-beads away with a scalpel.

- The sample can attach to the mask with the whole surface or only at single points, making alignment difficult to impossible. In general, longer softbake times will help against this problem if the whole sample attaches to the mask. Otherwise the problem can be related to the above mentioned edge beads. If attachment to the mask happens

only at few, small position, the following is often a practical solution: The sample is first pressed the sample into contact, then one goes completely back out of contact and only subsequent adjust the sample into contact for alignment. Note hat this process could potentially contaminate or even damage the mask. While a dirty mask can be cleaned e.g. in Piranha solution, the later will break the mask.

C.5 Dielectrics from PI 2610

Polyimide layers are well suited as dielectrics layers,[39] but also as smoothing layer. While photodefinable formulations exist, the more usual ones are not photodefinable. Nevertheless, the process parameters shall be given here, since the fabrication is similar to that of photoresist layers. The used polyimide precursor solution is the product PI 2610 from HD Microsystems. PI 2610 forms good dielectrics upon curing at 400°C, which limits the substrates it can be used on.

The precursor solution is dripped onto a suitable substrate and given some time to relax and dispense over the surface. Then it is spincoated and softbaked. Last, it is cured in the GERO-furnace under pure N_2 flow. The cure will start and drive the chemical reaction, imidization, of the precursor molecules to from a crosslinked layer. The process parameters are:

coat SU-8 2000.5	7 s @ 500 rpm	45 s @ 5000 rpm
softbake SU-8 2000.5	180 s @ 130°C	
GERO-furnace	100 l/s N_2	
PR	PL	PD
240	400	1.5
1000	22	End

Table C.8: Parameters to fabricate dielectrics from PI 2610.

For improving adhesion on e.g. glass slides, an adhesion promoter can be applied first. The company offers the adhesion promoters, however, from technical specifications APTES (Amino-propyl-triethoxysilan) should also be suitable. Otherwise, the fabricated layer can be peeled off from the substrate. This can be used to produce substrate free OFETs.

FLUID MEASUREMENT CHAMBER AND MEASUREMENT PROTOCOLS

D.1 FLUID MEASUREMENT CHAMBER ASSEMBLY

The measurement setup is based on a commercial flow chamber (see Fig. 3.1). Sticky Slides VI$^{0.4}$ from Ibidi are custom modified to attach and measure OFET samples. First, the original sticky tape is ripped of, since in subsequent steps the tape will be ruptured and spoil the driller head. Next, with a computer controlled CNC milling machine 0.8 mm diameter holes for electrical contacts are drilled into the flow chamber. Here, the slides are placed in a master plate and the driller adjusted to the master position of the milling program, which is marked on the master plate. After drilling, the holes are fettled with a 0.8 mm diameter steel wire and the slides are cleaned.

Onto the cleaned bottom, a sheet of ca. 20 mm times 25 mm of 467 MP adhesive tape (3 M) is applied. This sheet is than patterned by stamping out holes with the steel wire at the position of the vias drilled into the slide. The channels in the slides are opened again with a scalpel and the surplus glue in the channels is taken away.

After applying the glue, the electrode for use in the electrolyte is added. A piece of Pt or Pt/Ir wire of sufficient length (ca. 7 cm) is cut and glowed out in a bunsen burner flame. The wire is then placed in the channel with cleaned tweezers and pulled through the inlets/outlets. It is helpful to fix the wire to the slide at one inlet.

Last the OFET sample is placed on a plane are and the prepared flow chamber applied from the top, with the holes aligned to the electrodes on the sample. Note that one has only one try, since the glue is strongly adhesive. Attachment can be facilitated by applying pressure to the assembled sample-flow chamber stack. The glue should then give one night time to obtain a good seal versus solutions.

D.2   OFET MEASUREMENT PROTOCOLS

The different OFETs in each flow-channel were addressed individually. To decrease measurement time, the 6 OFETs in each channel were hot-switched through by a matrix card. Each OFETs source and drain electrode were serially connected via the matrix card to a Source Measurement Unit (SMU) with applied voltage (see Fig. D.1). For the bottom gate, the gate voltage was applied as a common gate to all 6 transistors in one flow-channel. Here, the OFETs must be checked for gate-leakage and broken devices disconnected via the cable. This test should be done at low voltages, lower than 1 V, for samples exposed to solutions. Otherwise, electrochemical reactions and the reaction products can damage or break the sample.

The solution side gate is connected via a cable attached to the wire in the flow-channel to a
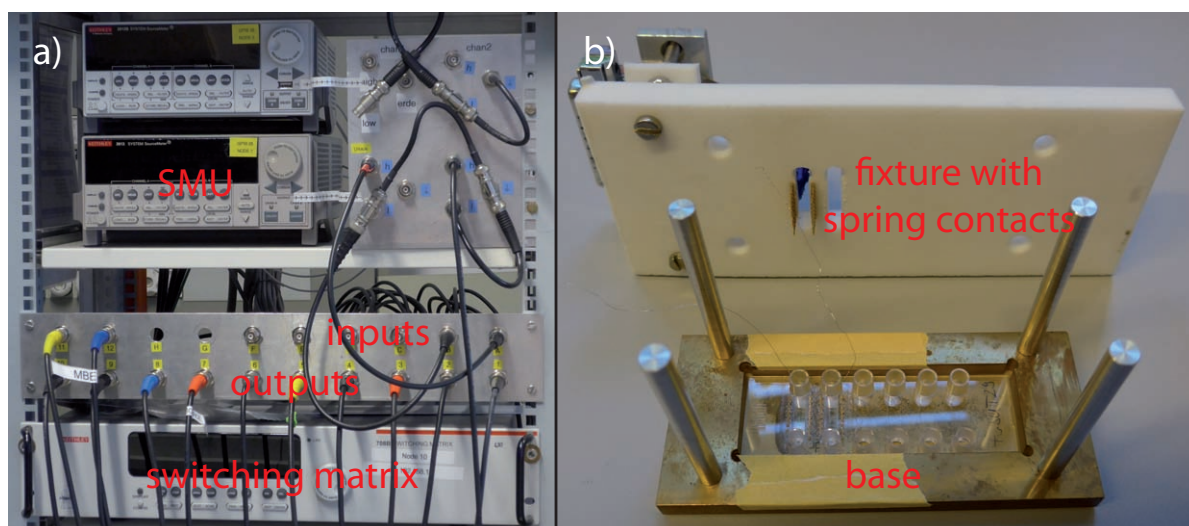
Figure D.1: *a) Wiring of the switching matrix. The drain (High of one SMU channel) is wired to the input of the matrix card, while the source (Low of one SMU channel, shorted with ground) is wired to another input. The standard inputs are A and B. The outputs of the switching matrix are then wired to the respective source and drain contacts of the OFETs. b) Measurement setup for OFETs (attached to flow cells). The OFETs are placed on the base and the fixture is put and top and fixed mechanically with a screw. The OFETs have to aligned to the spring contacts on the fixture. Apart from the displayed brass base, which is suitable for use in inverted microscopes, a base made from polytetrafluorethylen is available.*

SMU. All voltages are applied versus the Source, which is grounded. Typical operating voltages in electrolytes depend on the semiconductor used, however a limitation of the potentials |U| < 0.8 V proved useful. Practically, the voltage difference between Drain and Gate can sum up and should also kept below 0.8 V.

The solution can be applied before fixing the measurement chamber in the setup or afterward. Afterward, the solution can be applied through the measurement setup into the flow-chamber. This is beneficial, since it reduces the mechanical load on the wire as well as avoids problems with electrical contact between the spring contacts and the OFET contact pads.

Transient current response of OFETs can be obtained by wiring one OFET directly to the

SMUs and omitting the matrix card. Otherwise, the temporal resolution is insufficient in most cases.

BIBLIOGRAPHY

[1] F. Werkmeister and B. Nickel. Towards flexible organic thin film transistors (otfts) for biosensing. *Journal of Materials Chemistry B*, 1(31):3830–3835, 2013.

[2] Franz X. Werkmeister, Simon J. Noever, and Bert A. Nickel. Sub-monolayer percolation of pentacene on rough parylene-c dielectrics. *Organic Electronics*, 26:439–442, 2015.

[3] F. X. Werkmeister, T. Koide, and B. A. Nickel. Ammonia sensing for enzymatic urea detection with organic field effect transistors and a semipermeable membrane. *Journal of Materials Chemistry B*, 4(1):162–168, 2016.

[4] Franz X. Werkmeister and Bert A. Nickel. Fast detection of blood gases by solution gated organic field effect transistors. *Organic Electronics*, 39:113–117, 2016.

[5] H. Sirringhaus. 25th anniversary article: organic field-effect transistors: the path beyond amorphous silicon. *Adv Mater*, 26(9):1319–35, 2014.

[6] P. Heremans, A. K. Tripathi, A. de Jamblinne de Meux, E. C. Smits, B. Hou, G. Pourtois, and G. H. Gelinck. Mechanical and electronic properties of thin-film transistors on plastic, and their integration in flexible electronic applications. *Adv Mater*, 2015.

[7] Luisa Torsi, Maria Magliulo, Kyriaki Manoli, and Gerardo Palazzo. Organic field-effect transistor sensors: a tutorial review. *Chemical Society Reviews*, 42(22):8612–8628, 2013.

[8] D. A. Bernards, D. J. Macaya, M. Nikolou, J. A. DeFranco, S. Takamatsu, and G. G. Malliaras. Enzymatic sensing with organic electrochemical transistors. *Journal of Materials Chemistry*, 18(1):116–120, 2008.

[9] Gäetan Scheiblin, Abdelkader Aliane, Xenofon Strakosas, Vincenzo F. Curto, Romain Coppard, Gilles Marchand, Roisin M. Owens, Pascal Mailley, and George G. Malliaras. Screen-printed organic electrochemical transistors for metabolite sensing. *MRS Communications*, 5(03):507–511, 2015.

[10] Daniel R. Thevenot, Klara Toth, Richard A. Durst, and George S. Wilson. Electrochemical biosensors: recommended definitions and classification. *Biosensors and Bioelectronics*, 16:121–131, 2001.

[11] Ernest Peris, Maria-Jose Banuls, Rosa Puchades, and Angel Maquieira. Photoattachment of thiolated dna probes on su-8 spin-coated blu-ray disk surfaces for biosensing. *Journal of Materials Chemistry B*, 2013.

[12] J. L. Arlett, E. B. Myers, and M. L. Roukes. Comparative advantages of mechanical biosensors. *Nat Nano*, 6(4):203–215, 2011.

[13] Tatikonda Anand Kumar, Eyal Capua, Maria Tkachev, Samuel N. Adler, and Ron Naaman. Hybrid organic-inorganic biosensor for ammonia operating under harsh physiological conditions. *Advanced Functional Materials*, 24(37):5833–5840, 2014.

[14] Arshak Poghossian and Michael J. Schöning. Label-free sensing of biomolecules with field-effect devices for clinical applications. *Electroanalysis*, 26(6):1197–1213, 2014.

[15] Mallory L. Hammock, Oren Knopfmacher, Tse Nga Ng, Jeffrey B. H. Tok, and Zhenan Bao. Electronic readout enzyme-linked immunosorbent assay with organic field-effect transistors as a preeclampsia prognostic. *Advanced Materials*, 26(35):6138–6144, 2014.

[16] A. P. Turner. Biosensors: sense and sensibility. *Chem Soc Rev*, 42(8):3184–96, 2013.

[17] J. S. Daniels and N. Pourmand. Label-free impedance biosensors: Opportunities and challenges. *Electroanalysis*, 19(12):1239–1257, 2007.

[19] P. Bergveld. Thirty years of isfetology: What happened in the past 30 years and what may happen in the next 30 years. *Sensors and Actuators B: Chemical*, 88(1):1–20, 2003.

[18] P. Bergveld. Isfet, theory and practice. In *IEEE sensor conference Toronto*, 2003.

[21] D. Khodagholy, T. Doublet, P. Quilichini, M. Gurfinkel, P. Leleux, A. Ghestem, E. Ismailova, T. Herve, S. Sanaur, C. Bernard, and G. G. Malliaras. In vivo recordings of brain activity using organic transistors. *Nature Communications*, 4:1575, 2013.

[20] J. T. Mabeck and G. G. Malliaras. Chemical and biological sensors based on organic thin-film transistors. *Anal Bioanal Chem*, 384(2):343–53, 2006.

[22] Jonathan M. Rothberg, Wolfgang Hinz, Todd M. Rearick, Jonathan Schultz, William Mileski, Mel Davey, John H. Leamon, Kim Johnson, Mark J. Milgrew, Matthew Edwards, Jeremy Hoon, Jan F. Simons, David Marran, Jason W. Myers, John F. Davidson, Annika Branting, John R. Nobile, Bernard P. Puc, David Light, Travis A. Clark, Martin Huber, Jeffrey T. Branciforte, Isaac B. Stoner, Simon E. Cawley, Michael Lyons, Yutao Fu, Nils Homer, Marina Sedova, Xin Miao, Brian Reed, Jeffrey Sabina, Erika Feierstein, Michelle Schorn, Mohammad Alanjary, Eileen Dimalanta, Devin Dressman, Rachel Kasinskas, Tanya Sokolsky, Jacqueline A. Fidanza, Eugeni Namsaraev, Kevin J. McKernan, Alan Williams, G. Thomas Roth, and James Bustillo. An integrated semiconductor device enabling non-optical genome sequencing. *Nature*, 475(7356):348–352, 2011.

[23] K. V. Stepurska, C. O. Soldatkin, I. S. Kucherenko, V. M. Arkhypova, S. V. Dzyadevych, and A. P. Soldatkin. Feasibility of application of conductometric biosensor based on acetylcholinesterase for the inhibitory analysis of toxic compounds of different na-

ture. *Anal Chim Acta*, 854:161–168, 2015.

[24] Kyriaki Manoli, Maria Magliulo, Mohammad Yusuf Mulla, Mandeep Singh, Luigia Sabbatini, Gerardo Palazzo, and Luisa Torsi. Printable bioelectronics to investigate functional biological interfaces. *Angewandte Chemie International Edition*, 54(43):12562–12576, 2015.

[25] Enrico Bandiello, Michele Sessolo, and Henk J. Bolink. Electrolyte-gated nanostructured zno transistors for environmental and biological sensing. *Journal of Materials Chemistry C*, 2:10277–10281, 2014.

[26] E. D. Glowacki, R. R. Tangorra, H. Coskun, D. Farka, A. Operamolla, Y. Kanbur, F. Milano, L. Giotta, G. M. Farinola, and N. S. Sariciftci. Bioconjugation of hydrogen-bonded organic semiconductors with functional proteins. *Journal of Materials Chemistry C*, 3(25):6554–6564, 2015.

[27] M. Irimia-Vladu, N. S. Sariciftci, and S. Bauer. Exotic materials for bio-organic electronics. *Journal of Materials Chemistry*, 21(5):1350–1361, 2011.

[28] D. Khodagholy, T. Doublet, M. Gurfinkel, P. Quilichini, E. Ismailova, P. Leleux, T. Herve, S. Sanaur, C. Bernard, and G. G. Malliaras. Highly conformable conducting polymer electrodes for in vivo recordings. *Adv Mater*, 23(36):H268–272, 2011.

[29] Amanda Jonsson, Zhiyang Song, David Nilsson, Björn A. Meyerson, Daniel T. Simon, Bengt Linderoth, and Magnus Berggren. Therapy using implanted organic bioelectronics. *Science Advances*, 1(4), 2015.

[30] D. T. Simon, K. C. Larsson, D. Nilsson, G. Burstrom, D. Galter, M. Berggren, and A. Richter-Dahlfors. An organic electronic biomimetic neuron enables auto-regulated neuromodulation. *Biosens Bioelectron*, 71:359–64, 2015.

[31] Markus Schwoerer and Hans Christoph Wolf. *Organische molekulare Festkörper Einführung in die Physik von Pi-Systemen*. WILEY-VCH, Weinheim, 2005.

[32] Mark Geoghegan and Georges Hadziioannou. *Polymer electronics*. Oxford Univ. Press, Oxford, 1. ed. edition, 2013.

[33] Simon M. Sze and Kwok Kwok Ng. *Physics of semiconductor devices*. Wiley-Interscience, Hoboken, NJ, 3. ed. edition, 2007.

[34] J. Christopher Love, Lara A. Estroff, Jennah K. Kriebel, Ralph G. Nuzzo, and George M. Whitesides. Self-assembled monolayers of thiolates on metals as a form of nanotechnology. *Chemical Reviews*, 105(4):1103–1170, 2005.

[35] Antoine Kahn. Fermi level, work function and vacuum level. *Materials Horizons*, 3:7–10, 2016.

[36] Guillaume Schweicher, Yoann Olivier, Vincent Lemaur, and Yves Henri Geerts. What currently limits charge carrier mobility in crystals of molecular semiconductors? *Israel Journal of Chemistry*, 54(5-6):595–620, 2014.

[37] Simone Fratini, Didier Mayou, and Sergio Ciuchi. The transient localization scenario for charge transport in crystalline organic materials. *Advanced Functional Materials*, 26(14):2292–2315, 2016.

[38] Steffen Illig, Alexander S. Eggeman, Alessandro Troisi, Lang Jiang, Chris Warwick, Mark Nikolka, Guillaume Schweicher, Stephen G. Yeates, Yves Henri Geerts, John E. Anthony, and Henning Sirringhaus. Reducing dynamic disorder in small-molecule organic semiconductors by suppressing large-amplitude thermal motions. *Nat Commun*, 7, 2016.

[39] Yusaku Kato, Shingo Iba, Ryohei Teramoto, Tsuyoshi Sekitani, Takao Someya, Hiroshi Kawaguchi, and Takayasu Sakurai. High mobility of pentacene field-effect transistors with polyimide gate dielectric layers. *Applied Physics Letters*, 84(19):3789, 2004.

[40] Kung-Ching Liao, Ahmad G. Ismail, Laurent Kreplak, Jeffrey Schwartz, and Ian G. Hill. Designed organophosphonate self-assembled monolayers enhance device performance of pentacene-based organic thin-film transistors. *Advanced Materials*, 22(28):3081–3085, 2010.

[41] Ricardo Ruiz, Devashish Choudhary, Bert Nickel, Tullio Toccoli, Kee-Chul Chang, Alex C. Mayer, Paulette Clancy, Jack M. Blakely, Randall L. Headrick, Salvatore Iannotta, and George G. Malliaras. Pentacene thin film growth. *Chemistry of Materials*, 16(23):4497–4508, 2004.

[42] S. H. Kim, M. Jang, H. Yang, and C. E. Park. Effect of pentacene-dielectric affinity on pentacene thin film growth morphology in organic field-effect transistors. *Journal of Materials Chemistry*, 20(27):5612–5620, 2010.

[43] C. D. Dimitrakopoulos, A. R. Brown, and A. Pomp. Molecular beam deposited thin films of pentacene for organic field effect transistor applications. *Journal of Applied Physics*, 80(4):2501, 1996.

[44] Stefan Schiefer, Martin Huth, Alexander Dobrinevski, and Bert Nickel. Determination of the crystal structure of substrate-induced pentacene polymorphs in fiber structured thin films. *Journal of the American Chemical Society*, 129(34):10316–+, 2007.

[45] Q. Tang, D. Q. Zhang, S. L. Wang, N. Ke, J. B. Xu, J. C. Yu, and Q. Miao. A meaningful analogue of pentacene: Charge transport, polymorphs, and electronic structures of dihydrodiazapentacene. *Chemistry of Materials*, 21(7):1400–1405, 2009.

[46] T. Yamamoto and K. Takimiya. Facile synthesis of highly pi-extended heteroarenes, dinaphtho[2,3-b:2',3'-f]chalcogenopheno[3,2-b]chalcogenophenes, and their application to field-effect transistors. *Journal of the American Chemical Society*, 129(8):2224–2225, 2007.

[47] Eric Daniel Glowacki, Giuseppe Romanazzi, Cigdem Yumusak, Halime Coskun, Uwe Monkowius, Gundula Voss, Max Burian, Rainer T. Lechner, Nicola Demitri, Günther J. Redhammer, Nevsal Sünger, Gian Paolo Suranna, and Serdar Sariciftci. Epindolidiones-versatile and stable hydrogen-bonded pigments for organic field-effect transistors and light-emitting diodes. *Advanced Functional Materials*, 25(5):776–787, 2015.

[48] Ute Zschieschang, Frederik Ante, Daniel Kälblein, Tatsuya Yamamoto, Kazuo Takimiya, Hirokazu Kuwabara, Masaaki Ikeda, Tsuyoshi Sekitani, Takao Someya,

Jan Blochwitz Nimoth, and Hagen Klauk. Dinaphtho[2,3-b:2',3'-f]thieno[3,2-b]thiophene (dntt) thin-film transistors with improved performance and stability. *Organic Electronics*, 12(8):1370–1375, 2011.

[49] K. Kuribara, H. Wang, N. Uchiyama, K. Fukuda, T. Yokota, U. Zschieschang, C. Jaye, D. Fischer, H. Klauk, T. Yamamoto, K. Takimiya, M. Ikeda, H. Kuwabara, T. Sekitani, Y. L. Loo, and T. Someya. Organic transistors with high thermal stability for medical applications. *Nature Communications*, 3, 2012.

[50] M. C. Jung, M. R. Leyden, G. O. Nikiforov, M. V. Lee, H. K. Lee, T. J. Shin, K. Takimiya, and Y. Qi. Flat-lying semiconductor-insulator interfacial layer in dntt thin films. *ACS Appl Mater Interfaces*, 7(3):1833–40, 2015.

[51] Pollawat Prisawong, Peter Zalar, Amir Reuveny, Naoji Matsuhisa, Wonryung Lee, Tomoyuki Yokota, and Takao Someya. Vacuum ultraviolet treatment of self-assembled monolayers: A tool for understanding growth and tuning charge transport in organic field-effect transistors. *Advanced Materials*, 28(10):2049–2054, 2016.

[52] N. Padma, Shilpa N. Sawant, V. Sudarsan, Shaswati Sen, and S. K. Gupta. Comparison of the role of holes and electrons in hysteresis and threshold voltage stability of organic field effect transistors. *physica status solidi (a)*, 210(10):2111–2120, 2013.

[53] Yin Sun, Lining Zhang, Zubair Ahmed, and Mansun Chan. Characterization of interface trap dynamics responsible for hysteresis in organic thin-film transistors. *Organic Electronics*, 27:192–196, 2015.

[54] A. Facchetti, M. H. Yoon, and T. J. Marks. Gate dielectrics for organic field-effect transistors: New opportunities for organic electronics. *Advanced Materials*, 17(14):1705–1725, 2005.

[55] Gilles Horowitz. Organic field-effect transistors. *Advanced Materials*, 10(5):365–377, 1998.

[56] Daniele Braga and Gilles Horowitz. High-performance organic field-effect transistors. *Advanced Materials*, 21(14-15):1473–1486, 2009.

[57] L. Kergoat, B. Piro, M. Berggren, G. Horowitz, and M. C. Pham. Advances in organic transistor-based biosensors: from organic electrochemical transistors to electrolyte-gated organic field-effect transistors. *Anal Bioanal Chem*, 402(5):1813–26, 2012.

[58] Dion Khodagholy, Jonathan Rivnay, Michele Sessolo, Moshe Gurfinkel, Pierre Leleux, Leslie H. Jimison, Eleni Stavrinidou, Thierry Herve, Sebastien Sanaur, Roisin M. Owens, and George G. Malliaras. High transconductance organic electrochemical transistors. *Nat Commun*, 4:2133, 2013.

[59] Xenofon Strakosas, Michele Sessolo, Adel Hama, Jonathan Rivnay, Eleni Stavrinidou, George G. Malliaras, and Roisin M. Owens. A facile biofunctionalisation route for solution processable conducting polymer devices. *Journal of Materials Chemistry B*, 2014.

[60] Loig Kergoat, Piro Benoit, Daniel T. Simon, Minh-Chau Pham, Vincent Noel, and Magnus Berggren. Detection of glutamate and acetylcholine with organic electrochemical

transistors based on conducting polymer/platinum nanoparticle composites. *Advanced Materials*, 26(32):5658–5664, 2014.

[61] Caizhi Liao, Chunhin Mak, Meng Zhang, Helen L. W. Chan, and Feng Yan. Flexible organic electrochemical transistors for highly selective enzyme biosensors and used for saliva testing. *Advanced Materials*, pages n/a–n/a, 2014.

[62] Allen J. Bard and Larry R. Faulkner. *Electrochemical methods: fundamentals and applications*. John Wiley and Sons, New York, Chichester, Weinheim, Brisbane, Singapore, Toronto, 2nd edition, 2001.

[63] M. J. Spijkman, J. J. Brondijk, T. C. T. Geuns, E. C. P. Smits, T. Cramer, F. Zerbetto, P. Stoliar, F. Biscarini, P. W. M. Blom, and D. M. de Leeuw. Dual-gate organic field-effect transistors as potentiometric sensors in aqueous solution. *Advanced Functional Materials*, 20(6):898–905, 2010.

[64] Martin Göllner, Georg Glasbrenner, and Bert Nickel. An electrochemical transducer based on a pentacene double-gate thin-film transistor. *Electroanalysis*, 24(2):214–218, 2012.

[65] H. K. Lim and J. G. Fossum. Threshold voltage of thin-film silicon-on-insulator (soi) mosfets. *Ieee Transactions on Electron Devices*, 30(10):1244–1251, 1983.

[66] L. Torsi, A. Dodabalapur, L. Sabbatini, and P. G. Zambonin. Multi-parameter gas sensors based on organic thin-film-transistors. *Sensors and Actuators B-Chemical*, 67(3):312–316, 2000.

[67] Sejin Park, Hankil Boo, Yunmee Kim, Ji-Hyung Han, Hee Chan Kim, and Taek Dong Chung. ph-sensitive solid-state electrode based on electrodeposited nanoporous platinum. *Analytical Chemistry*, 77(23):7695–7701, 2005.

[68] Kerstin Schmoltner, Johannes Kofler, Andreas Klug, and Emil J. W. List-Kratochvil. Electrolyte-gated organic field-effect transistor for selective reversible ion detection. *Advanced Materials*, 25(47):6895–6899, 2013.

[69] Katharina Melzer, Alexandra Mara Münzer, Ewa Jaworska, Krzysztof Maksymiuk, Agata Michalska, and Giuseppe Scarpa. Polymeric ion-selective membrane functionalized gate-electrodes: Ion-selective response of electrolyte-gated poly (3-hexylthiophene) field-effect transistors. *Organic Electronics*, 15(2):595–601, 2014.

[70] Mallory L. Hammock, Oren Knopfmacher, Benjamin D. Naab, Jeffrey B. H. Tok, and Zhenan Bao. Investigation of protein detection parameters using nanofunctionalized organic field-effect transistors. *ACS Nano*, 7(5):3970–3980, 2013.

[71] Gerardo Palazzo, Donato De Tullio, Maria Magliulo, Antonia Mallardi, Francesca Intranuovo, Mohammad Yusuf Mulla, Pietro Favia, Inger Vikholm-Lundin, and Luisa Torsi. Detection beyond debye's length with an electrolyte-gated organic field-effect transistor. *Advanced Materials*, 27(5):911–916, 2014.

[72] Mohammad Yusuf Mulla, Elena Tuccori, Maria Magliulo, Gianluca Lattanzi, Gerardo Palazzo, Krishna Persaud, and Luisa Torsi. Capacitance-modulated transistor detects odorant binding protein chiral interactions. *Nat Commun*, 6, 2015.

[73] Tsukuru Minamiki, Tsuyoshi Minami, Ryoji Kurita, Osamu Niwa, Shin-ichi Wakida, Kenjiro Fukuda, Daisuke Kumaki, and Shizuo Tokito. Accurate and reproducible detection of proteins in water using an extended-gate type organic transistor biosensor. *Applied Physics Letters*, 104(24):243703, 2014.

[74] N. C. S. Vieira, A. Figueiredo, E. G. R. Fernandes, F. E. G. Guimaraes, and V. Zucolotto. Nanostructured polyaniline thin films as urea-sensing membranes in field-effect devices. *Synthetic Metals*, 175:108–111, 2013.

[75] S. Lai, M. Demelas, G. Casula, P. Cosseddu, M. Barbaro, and A. Bonfiglio. Ultralow voltage, otft-based sensor for label-free dna detection. *Adv Mater*, 25(1):103–7, 2013.

[76] Monia Demelas, Stefano Lai, Andrea Spanu, Sergio Martinoia, Piero Cosseddu, Massimo Barbaro, and Annalisa Bonfiglio. Charge sensing by organic charge-modulated field effect transistors: application to the detection of bio-related effects. *Journal of Materials Chemistry B*, 1(31):3811–3819, 2013.

[77] Maria Magliulo, Kyriaki Manoli, Eleonora Macchia, Gerardo Palazzo, and Luisa Torsi. Tailoring functional interlayers in organic field-effect transistor biosensors. *Advanced Materials*, 27(46):7528–7551, 2015.

[78] M. Magliulo, D. Altamura, C. Di Franco, M. V. Santacroce, K. Manoli, A. Mallardi, G. Palazzo, G. Scamarcio, C. Giannini, and L. Torsi. Structural and morphological study of a poly(3-hexylthiophene)/streptavidin multi layer structure serving as active layer in ultra-sensitive ofet biosensors. *Journal of Physical Chemistry C*, 118(29):15853–15862, 2014.

[79] M. Göllner, M. Huth, and B. Nickel. Pentacene thin-film transistors encapsulated by a thin alkane layer operated in an aqueous ionic environment. *Adv Mater*, 22(39):4350–4, 2010.

[80] C. D. Dimitrakopoulos, B. K. Furman, T. Graham, S. Hegde, and S. Purushothaman. Field-effect transistors comprising molecular beam deposited alpha,omega-di-hexyl-hexathienylene and polymeric insulator. *Synthetic Metals*, 92(1):47–52, 1998.

[81] A. Vincze, J. Jakabovic, R. Srnanek, A. Satka, J. Kovac, and J. Kovac. Surface and interface properties of thin pentacene and parylene layers. *Central European Journal of Physics*, 7(2):270–278, 2009.

[82] V. A. Skryshevsky, J. Tardy, M. Phaner-Goutorbe, E. Souteyrand, R. Villey, M. Erquel, and M. Iazykov. An afm investigation of surface energy of pentacene films on parylene-c and benzocyclobutene. *Functional Materials Letters*, 05(01):1250016, 2012.

[83] Minni Singh, Neelam Verma, Arun Kumar Garg, and Niha Redhu. Urea biosensors. *Sensors and Actuators B: Chemical*, 134(1):345–351, 2008.

[84] Gunjan Dhawan, Gajjala Sumana, and B. D. Malhotra. Recent developments in urea biosensors. *Biochemical Engineering Journal*, 44(1):42–52, 2009.

[85] B. Azeem, K. KuShaari, Z. B. Man, A. Basit, and T. H. Thanh. Review on materials & methods to produce controlled release coated urea fertilizer. *J Control Release*, 181:11–21, 2014.

[86] Liqiang Li, Peng Gao, Martin Baumgarten, Klaus Müllen, Nan Lu, Harald Fuchs, and Lifeng Chi. High performance field-effect ammonia sensors based on a structured ultrathin organic semiconductor film. *Advanced Materials*, 25(25):3419–3425, 2013.

[87] Jeremy Golden, Harris Miller, Dan Nawrocki, and Jack Ross. Optimization of bi-layer lift-off resist process. CS MANTECH conference, Tampa, Florida, USA, 2009.

[88] Yingtao Xie, Shihong Ouyang, Dongping Wang, Wen-Ya Lee, Zhenan Bao, James R. Matthews, Weijun Niu, Robert A. Bellman, Mingqian He, and Hon Hang Fong. High performance top contact fused thiophene-diketopyrrolopyrrole copolymer transistors using a photolithographic metal lift-off process. *Organic Electronics*, 20(0):55–62, 2015.

[89] L. L. Chua, J. Zaumseil, J. F. Chang, E. C. W. Ou, P. K. H. Ho, H. Sirringhaus, and R. H. Friend. General observation of n-type field-effect behaviour in organic semiconductors. *Nature*, 434(7030):194–199, 2005.

[90] S. Y Yang, K. Shin, and C. E Park. The effect of gate-dielectric surface energy on pentacene morphology and organic field-effect transistor characteristics. *Advanced Functional Materials*, 15(11):1806–1814, 2005.

[91] T. Sekitani, Y. Kato, S. Iba, H. Shinaoka, T. Someya, T. Sakurai, and S. Takagi. Bending experiment on pentacene field-effect transistors on plastic films. *Applied Physics Letters*, 86(7):073511, 2005.

[92] Deyang Ji, Lang Jiang, Xiaozhou Cai, Huanli Dong, Qing Meng, Guofeng Tian, Dezhen Wu, Jingze Li, and Wenping Hu. Large scale, flexible organic transistor arrays and circuits based on polyimide materials. *Organic Electronics*, 14(10):2528–2533, 2013.

[93] Jeffrey B. Fortin and Toh-Ming Lu. *Chemical Vapor Deposition Polymerization The Growth and Properties of Parylene Thin Films*. Springer Science & Business Media, 2003.

[94] Y. S. Yeh, W. J. James, and H. Yasuda. Polymerization of para-xylylene derivatives. vi. morphology of parylene n and parylene c films investigated by gas transport characteristics. *Journal of Polymer Science Part B: Polymer Physics*, 28(4):545–568, 1990.

[95] P. Kramer, A. K. Sharma, E. E. Hennecke, and H. Yasuda. Polymerization of para-xylylene derivatives (parylene polymerization). i. deposition kinetics for parylene n and parylene c. *Journal of Polymer Science: Polymer Chemistry Edition*, 22(2):475–491, 1984.

[96] M. Gazicki, G. Surendran, W. James, and H. Yasuda. Polymerization of para-xylylene derivatives (parylene polymerization). ii. heat effects during deposition of parylene c at different temperatures. *Journal of Polymer Science: Polymer Chemistry Edition*, 23(8):2255–2277, 1985.

[97] M. Gazicki, G. Surendran, W. James, and H. Yasuda. Polymerization of para-xylylene derivatives (parylene polymerization) .3. heat-effects during deposition of parylene-n at different temperatures. *Journal of Polymer Science Part a-Polymer Chemistry*, 24(2):215–240, 1986.

[98] G. Surendran, M. Gazicki, W. J. James, and H. Yasuda. Polymerization of para-xylylene derivatives (parylene polymerization). iv. effects of the sublimation rate of di-p-xylylene on the morphology and crystallinity of parylene n deposited at different temperatures. *Journal of Polymer Science Part A: Polymer Chemistry*, 25(6):1481–1503, 1987.

[99] G. Surendran, M. Gazicki, W. J. James, and H. Yasuda. Polymerization of para-xylylene derivatives. v. effects of the sublimation rate of di-p-xylylene on the crystallinity of parylene c deposited at different temperatures. *Journal of Polymer Science Part A: Polymer Chemistry*, 25(8):2089–2106, 1987.

[100] Franz Xaver Werkmeister. Flexible and micropatterned organic field effect transistors. Master's thesis, LMU Munich, 2012.

[101] Kathleen M. Vaeth and Klavs F. Jensen. Transition metals for selective chemical vapor deposition of parylene-based polymers. *Chemistry of Materials*, 12(5):1305–1313, 2000.

[102] H. Y. Chen, J. H. Lai, X. W. Jiang, and J. Lahann. Substrate-selective chemical vapor deposition of reactive polymer coatings. *Advanced Materials*, 20(18):3474–3480, 2008.

[103] P. Cosseddu, A. Piras, and A. Bonfiglio. Fully deformable organic thin-film transistors with moderate operation voltage. *Electron Devices, IEEE Transactions on*, 58(10):3416–3421, 2011.

[104] Martin Kaltenbrunner, Tsuyoshi Sekitani, Jonathan Reeder, Tomoyuki Yokota, Kazunori Kuribara, Takeyoshi Tokuhara, Michael Drack, Reinhard Schwodiauer, Ingrid Graz, Simona Bauer-Gogonea, Siegfried Bauer, and Takao Someya. An ultra-lightweight design for imperceptible plastic electronics. *Nature*, 499(7459):458–463, 2013.

[105] Ute Zschieschang and Hagen Klauk. Low-voltage organic transistors with steep sub-threshold slope fabricated on commercially available paper. *Organic Electronics*, 25:340–344, 2015.

[106] Stefan Thiemann, Swetlana J. Sachnov, Fredrik Pettersson, Roger Bollström, Ronald Österbacka, Peter Wasserscheid, and Jana Zaumseil. Cellulose-based ionogels for paper electronics. *Advanced Functional Materials*, 24:625–634, 2013.

[107] T. Sekitani, U. Zschieschang, H. Klauk, and T. Someya. Flexible organic transistors and circuits with extreme bending stability. *Nat Mater*, 9(12):1015–22, 2010.

[108] Yanfei Wu, Annabel R. Chew, Geoffrey A. Rojas, Gjergji Sini, Greg Haugstad, Alex Belianinov, Sergei V. Kalinin, Hong Li, Chad Risko, Jean-Luc Brédas, Alberto Salleo, and C. Daniel Frisbie. Strain effects on the work function of an organic semiconductor. *Nature Communications*, 7:10270, 2016.

[109] C. Yang, J. Yoon, S. H. Kim, K. Hong, D. S. Chung, K. Heo, C. E. Park, and M. Ree. Bending-stress-driven phase transitions in pentacene thin films for flexible organic field-effect transistors. *Applied Physics Letters*, 92(24):243305, 2008.

[110] V. Scenev, P. Cosseddu, A. Bonfiglio, I. Salzmann, N. Severin, M. Oehzelt, N. Koch, and J. P. Rabe. Origin of mechanical strain sensitivity of pentacene thin-film transistors.

Organic Electronics, 14(5):1323–1329, 2013.

[111] P. Cosseddu, G. Tiddia, S. Milita, and A. Bonfiglio. Continuous tuning of the mechanical sensitivity of pentacene otfts on flexible substrates: From strain sensors to deformable transistors. *Organic Electronics*, 14(1):206–211, 2013.

[112] Ingrid M. Graz, Darryl P. J. Cotton, Adam Robinson, and Stephanie P. Lacour. Silicone substrate with in situ strain relief for stretchable thin-film transistors. *Applied Physics Letters*, 98(12):124101, 2011.

[113] Richard Moser, Gerald Kettlgruber, Christian M. Siket, Michael Drack, Ingrid M. Graz, Umut Cakmak, Zoltan Major, Martin Kaltenbrunner, and Siegfried Bauer. From playroom to lab: Tough stretchable electronics analyzed with a tabletop tensile tester made from toy-bricks. *Advanced Science*, 3(4), 2016.

[114] Andrei Ionut Mardare, Martin Kaltenbrunner, Niyazi Serdar Sariciftci, Siegfried Bauer, and Achim Walter Hassel. Ultra-thin anodic alumina capacitor films for plastic electronics. *physica status solidi (a)*, 209(5):813–818, 2012.

[115] Soeren Steudel, Stijn De Vusser, Stijn De Jonge, Dimitri Janssen, Stijn Verlaak, Jan Genoe, and Paul Heremans. Influence of the dielectric roughness on the performance of pentacene transistors. *Applied Physics Letters*, 85(19):4400, 2004.

[116] Hong-Gi Min, Eunsuk Seo, Junghwi Lee, Namwoo Park, and Hwa Sung Lee. Behavior of pentacene molecules deposited onto roughness-controlled polymer dielectrics films and its effect on fet performance. *Synthetic Metals*, 163:7–12, 2013.

[117] Kwonwoo Shin, Chanwoo Yang, Sang Yoon Yang, Hayoung Jeon, and Chan Eon Park. Effects of polymer gate dielectrics roughness on pentacene field-effect transistors. *Applied Physics Letters*, 88(7):072109, 2006.

[118] K. Shin, S. Y. Yang, C. W. Yang, H. Jeon, and C. E. Park. Effects of polar functional groups and roughness topography of polymer gate dielectric layers on pentacene field-effect transistors. *Organic Electronics*, 8(4):336–342, 2007.

[119] Guangqing Lin, Qinghe Wang, Li Peng, Minghui Wang, Hongbo Lu, Guobing Zhang, Guoqiang Lv, and Longzhen Qiu. Impact of the lateral length scales of dielectric roughness on pentacene organic field-effect transistors. *Journal of Physics D: Applied Physics*, 48(10):105103, 2015.

[120] Sandra E. Fritz, Tommie Wilson Kelley, and C. Daniel Frisbie. Effect of dielectric roughness on performance of pentacene tfts and restoration of performance with a polymeric smoothing layer. *The Journal of Physical Chemistry B*, 109(21):10574–10577, 2005.

[121] M J Blumenkrantz, J D Kopple, R A Gutman, Y K Chan, G L Barbour, C Roberts, F H Shen, V C Gandhi, C T Tucker, F K Curtis, and J W Coburn. Methods for assessing nutritional status of patients with renal failure. *The American Journal of Clinical Nutrition*, 33(7):1567–85, 1980.

[122] I. Gotsman, D. Zwas, D. Planer, D. Admon, C. Lotan, and A. Keren. The significance of serum urea and renal function in patients with heart failure. *Medicine*, 89(4):197–203,

2010.

[123] S Stiller, A Al-Bashir, and Helmut Mann. On-line urea monitoring during hemodialysis: A review. *Saudi J Kidney Dis Transplant*, 12(3):364–374, 2001.

[124] W. T. Chin and W. Kroontje. Conductivity method for determination of urea. *Analytical Chemistry*, 33(12):1757–1760, 1961.

[125] D. Niwa, K. Omichi, N. Motohashi, T. Homma, and T. Osaka. Organosilane self-assembled monolayer-modified field effect transistors for on-chip ion and biomolecule sensing. *Sensors and Actuators B-Chemical*, 108(1-2):721–726, 2005.

[126] Manvi Tak, Vinay Gupta, and Monika Tomar. Zinc oxide-multiwalled carbon nanotubes hybrid nanocomposite based urea biosensor. *Journal of Materials Chemistry B*, 1(46):6392–6401, 2013.

[127] M. Sheliakina, V. Arkhypova, O. Soldatkin, O. Saiapina, B. Akata, and S. Dzyadevych. Urease-based isfet biosensor for arginine determination. *Talanta*, 121:18–23, 2014.

[128] R. G. Bates and G. D. Pinching. Acidic dissociation constant of ammonium ion at 0-degrees to 50-degrees-c, and the base strength of ammonia. *Journal of Research of the National Bureau of Standards*, 42(5):419–430, 1949.

[129] J. S. Yu, X. G. Yu, L. Zhang, and H. J. Zeng. Ammonia gas sensor based on pentacene organic field-effect transistor. *Sensors and Actuators B-Chemical*, 173:133–138, 2012.

[130] Xinge Yu, Nanjia Zhou, Shijiao Han, Hui Lin, Donald B. Buchholz, Junsheng Yu, Robert P. H. Chang, Tobin J. Marks, and Antonio Facchetti. Flexible spray-coated tips-pentacene organic thin-film transistors as ammonia gas sensors. *Journal of Materials Chemistry C*, 1(40):6532–6535, 2013.

[131] Anamika Kalita, Sameer Hussain, Akhtar Hussain Malik, Nimmakayala V. V. Subbarao, and Parameswar K. Iyer. Vapor phase sensing of ammonia at the sub-ppm level using a perylene diimide thin film device. *Journal of Materials Chemistry C*, 3(41):10767–10774, 2015.

[132] F. Winquist, A. Spetz, I. Lundstrom, and B. Danielsson. Determination of urea with an ammonia gas-sensitive semiconductor-device in combination with urease. *Analytica Chimica Acta*, 163(SEP):143–149, 1984.

[133] D. J. Gundlach, L. Zhou, J. A. Nichols, T. N. Jackson, P. V. Necliudov, and M. S. Shur. An experimental study of contact effects in organic thin film transistors. *Journal of Applied Physics*, 100(2):024509, 2006.

[134] Mark E. Roberts, Stefan C. B. Mannsfeld, Randall M. Stoltenberg, and Zhenan Bao. Flexible, plastic transistor-based chemical sensors. *Organic Electronics*, 10(3):377–383, 2009.

[135] Kerstin Länge, Sebastian Grimm, and Michael Rapp. Chemical modification of parylene c coatings for saw biosensors. *Sensors and Actuators B: Chemical*, 125(2):441–446, 2007.

[136] M. Mirza, J. Wang, D. Li, S. A. Arabi, and C. Jiang. Novel top-contact monolayer pentacene-based thin-film transistor for ammonia gas detection. *ACS Appl Mater Inter-*

faces, 6(8):5679–5684, 2014.

[137] S. H. Yu, J. Cho, K. M. Sim, J. U. Ha, and D. S. Chung. Morphology-driven high-performance polymer transistor-based ammonia gas sensor. *ACS Appl Mater Interfaces*, 8(10):6750–6756, 2016.

[138] L. Torsi, A. J. Lovinger, B. Crone, T. Someya, A. Dodabalapur, H. E. Katz, and A. Gelperin. Correlation between oligothiophene thin film transistor morphology and vapor responses. *The Journal of Physical Chemistry B*, 106(48):12563–12568, 2002.

[139] A. del Campo and C. Greiner. Su-8: a photoresist for high-aspect-ratio and 3d submicron lithography. *Journal of Micromechanics and Microengineering*, 17(6):R81–R95, 2007.

[140] Joost Melai, Cora Salm, Sander Smits, Jan Visschers, and Jurriaan Schmitz. The electrical conduction and dielectric strength of su-8. *Journal of Micromechanics and Microengineering*, 19(6):065012, 2009.

[141] C. H. Kim, D. Tondelier, B. Geffroy, Y. Bonnassieux, and G. Horowitz. Characterization of the pentacene thin-film transistors with an epoxy resin-based polymeric gate insulator. *The European Physical Journal Applied Physics*, 57(2):20201, 2011.

[142] Narayanan Padma, Priya Maheshwari, Debarati Bhattacharya, Raj B. Tokas, Shashwati Sen, Yoshihide Honda, Saibal Basu, Pradeep Kumar Pujari, and T. V. Chandrasekhar Rao. Investigations on substrate temperature-induced growth modes of organic semiconductors at dielectric/semiconductor interface and their correlation with threshold voltage stability in organic field-effect transistors. *ACS Applied Materials & Interfaces*, 8(5):3376–3385, 2016.

[143] Henrik Toss, Clement Suspene, Benoit Piro, Abderrahim Yassar, Xavier Crispin, Loig Kergoat, Minh-Chau Pham, and Magnus Berggren. On the mode of operation in electrolyte-gated thin film transistors based on different substituted polythiophenes. *Organic Electronics*, 15(10):2420–2427, 2014.

[144] S. Cotrone, D. Cafagna, S. Cometa, E. De Giglio, M. Magliulo, L. Torsi, and L. Sabbatini. Microcantilevers and organic transistors: two promising classes of label-free biosensing devices which can be integrated in electronic circuits. *Anal Bioanal Chem*, 402(5):1799–811, 2012.

[145] T. Cramer, A. Kyndiah, M. Murgia, F. Leonardi, S. Casalini, and F. Biscarini. Double layer capacitance measured by organic field effect transistor operated in water. *Applied Physics Letters*, 100(14):143302, 2012.

[146] M. Magliulo, A. Mallardi, M. Y. Mulla, S. Cotrone, B. R. Pistillo, P. Favia, I. Vikholm-Lundin, G. Palazzo, and L. Torsi. Electrolyte-gated organic field-effect transistor sensors based on supported biotinylated phospholipid bilayer. *Adv Mater*, 25(14):2090–4, 2013.

[147] M. Y. Mulla, P. Seshadri, L. Torsi, K. Manoli, A. Mallardi, N. Ditaranto, M. V. Santacroce, C. Di Franco, G. Scamarcio, and M. Magliulo. Uv crosslinked poly(acrylic acid): a simple method to bio-functionalize electrolyte-gated ofet biosensors. *Journal*

of Materials Chemistry B, 3(25):5049–5057, 2015.

[148] Rossella Porrazzo, Sebastiano Bellani, Alessandro Luzio, Erica Lanzarini, Mario Caironi, and Maria Rosa Antognazza. Improving mobility and electrochemical stability of a water-gated polymer field-effect transistor. *Organic Electronics*, 15(9):2126–2134, 2014.

[149] R. Hofmockel, U. Zschieschang, U. Kraft, R. Rodel, N. H. Hansen, M. Stolte, F. Wurthner, K. Takimiya, K. Kern, J. Pflaum, and H. Klauk. High-mobility organic thin-film transistors based on a small-molecule semiconductor deposited in vacuum and by solution shearing. *Organic Electronics*, 14(12):3213–3221, 2013.

[150] Yuanyuan Hu, Vincenzo Pecunia, Lang Jiang, Chong-An Di, Xike Gao, and Henning Sirringhaus. Scanning kelvin probe microscopy investigation of the role of minority carriers on the switching characteristics of organic field-effect transistors. *Advanced Materials*, 28(23):4713–4719, 2016.

[151] F. Buth, A. Donner, M. Sachsenhauser, M. Stutzmann, and J. A. Garrido. Biofunctional electrolyte-gated organic field-effect transistors. *Adv Mater*, 24(33):4511–7, 2012.

[152] Rodrigo Lerchundi, Ignacio Fernandez-Moncada, Yasna Contreras-Baeza, Tamara Sotelo-Hitschfeld, Philipp Mächler, Matthias T. Wyss, Jillian Stobart, Felipe Baeza-Lehnert, Karin Alegria, Bruno Weber, and L. Felipe Barros. Nh4+ triggers the release of astrocytic lactate via mitochondrial pyruvate shunting. *Proceedings of the National Academy of Sciences*, 112(35):11090–11095, 2015.

[153] P. Mamczur, B. Borsuk, J. Paszko, Z. Sas, J. Mozrzymas, J. R. Wisniewski, A. Gizak, and D. Rakus. Astrocyte-neuron crosstalk regulates the expression and subcellular localization of carbohydrate metabolism enzymes. *Glia*, 63(2):328–40, 2015.

[154] D. Rabinovich, S. P. Yaniv, I. Alyagor, and O. Schuldiner. Nitric oxide as a switching mechanism between axon degeneration and regrowth during developmental remodeling. *Cell*, 164(1-2):170–82, 2016.

[155] F. Marinelli, A. Dell'Aquila, L. Torsi, J. Tey, G. P. Suranna, P. Mastrorilli, G. Romanazzi, C. F. Nobile, S. G. Mhaisalkar, N. Cioffi, and F. Palmisano. An organic field effect transistor as a selective nox sensor operated at room temperature. *Sensors and Actuators B: Chemical*, 140(2):445–450, 2009.

[156] Anne-Marije Andringa, Mark-Jan Spijkman, Edsger C. P. Smits, Simon G. J. Mathijssen, Paul A. van Hal, Sepas Setayesh, Nico P. Willard, Oleg V. Borshchev, Sergei A. Ponomarenko, Paul W. M. Blom, and Dago M. de Leeuw. Gas sensing with self-assembled monolayer field-effect transistors. *Organic Electronics*, 11(5):895–898, 2010.

[157] B. Crone, A. Dodabalapur, A. Gelperin, L. Torsi, H. E. Katz, A. J. Lovinger, and Z. Bao. Electronic sensing of vapors with organic transistors. *Applied Physics Letters*, 78(15):2229, 2001.

[158] Weiguo Huang, Jasmine Sinha, Ming-Ling Yeh, Josue F. Martinez Hardigree, Rachel LeCover, Kalpana Besar, Ana Maria Rule, Patrick N. Breysse, and Howard E. Katz.

Diverse organic field-effect transistor sensor responses from two functionalized naph-thalenetetracarboxylic diimides and copper phthalocyanine semiconductors distin-guishable over a wide analyte range. *Advanced Functional Materials*, 23(33):4094–4104, 2013.

[159] Wolfgang Kalb, Philippe Lang, Mohamad Mottaghi, Herve Aubin, Gilles Horowitz, and Matthias Wuttig. Structure-performance relationship in pentacene/al2o3 thin-film transistors. *Synthetic Metals*, 146(3):279–282, 2004.

[160] Shun-Wei Liu, Chih-Chien Lee, Hung-Lin Tai, Je-Min Wen, Jiun-Haw Lee, and Chin-Ti Chen. In situ electrical characterization of the thickness dependence of organic field-effect transistors with 1-20 molecular monolayer of pentacene. *ACS Applied Materials & Interfaces*, 2(8):2282–2288, 2010.

[161] T. Cramer, A. Kyndiah, A. Kloes, M. Murgia, B. Fraboni, and F. Biscarini. Charge density increase in submonolayer organic field-effect transistors. *Physical Review B*, 91(20), 2015.

[162] R. D. Tacito and C. Steinbruchel. Fine-line patterning of parylene-n by reactive ion etching for application as an interlayer dielectric. *Journal of the Electrochemical Society*, 143(6):1974–1977, 1996.

[163] Ramesh R. Navan, K. Prashanthi, M. Shojaei Baghini, and V. Ramgopal Rao. Solu-tion processed photopatternable high-k nanocomposite gate dielectric for low voltage organic field effect transistors. *Microelectronic Engineering*, 96:92–95, 2012.

[164] N. Sani, M. Robertsson, P. Cooper, X. Wang, M. Svensson, P. Andersson Ersman, P. Norberg, M. Nilsson, D. Nilsson, X. Liu, H. Hesselbom, L. Akesso, M. Fahlman, X. Crispin, I. Engquist, M. Berggren, and G. Gustafsson. All-printed diode operating at 1.6 ghz. *Proc Natl Acad Sci U S A*, 111(33):11943–8, 2014.

[165] F. Buth, D. Kumar, M. Stutzmann, and J. A. Garrido. Electrolyte-gated organic field-effect transistors for sensing applications. *Applied Physics Letters*, 98(15):153302, 2011.